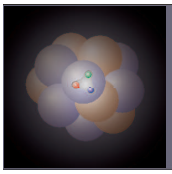

Institut für
Theoretische Physik I

JUSTUS-LIEBIG-
UNIVERSITÄT
GIESSEN

Low-energy pions in a Boltzmann-Uehling-Uhlenbeck transport simulation

Niederenergetische Pionen in einer
Boltzmann-Uehling-Uhlenbeck
Transportsimulation

Diploma thesis presented by

Oliver Buß

from Gambach / Hessen

Giessen, 30th of March, 2004

Contents

Introduction

A problem worth hitting, is very probable to hit you back.
Paul Erdös

Differences can be observed when comparing the way of walking of a man on a lonely path in the forest on a sunny winter day to his gait on a Saturday afternoon in the pedestrian precinct of Giessen. In the pedestrian precinct he will interact with various shoppers and will need to vary his speed according to the density of those shoppers because they are obstructing him. All together his gait will be sluggish as compared to his gait on the forest path. He might feel like he got attached ball and chain. Finally the stress in the pedestrian precinct will also have a negative impact on his life time.

The same might happen to a hadron which is traveling in nuclear matter. It interacts with the matter and thereby its mass and lifetime changes. Those changes are for sure dependent on density, structure and temperature of the medium.

According to present knowledge the physics at subnuclear scale is governed by the Standard Model. The elementary degrees of freedom in this theory are quarks, leptons and the gauge bosons (photon, gluon, $W^{\pm}$- and Z-boson) which mediate the interactions. Despite all efforts one was never able to observe a single quark. They have only been observed as compound states, the so-called hadrons. The most simple hadrons consist of three quarks (baryonic hadrons) or one quark and one anti-quark (mesonic hadrons). At low energies these hadrons are the relevant degrees of freedom. Compound states are always hard to describe and therefore one might think that life is getting even more complicated if one embeds those states into a nuclear medium. Nevertheless one can learn a lot about the elementary degrees of freedoms - the quarks - by examining those compound states. Especially interesting is the dependence of the hadron's properties on the surrounding nuclear medium. Based on Quantum Chromo Dynamics (QCD),

which is part of the Standard Model and describes the dynamics of the quarks, one expects the restauration of the so-called 'chiral symmetry' in a high density medium, e.g. [BW96]. The restauration of this symmetry should also have profound impact on the masses and lifetimes of the hadrons. Therefore one studies hadrons like the π-, ω-, ϕ- or ρ-meson in nuclear matter and compares those observations to vacuum results. The nuclear matter we want to look at are nuclei in their ground state - that means at temperature $T = 0$. In contrast to this one can also examine heavy-ion collisions which produce a so-called fire ball. This fire ball consists of excited high density nuclear matter at finite temperature.

Intention of this work. In this diploma thesis the influence of the pionic self energy on processes at low pion momenta is examined. We will especially utilize the so-called Boltzmann-Uehling-Uhlenbeck (BUU) transport model to describe low energy scattering data. Models like the BUU model are important tools to simulate complex γ-nucleus reactions and heavy-ion collisions. This diploma thesis examines the possibility of describing low energy processes with such a semi-classical transport model. Our interest in those low energy events is triggered by an experiment of the TAPS collaboration [M$^+$02], which investigates the photoproduction of pions off complex nuclei. The incident beam energy of $400 - 460\ MeV$ allows also the production of two pions in one absorption event. The kinetic energy of one of those correlated pions amounts up to 120 MeV. Measuring the invariant mass of the pions outside the nuclear medium, the collaboration claims to see first signs of a chiral symmetry restauration in matter. Another experiment by the CHAOS collaboration addresses the same energy regime [B$^+$96][B$^+$00]. Here the two-pion production is induced by a π^+ beam with an incident kinetic pion energy of 283 MeV. Also their results hint to a partial chiral symmetry restauration in nuclear matter.

Final state effects are extremely important for those experiments. For this reason it is necessary to apply an approved transport simulation in the analysis of such experiments. The BUU transport model which was developed in Giessen during the last two decades is such a simulation. It was utilized in heavy-ion collisions as well as in γ-nucleus processes and has a long-standing history in our working group. BUU models are the successors of the Cascade models which are being replaced by the BUU models since the early 1980's.

In spite of its merits the BUU transport model is semi-classical. Hence it is important to check whether this model can make meaningful predictions also at low energies where the wavelength of the pions is of the size of the nucleus itself.

Structure of this work. Starting with an introduction into basic ideas of field theory we will thereafter introduce the so-called 'Δ-hole model' which describes low energy pion-nucleon scattering. After a short detour covering basic facts of optical potentials we will introduce the BUU transport model. Hereafter results

on the mean free path of a π-meson in nuclear matter are presented. Then results of the BUU simulations on pion-induced scattering events and γ-induced two-pion production will be compared to experimental data. In the end we will summarize and have an outlook on the possibilities of this simulation in future.

A summary in German language of the whole thesis can be found in Appendix E.

Part I

Theoretical background

Chapter 1

Field theory

1.1 Particles and matter fields

Modern particle physics is based on quantum field theory. This theory describes particles as excitations of matter fields. For each type of particle one defines a distinct field. Finally the quantum field theory describes the propagation of these matter fields in space-time and the interactions among the distinct fields. Especially important are the so-called 'Green's functions' or 'propagators' of the fields.

1.1.1 The Propagator

The propagator describes the propagation of a field from space-time point (r_1, t_1) to (r_2, t_2). If the Hamiltonian of the system does not explicitly depend on time, then all physical observables are invariant against time shifts and can only depend on time differences. We want to consider such a time-independent Hamiltonian. One defines the so-called 'causal propagator' as

$$G(r_2, r_1, t_2 - t_1) \;=\; \frac{\langle \Psi_0 | T \left\{ \psi_H(r_2, t_2) \psi_H^\dagger(r_1, t_1) \right\} | \Psi_0 \rangle}{\langle \Psi_0 | \Psi_0 \rangle} \,. \tag{1.1}$$

Ψ_0 is the vacuum of the many-body problem and T is Wick's time-ordering-operator. All operators are Heisenberg-Operators. The knowledge of this 'one-particle Green's function' is sufficient to evaluate all expectation values of any one-body operator in the ground state of the system. The causal propagator can be evaluated with the help of Wick's theorem. Using Feynman diagrams the calculations are often visualized in an intuitive way and therefore simplified.

1.1.2 Perturbation Theory

Perturbation theory deals with interacting theories where the interacting term in the Hamiltonian is small. Denoting this interacting term with $\widehat{H}_{int}$ and the

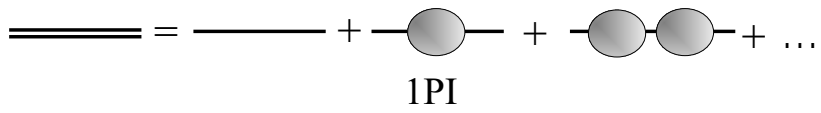

Figure 1.1: Perturbation expansion of the propagator. The bubble labeled '1PI' denotes the sum of all one-particle-irreducible diagrams.

non-interacting term with H_0 one can split the Hamiltonian into two pieces:

$$H = H_0 + \widehat{H}_{int} \; .$$

Now one introduces the interaction picture where

$$\begin{aligned} \Psi_{int}(t,x) &= e^{iH_0(t-t_0)}\Psi_S(t_0,x)e^{-iH_0(t-t_0)} \\ H_{int} &= e^{iH_0(t-t_0)}\widehat{H}_{int}e^{-iH_0(t-t_0)} \; . \end{aligned}$$

In the Heisenberg picture the operators are given by

$$\Psi_H(t,x) = e^{iH(t-t_0)}\Psi_S(t_0,x)e^{-iH(t-t_0)} \; .$$

Consequently

$$\Psi_H(t,x) = e^{iH(t-t_0)}e^{-iH_0(t-t_0)}\Psi_{int}(t_0,x)e^{iH_0(t-t_0)}e^{-iH(t-t_0)} \; .$$

In the end one can show that [PS95]

$$\begin{aligned} G(r_2,r_1,t_2-t_1) &= \frac{\langle\Psi_0|T\left\{\psi_H(r_2,t_2)\psi_H^\dagger(r_1,t_1)\right\}|\Psi_0\rangle}{\langle\Psi_0|\Psi_0\rangle} \\ &= \lim_{T\to(\infty-i\epsilon)} \frac{\langle\Psi_0|T\left\{\psi_I(r_2,t_2)\psi_I^\dagger(r_1,t_1)exp\left(-i\int_{-T}^{T}dtH_{int}(t)\right)\right\}|\Psi_0\rangle}{\langle\Psi_0|T\left\{exp\left(-i\int_{-T}^{T}dtH_{int}(t)\right)\right\}|\Psi_0\rangle} \; . \end{aligned}$$

This equation is the basis for all perturbative studies. To do a perturbation expansion one retains as many terms as desired in the Taylor series expansion of the exponentials. Using Wick's theorem one finally arrives at the point, where one can introduce the language of Feynman diagrams. In this schematic language the propagator can be visualized like in figure 1.1. The term 1PI stands for 'one-particle-irreducible diagrams', denoting the sum of all those diagrams which cannot be split into two pieces just by cutting one line of the regarded field.

1.2 The Pion Field

The long ongoing story of the pion starts in the middle of the 30s of the last century. In those days the Japanese physicist Hideki Yukawa presented his meson hypothesis to explain the forces which bind the nucleons to form a nucleus[1].

[1]Nobel price 1949

In this framework he predicted the existence of the so-called π-mesons (short: pions), which were supposed to mediate the binding forces. After a hard experimental struggle, the charged π^+- and π^-- mesons were finally detected in 1947 in atmospheric showers[2]. Nevertheless it took three more years to proof the existence of the short-living and uncharged π^0-meson[3]. In figure 1.2 an old bubble chamber photograph of pions scattering on a carbon target is shown.

meson	mass [MeV]	charge [e]	lifetime [s]	spin	isospin	parity	decay channels in vacuum
π^+	139.6	+1	$2.6\ 10^{-8}$	0	1	-	99.9% $\mu^+\nu_\mu$
π^-	139.6	-1	$2.6\ 10^{-8}$	0	1	-	99.9% $\mu^-\overline{\nu}_\mu$
π^0	135.0	0	$8.4\ 10^{-17}$	0	1	-	98.8% 2γ

Table 1.1: Properties of the π-mesons [H$^+$02a].

In our days we know a lot more about those particles. They are the lightest of all hadrons and are made of up- and down- quarks and their anti-particles. All three pions have nearly identical quantum numbers and only differentiate each other by their masses, charges and lifetimes. The lifetime difference and the small mass difference is understood to be in leading order a result of the electroweak interaction which couples to the electric charge. If one only considers the strong interaction and neglects the electroweak interaction, the three pions get nearly indistinguishable. They now can be classified as elements of a triplet of the isospin-symmetry-group SU(2), which governs the strong interaction of light matter. The Lagrange density of this isospin-triplet must be invariant under SU(2)- transformations. The pion is as well a spin S=0 particle and is therefore represented by a Lorentz-scalar field. Result of these prerequisites is

$$L = \frac{1}{2}\left((\partial^\mu \pi)^2 - m^2\pi^2\right) \ .$$

Where $\pi = (\pi_1, \pi_2, \pi_3)^t$ is the Cartesian representation of the triplet basis. By a basis transformation[4] one finally gets the physical excitations:

$$\begin{aligned} \pi^+ &= \frac{1}{\sqrt{2}}(\pi_1 - i\pi_2) \\ \pi^- &= \frac{1}{\sqrt{2}}(\pi_1 + i\pi_2) \\ \pi^0 &= \pi_3 \ . \end{aligned}$$

[2]C.F. Powell, C.M.G. Lattes, G.P.S. Occialini; Nobel price 1950 to Powell
[3]cyclotron based experiments by Bjorklund et al..
[4]More details in [Mos99]

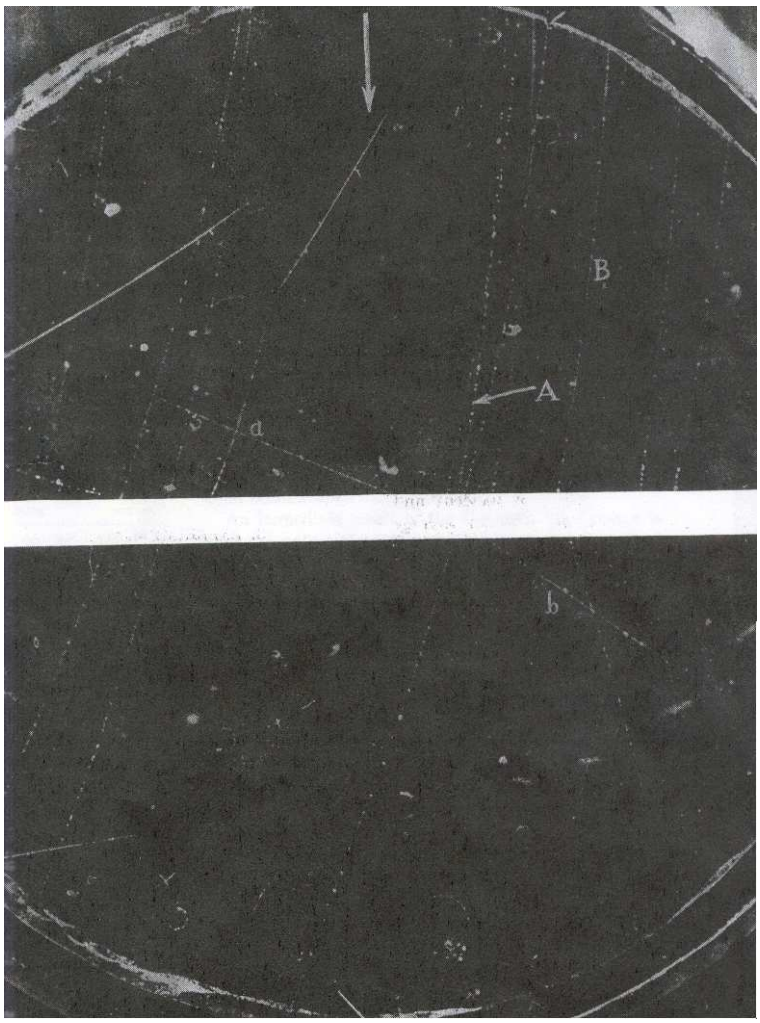

Figure 1.2: Bubble chamber photograph of a 70 MeV pion beam incoming from the top onto a carbon target. The white strip between the two pictures is where the target is fixed. One sees a pion A, which yields a two particle final state a and b. Pion B is elastically scattered through an angle of 32°. This picture was taken in 1951 [BKL$^+$52].

In this representation the Lagrange density becomes a sum of the Lagrange density for a complex field and the Lagrange density for a real field.

$$L = \partial^\mu \pi^+ \partial_\mu \pi^- - m^2 \pi^+ \pi^- + \frac{1}{2}\left(\left(\partial^\mu \pi^0\right)^2 - m^2\left(\pi^0\right)^2\right) .$$

For all three pions one gets the same equations of motion

$$\partial^\mu \partial_\mu \pi^i + m^2 \pi^i = 0$$

with $i = +, -, 0$. Therefore each pion is described by the well known Klein-Gordon equation.

1.2.1 The pion propagator in vacuum

In equation (1.1) we defined the causal propagator of matter fields. In vacuum the causal propagator of the pion can be computed to be [PS95]

$$iG(x-y) = \int \frac{d^4p}{(2\pi)^4} \frac{i}{p^2 - m^2 + i\epsilon} e^{-ip(x-y))} \tag{1.2}$$

with the Fourier transform

$$iG(p_0, \vec{p}) = \frac{i}{p^2 - m^2 + i\epsilon} . \tag{1.3}$$

Interpretation

Let us have a closer look at the interpretation of the propagator in terms of probabilities assuming that the vacuum is normalized ($\langle \Psi_0 | \Psi_0 \rangle = 1$).

$$\begin{aligned} G(r_2, r_1, t_2, t_1) &= \langle \Psi_0 | T\left\{\phi(r_2, t_2), \phi^\dagger(r_1, t_1)\right\} | \Psi_0 \rangle \\ &= \Theta(t_2 - t_1) \langle \Psi_0 | \phi(r_2, t_2)\ \phi^\dagger(r_1, t_1) | \Psi_0 \rangle \\ &\quad + \Theta(t_1 - t_2) \langle \Psi_0 | \phi^\dagger(r_1, t_1)\ \phi(r_2, t_2) | \Psi_0 \rangle . \end{aligned}$$

In terms of second quantization $\phi^\dagger$ has to be understood as a particle creation operator or antiparticle annihilation operator, whereas ϕ just performs the opposite operations. For a complex Klein-Gordon-theory we have a charged field. Here one defines the particle to be the negative charged excitation and the antiparticle to be the positive one. For a real Klein-Gordon-theory the particle is its own antiparticle. On the one hand

$$\Theta(t_2 - t_1) \langle \Psi_0 | \phi(r_2, t_2) \phi^\dagger(r_1, t_1) | \Psi_0 \rangle$$

expresses the probability amplitude for an overlap between a particle produced at (r_1, t_1) with another particle at later time t_2 and position r_2. On the other hand

$$\Theta(t_1 - t_2) \langle \Psi_0 | \phi^\dagger(r_1, t_1) \phi(r_2, t_2) | \Psi_0 \rangle$$

gives the overlap between an antiparticle, which is produced at time t_2 and at position r_2, with another one at later time t_1 and at position r_1. It can either be interpreted as an antiparticle running forward in time from r_2 to r_1 or an particle running backward in time from r_1 to r_2.

Therefore both parts of he propagator probability amplitudes add up to one amplitude, which stands for the probability amplitude to measure a particle at (r_2, t_2), which has been produced at (r_1, t_1). In these terms the causal propagator has a well defined probability interpretation.

$$|G(r_2, r_1, t_2, t_1)|^2 \quad = \quad \begin{array}{l}\text{probability to measure a} \\ \text{particle at } (r_2, t_2), \text{ which} \\ \text{has been produced at } (r_1, t_1)\end{array} \tag{1.4}$$

1.2.2 Self energy of the pion

We want to have a closer look at a pion which is interacting with other matter fields. The free pion propagator in momentum space was already stated in equation (1.3). In figure 1.1 the calculation of the propagator is described in the language of Feynman diagrams. Defining

$$-i\Pi(p) = \text{sum of all 1PI diagrams in momentum space}$$

one can now evaluate the propagator of the interacting theory just by translating figure 1.1:

$$\begin{aligned} G(\vec{p}, E) &= \int d^4x \frac{\langle \Psi_0 | T \left\{ \psi_H(r_2, t_2) \psi_H^\dagger(r_1, t_1) \right\} | \Psi_0 \rangle}{\langle \Psi_0 | \Psi_0 \rangle} e^{ipx} \\ &= \frac{i}{p^2 - m^2 + i\epsilon} + \frac{i}{p^2 - m^2 + i\epsilon}(-i\Pi(p))\frac{i}{p^2 - m^2 + i\epsilon} \\ &+ \frac{i}{p^2 - m^2 + i\epsilon}(-i\Pi(p))\frac{i}{p^2 - m^2 + i\epsilon}(-i\Pi(p))\frac{i}{p^2 - m^2} + \dots \ . \end{aligned}$$

Fortunately the sum of all diagrams forms a geometric series due to the fact that p and $\Pi(p)$ commute. Consequently,

$$G(\vec{p}, E) = \frac{i}{p^2 - m^2 + i\epsilon - \Pi(p)} \ .$$

The term $\Pi(p)$ is also called the self energy of the pion. Its real part can be understood as an effective additive mass term due to the medium. The imaginary part of the self energy shifts the pole of the propagator away from the real axis into the complex plane. The result of the imaginary part is a change in the lifetime of the pion.

1.2.3 Self energy and decay rates

The propagator can be interpreted as the probability amplitude for a particle traveling from space point A at time t_1 to space point B at time t_2. We assume $t_2 > t_1$. By residual calculus

$$\begin{aligned} G(\vec{p}, t_2 - t_1) &= \int_{-\infty}^{\infty} G(\vec{p}, E) e^{-iE(t_2-t_1)} dE \\ &= \int_{-\infty}^{\infty} \frac{i}{E^2 - \vec{p}^2 - m^2 - \Pi(E, \vec{p})} e^{-iE(t_2-t_1)} dE \\ &= \sum_i \underbrace{-2\pi \left(\frac{E - \omega_i}{E^2 - \vec{p}^2 - m^2 - \Pi(E, \vec{p})} \right)_{E=\omega_i}}_{=a_i} e^{-i\omega_i(t_2-t_1)} \\ &= \sum_i a_i e^{-i\omega_i(t_2-t_1)} \end{aligned}$$

with the index i counting the numbers of solutions to the dispersion relation

$$\omega_i^2 = \vec{p}^2 + m^2 + \Pi(\omega_i, \vec{p})$$

in the lower complex half plane. The imaginary parts of the solutions are given by

$$\begin{aligned} \Im(\omega_i) &= \frac{\Im(\omega_i^2)}{2\Re(\omega_i)} \\ &= \frac{\Im\left(\Pi(\omega_i, \vec{p})\right)}{2\Re\left(\sqrt{\vec{p}^2 + m^2 + \Pi(\omega_i, \vec{p})}\right)} \,. \end{aligned}$$

Therefore

$$G(\vec{p}, t_2 - t_1) = \sum_i \left[a_i \ \exp\left(-i\Re\left[\omega_i \left(t_2 - t_1\right)\right]\right) \ \exp\left(\frac{\Im\left(\Pi(\omega_i, \vec{p})\right)}{2\Re\left(\sqrt{\vec{p}^2 + m^2 + \Pi(\omega_i, \vec{p})}\right)} (t_2 - t_1) \right) \right] .$$

The propagator has different parts due to different solutions of the dispersion relation. The individual terms decay with the decay constant

$$\Gamma_i = -\frac{\Im\left(\Pi(\omega_i, \vec{p})\right)}{2 \ \Re\left(\sqrt{\vec{p}^2 + m^2 + \Pi(\omega_i, \vec{p})}\right)}$$

which can be approximated by for $|\Pi| \lll \vec{p}^2 + m^2$

$$\begin{aligned} \Gamma_i &\simeq -\frac{\Im\left(\Pi(\omega_i, \vec{p})\right)}{2\ \sqrt{\vec{p}^2 + m^2}} \\ &= -\frac{\Im\left(\Pi(\omega_i, \vec{p})\right)}{2\ E_{Free}} \,. \end{aligned} \tag{1.5}$$

Assuming there is only one solution to the dispersion relation in the lower half plane one gets finally

$$\begin{aligned} \text{Probability to travel from A at time } t_1 \text{ to B at } t_2 &= |G(\vec{p}, t_2 - t_1)|^2 \\ &\sim exp\left(-\Gamma(t_2 - t_1)\right) \ . \end{aligned}$$

The decay constant therefore describes, due to the probability interpretation of the propagator, the decay rate of the particle which is described by the specific propagator.

1.2.4 Lehmann representation of the pion

One of the most important quantities in many-body physics is the so-called 'spectral function'. This function contains the whole information concerning the analytic structure of the propagator. It has also an interesting probability interpretation.

For the pion the derivation of the spectral function is simplified by the fact that the pion is a scalar particle [PS95]. We demand that the vacuum is normalized ($\langle\Psi_0|\Psi_0\rangle = 1$). In this case the propagator is given by

$$iG(r_2, r_1, t_2 - t_1) = \langle\Psi_0|T\left\{\phi(r_2, t_2)\phi(r_1, t_1)\right\}|\Psi_0\rangle \ . \tag{1.6}$$

In a system which is invariant under translation the three-momentum operator P and the Hamiltonian H commute. Therefore it is possible to find a complete set of momentum eigenfunctions, which are also eigenfunctions of the Hamiltonian. Out of each momentum eigenfunction λ_0 with $P|\lambda_0\rangle = 0$ one can generate other eigenfunctions of P by Lorentz-boosting λ_0 to λ_p with $E_p(\lambda) = \sqrt{p^2 + m_\lambda^2}$. Here λ denotes one special particle species or state and m_λ denotes its mass.

A complete set of momentum eigenfunctions is therefore

$$1 = |\Psi_0\rangle\langle\Psi_0| + \sum_\lambda \int \frac{d^3p}{(2\pi)^3\ 2E_p(\lambda)} |\lambda_p\rangle\langle\lambda_p| \ . \tag{1.7}$$

The summation goes over all zero momentum states λ_0. Now one inserts this into (1.6). Considering only the case $t_2 > t_1$ one gets:

$$\begin{aligned} & \langle\Psi_0|\phi(r_2, t_2)\phi(r_1, t_1)|\Psi_0\rangle \\ = \ & \langle\Psi_0|\phi(r_2, t_2)\left(|\Psi_0\rangle\langle\Psi_0| + \sum_\lambda \int \frac{d^3p}{(2\pi)^3\ 2E_p(\lambda)} |\lambda_p\rangle\langle\lambda_p|\right) \\ & \phi(r_1, t_1)|\Psi_0\rangle \\ = \ & \langle\Psi_0|\phi(r_2, t_2)|\Psi_0\rangle\langle\Psi_0|\phi(r_1, t_1)|\Psi_0\rangle \\ & + \sum_\lambda \int \frac{d^3p}{(2\pi)^3\ 2E_p(\lambda)} \langle\Psi_0|\phi(r_2, t_2)|\lambda_p\rangle\langle\lambda_p|\phi(r_1, t_1)|\Psi_0\rangle \ . \end{aligned}$$

The constant

$$\langle\Psi_0|\phi(r_2,t_2)|\Psi_0\rangle\langle\Psi_0|\phi(r_1,t_1)|\Psi_0\rangle$$

can always be set to zero by

$$\phi(r,t) \rightarrow \phi(r,t) + const\ .$$

One is now left with

$$\begin{aligned}&\langle\Psi_0|\phi(r_2,t_2)\phi(r_1,t_1)|\Psi_0\rangle = \\ &\sum_\lambda \int \frac{d^3p}{(2\pi)^3\ 2E_p(\lambda)} \langle\Psi_0|\phi(r_2,t_2)|\lambda_p\rangle\langle\lambda_p|\phi(r_1,t_1)|\Psi_0\rangle\ . \end{aligned} \tag{1.8}$$

The unitary operator $e^{i\widehat{P}_\mu x^\mu}$ with $\widehat{P}_\mu = (H,P)$ generates a translation in spacetime by x^μ. Consequently,

$$\phi(r,t) = e^{iP_\mu x^\mu}\phi(0,0)e^{-iPx^\mu} \text{ with } x^\mu = (t,\vec{r})\ .$$

Now one is making use of Lorentz transformations. Demanding that there are no zero mass states besides the vacuum, there is always a Lorentz transformation U with $U|\lambda_p\rangle = |\lambda_0\rangle$. The vacuum is invariant under Lorentz transformations, the scalar operator $\phi(0,0)$ too. As a consequence

$$\begin{aligned}\langle\Psi_0|\phi(r,t)|\lambda_p\rangle &= \langle\Psi_0|e^{i\widehat{P}_\mu x^\mu}\phi(0,0)e^{-i\widehat{P}_\mu x^\mu}|\lambda_p\rangle \\ &= \langle\Psi_0|e^{i0}\phi(0,0)e^{-ip_\mu x^\mu}|\lambda_p\rangle \\ &= \langle\Psi_0|\phi(0,0)|\lambda_p\rangle e^{-ip_\mu x^\mu} \\ &= \langle\Psi_0|U^{-1}U\phi(0,0)U^{-1}U|\lambda_p\rangle e^{-ip_\mu x^\mu} \\ &= \left(\langle\Psi_0|U^{-1}\right)\left(U\phi(0,0)U^{-1}\right)|\lambda_0\rangle e^{-ip_\mu x^\mu} \\ &= \langle\Psi_0|\phi(0,0)|\lambda_0\rangle e^{-ip_\mu x^\mu} \text{ with } p_\mu = (E_p,p)\ .\end{aligned}$$

Now one uses this identity in equation (1.8):

$$\begin{aligned}\langle\Psi_0|\phi(r_2,t_2)\phi(r_1,t_1)|\Psi_0\rangle &= \sum_\lambda \int \frac{d^3p}{(2\pi)^3\ 2E_p(\lambda)} \langle\Psi_0|\phi(0,0)|\lambda_0\rangle \\ &\quad \langle\lambda_0|\phi(0,0)|\Psi_0\rangle e^{-ip_\mu(x_2^\mu - x_1^\mu)}|_{p_0=E_p}\ .\end{aligned}$$

Since $t_2 > t_1$ one can now use residual calculus to restate this:

$$\begin{aligned}\langle\Psi_0|\phi(r_2,t_2)\phi(r_1,t_1)|\Psi_0\rangle &= \sum_\lambda \int \frac{d^4p}{(2\pi)^4} \frac{i}{p^2 - m_\lambda^2 + i\epsilon} \\ &\quad e^{-ip_\mu(x_2^\mu - x_1^\mu)}|\langle\Psi_0|\phi(0,0)|\lambda_0\rangle|^2\ .\end{aligned}$$

The case $t_2 < t_1$ leads to the same result [PS95]. In the end one gets the so-called 'Lehmann representation' of the propagator.

$$\begin{aligned} iG(r_2, r_1, t_2 - t_1) &= \langle \Psi_0 | T \left\{ \phi(r_2, t_2) \phi(r_1, t_1) \right\} | \Psi_0 \rangle \\ &= \sum_\lambda \int \frac{d^4p}{(2\pi)^4} \frac{i}{p^2 - m_\lambda^2 + i\epsilon} e^{-ip_\mu (x_2^\mu - x_1^\mu)} |\langle \Psi_0 | \phi(0,0) | \lambda_0 \rangle|^2 \\ &= \sum_\lambda \int \frac{d^4p}{(2\pi)^4} D_F(p_\mu, m_\lambda^2) e^{-ip_\mu (x_2^\mu - x_1^\mu)} |\langle \Psi_0 | \phi(0,0) | \lambda_0 \rangle|^2 \\ &= \sum_\lambda D_F(x_2 - x_1, t_2 - t_1, m_\lambda^2) |\langle \Psi_0 | \phi(0,0) | \lambda_0 \rangle|^2 \\ &= \int_0^\infty dM^2 D_F(x_2 - x_1, t_2 - t_1, M^2) \rho(M^2) \end{aligned} \tag{1.9}$$

or

$$iG(k_\mu) = \int_0^\infty dM^2 D_F(k_\mu, M^2) \rho(M^2) \; . \tag{1.10}$$

The spectral function was hereby defined as

$$\rho(M^2) = \sum_\lambda \delta(M^2 - m_\lambda^2) |\langle \Psi_0 | \phi(0,0) | \lambda_0 \rangle|^2 \; . \tag{1.11}$$

There is an easy way to extract the spectral function out of the propagator $iG(k_\mu)$. Using the formula (B.1) with (1.10) one gets

$$\begin{aligned} G(k_\mu) &= \frac{1}{i} \int_0^\infty dM^2 D_F(k_\mu, M^2) \rho(M^2) \\ &= \underbrace{\wp \int_0^\infty dM^2 \frac{1}{k^2 - M^2} \rho(M^2)}_{\in \Re} - i\pi \rho(k^2) \; \theta(k^2) \\ \Longrightarrow \quad \rho(k^2) &= -\frac{1}{\pi} \Im \left(G(k_\mu) \right) \; \theta(k^2) \; . \end{aligned} \tag{1.12}$$

Interpretation

In classical terms one could interpret equation (1.9) in such a way, that the interacting particle is made out of a sum (or integral) of different particles, which only differ by mass.

This interpretation one has to keep in mind to understand the philosophy of off-shell transport simulations. In off-shell transport simulations the mass of the particle is different to the vacuum mass. One represents each real particle by several test-particles with distinct masses according to the Lehmann representation.

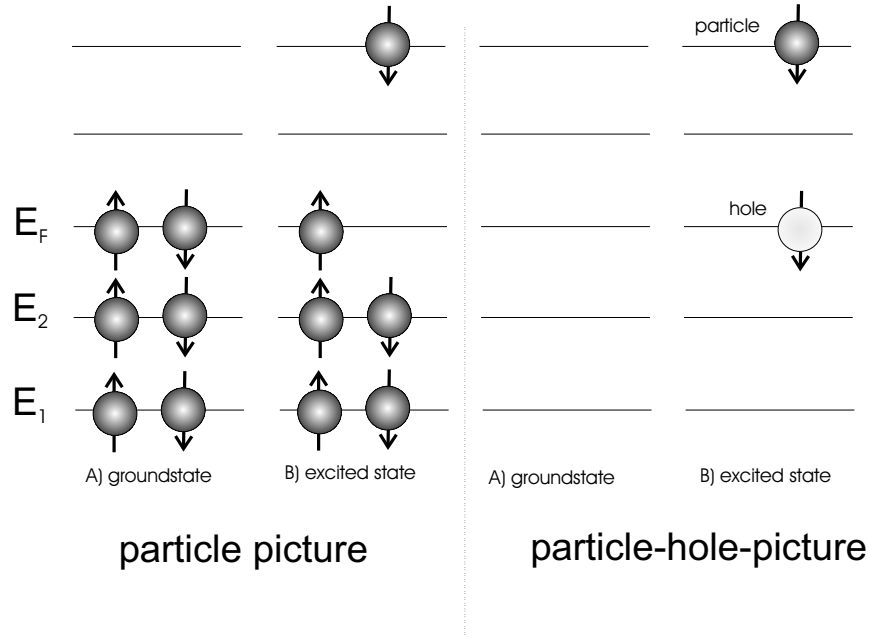

Figure 1.3: Particle-hole picture: One considers only particles above the Fermi surface and holes in the sea of fermions below this surface.

1.3 The Nucleon Field

We want to consider nuclear matter, which is a translation invariant system of nucleons. We assume that we can neglect all nucleon-nucleon interactions. The energy eigenstates of the single nucleons are simple plane waves and due to Pauli-Blocking the ground state of an ensemble of nucleons are two spheres - one for the protons and one for the neutrons - in momentum space with radius

$$\begin{aligned} p_f^p &= \sqrt{2mE_f^p} = \left(3\pi^2\rho_p\right)^{1/3} \\ p_f^n &= \sqrt{2mE_f^n} = \left(3\pi^2\rho_n\right)^{1/3} \end{aligned}$$

where $\rho_{n,p}$ are the densities of the protons and neutrons. A typical value for p_f in symmetric nuclear matter is around 250 MeV. The surfaces of those spheres are called Fermi surfaces.

1.3.1 Particle-hole notation

The so-called particle-hole description only deals with particles above the Fermi surface and holes in the sea of fermions below this surface. Hence the sea of fermions below the Fermi surface is still physically present, but removed from the picture. An illustration for this notation is given in figure 1.3.

1.3.2 The nucleon propagator in particle-hole notation

Following the notation of [FW71] one defines the nucleonic field in second quantized form by

$$\psi_H(x) = \sum_{\vec{p},\lambda} \psi_{\vec{p},\lambda}(x)\ e^{-i\omega_{\vec{p}}t}\ c_{\vec{p},\lambda}$$

where $c_{\vec{p},\lambda}$ is the particle annihilation operator and $\omega_{\vec{p}} = \sqrt{\vec{p}^2 + m^2}$. $\vec{p}$ denotes the momentum of the particle and λ its inner degrees of freedom. Now one transforms this into the particle-hole picture by

$$c_{\vec{p},\lambda} = \begin{cases} a_{\vec{p},\lambda} & |\vec{p}| > p_f \quad \text{particles} \\ b^\dagger_{-\vec{p},\lambda} & |\vec{p}| < p_f \quad \text{holes} \end{cases} .$$

The operator $a_{\vec{p},\lambda}$ is annihilating particles above the Fermi sea and its hermitian conjugate $a^\dagger_{\vec{p},\lambda}$ is creating particles above the Fermi sea. $b^\dagger_{-\vec{p},\lambda}$ removes particles from the Fermi sea and is therefore a hole-creation-operator, its counterpart $b_{-\vec{p},\lambda}$ annihilates holes. Therefore our field is now represented by

$$\psi_H(x) = \sum_{|\vec{p}|>p_f,\lambda} \psi_{\vec{p},\lambda}(x)\ e^{-i\omega_{\vec{p}}t}\ a_{\vec{p},\lambda} + \sum_{|\vec{p}|\le p_f,\lambda} \psi_{\vec{p},\lambda}(x)\ e^{-i\omega_{\vec{p}}t}\ b^\dagger_{-\vec{p},\lambda} .$$

The anti-commutation relations of the $c_{\vec{p},\lambda}$ operators translate directly into:

$$\begin{aligned} \left\{a_{\vec{p},\lambda}, a^\dagger_{\vec{p}',\lambda'}\right\} &= \left\{b_{\vec{p},\lambda}, b^\dagger_{\vec{p}',\lambda'}\right\} = \delta_{\vec{p},\vec{p}'}\delta_{\lambda,\lambda'} \\ \left\{a_{\vec{p},\lambda}, b^\dagger_{\vec{p}',\lambda'}\right\} &= \left\{a^\dagger_{\vec{p},\lambda}, b_{\vec{p}',\lambda'}\right\} = 0 . \end{aligned}$$

Now one inserts this form of the field operator in the definition of the propagator

$$G_{\alpha\beta}(r_1, r_2, t_2 - t_1) = \left\langle \Psi_0 | T\left[\psi_H(r_2, t_2, \alpha)\psi^\dagger_H(r_1, t_1, \beta)\right] |\Psi_0\right\rangle$$

where α, β denote inner degrees of freedom of the fields. As a result one gets after some commutator algebra in the infinite volume limit

$$\begin{aligned} &G_{\alpha\beta}(r_2, r_1, t_2 - t_1) \\ &= \delta_{\alpha\beta} \int \frac{d^3p\ dE}{(2\pi^4)} e^{i\vec{p}(\vec{r_2}-\vec{r_1})} e^{-iE(t_2-t_1)} \left(\frac{\theta(|\vec{p}| - p_F)}{E - \omega_{\vec{p}} + i\eta} + \frac{\theta(p_F - |\vec{p}|)}{E - \omega_{\vec{p}} - i\eta}\right) \end{aligned}$$

with the Fourier transform

$$G_{\alpha\beta}(\vec{p}, E) = \delta_{\alpha\beta} \left(\frac{\theta(|\vec{p}| - p_F)}{E - \omega_{\vec{p}} + i\eta} + \frac{\theta(p_F - |\vec{p}|)}{E - \omega_{\vec{p}} - i\eta}\right) . \tag{1.13}$$

Therefore the nucleon propagator in the nucleon-hole-picture now consists of a hole and a particle contribution.

Chapter 2

The Δ-Hole Model

The purpose of this chapter is to obtain a self energy for the pions. The self energy is used as an input for the transport simulations and modifies the dynamics of the pion while being propagated through nuclear matter in the simulation.

The Δ-hole model is a widely used field theoretical ansatz to evaluate pionic interactions in the nuclear medium. The Δ-hole model provides also a more elaborate understanding of the processes involved in pion absorption than other phenomenological optical potentials do, which are mainly fitted to data[1]. But the fitted optical potentials work very well, and serve therefore as an important benchmark for self energies derived by field theoretical arguments.

pole mass $[MeV]$	charge $[e]$	decay width in vacuum $[MeV]$
$1230 - 1234$	$-1, 0, +1, +2$	$115 - 125$

spin	isospin	parity	decay channels in vacuum
$\frac{3}{2}$	$\frac{3}{2}$	$+$	$> 99\% N\pi$

Table 2.1: Characteristics of the Δ-resonance in vacuum [H$^+$02a].

Already in other works by A. Larionov et al. [LM$^+$02] and W. Ehehalt et al. [Ehe92], the Δ-hole model was introduced to derive transport properties. In comparison to A. Larionov we are going to take a different approach. While Larionov was focusing on the implementation of the full spectral function and neglecting the real dynamics of the spectral function due to the self energy, we are mainly focusing on the dynamics while neglecting the width of the spectral function. This ansatz corresponds to the work of Wolfgang Ehehalt, who worked at higher energies and used a different prescription for the Δ properties.

[1] e.g. [SMC79] and [AR02]

2.1 Formalism

In a fully relativistic ansatz (e.g.[LP03]) one can write the Lagrangian density for the pion, nucleon and Δ-system in the following form

$$\begin{aligned} L &= \underbrace{\sum_{a=1}^{3}\left(-\frac{f}{m_\pi}\overline{\Psi}_N\gamma^\mu\gamma_5\tau_a\Psi_N\partial_\mu\pi_a + \frac{f_\Delta}{m_\pi}\overline{\Psi}^\mu_\Delta T_a^\dagger\Psi_N\partial_\mu\pi_a + \frac{f_\Delta}{m_\pi}\overline{\Psi}_N T_a\Psi^\mu_\Delta\partial_\mu\pi_a\right)}_{L_{int}} \\ &+ L^{\Delta N}_{\text{short range}} + L^\pi_{free} + L^\Delta_{free} + L^N_{free}. \end{aligned} \tag{2.1}$$

Here π is the pseudo-scalar isovector pion field, while Ψ^μ_Δ is the Rarita-Schwinger spinor of the Δ-resonance. f_Δ and f are the coupling constants. L^π_{free}, L^Δ_{free} and L^N_{free} are the free Lagrangian densities of the three different fields. The term $L_{\text{short range}}$ describes all sort of short range correlations between nucleons and Δ's and leads to the so-called 'Lorentz-Lorenz' correction. In the nonrelativistic limit it can be shown [EW88] that the interacting Lagrangian L_{int} reduces to

$$\begin{aligned} L^{NR}_{int} &= \sum_{a=1}^{3}\sum_{i,i',s,s'=-\frac{1}{2},\frac{1}{2}} \frac{f}{m_\pi}\left(\overline{\Psi}_N\right)_{s,i}\left(\vec{\sigma}\vec{\nabla}\right)_{s,s'}\left(\tau_a\pi_a\right)_{i,i'}\left(\Psi_N\right)_{s',i'} \\ &+ \sum_{a=1}^{3}\sum_{i,s=-\frac{1}{2},\frac{1}{2}}\sum_{i',s'=-\frac{3}{2},\frac{3}{2}}\left(\frac{f_\Delta}{m_\pi}\left(\overline{\Psi}_N\right)_{s,i}\left(\vec{S}\vec{\nabla}\right)_{s,s'}\left(T_a\pi_a\right)_{i,i'}\right. \\ &\left.\left(\Psi_\Delta\right)_{s',i'} + h.c.\right) \end{aligned} \tag{2.2}$$

with non-relativistic matter fields. The indices are explicitly written down to show the spin and isospin dependences. s and s' are spin indices, i and i' label isospin. T_a is the isospin transition operator and defined by Clebsch-Gordan elements in the following way

$$\left(T_a\right)_{ij} = \left\langle 1, a; \frac{1}{2}, i \middle| \frac{3}{2}, j \right\rangle \text{ with } i = -\frac{1}{2}, \frac{1}{2} \text{ and } j = -\frac{3}{2}, \ldots, \frac{3}{2} \tag{2.3}$$

and the spin transition operator $\left(S_a\right)_{ij}$ is defined in the same way. σ_a and τ_a are Pauli matrices.

2.2 Pion self energy

Already in paragraph 1.2.2 on page 8 it was described how the self energy for the pion can be calculated by summing up all 'one-particle-irreducible' graphs. Those graphs can not be split into two by just cutting one pion propagator line. Considering only Δ-hole loops in the propagator and no nucleon-hole loops, the resulting series of graphs is shown in figure 2.1. The wiggly lines connecting different Δ-hole loops are the short- range correlations mentioned earlier.

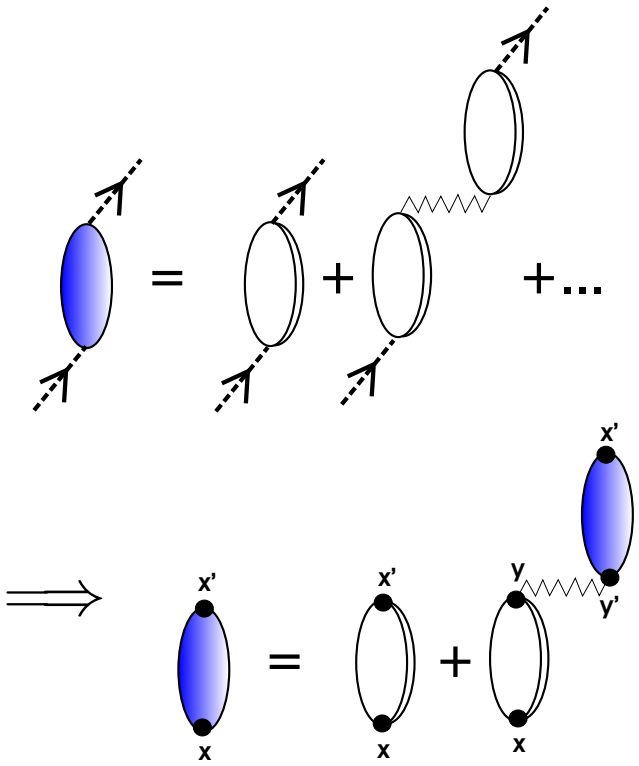

Figure 2.1: Dyson-equation for the self energy of the pion in the Δ-hole model with short-range correlations.

2.2.1 Lorentz-Lorenz correction

The upper graphs of figure 2.1 can be rearranged to a Dyson-equation. This Dyson-equation is shown in the lower part of the figure 2.1. Defining

$i\Delta(x,x') =$

$iP(x,x') =$

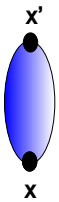

and the short-range correlations as $g(x, x')$ one can write down the Dyson-equation in position space:

$$P(x, x') = \Delta(x, x') + \int d^4y \int d^4y' \Delta(x, y) g(y, y') P(y', x').$$

Going to momentum space and using the convolution theorem twice on the integrals gives

$$P(\omega, p) = \Delta(\omega, p) + \Delta(\omega, p) g(\omega, p) P(\omega, p).$$

Therefore

$$P(\omega, p) = \frac{\Delta(\omega, p)}{1 - g(\omega, p)\Delta(\omega, p)}. \tag{2.4}$$

This result due to the short-range correlations is called the 'Lorentz-Lorenz' correction. In the literature [EW88] one can find this effect also described in analogy to the scattering of light in a dense medium. The short-range correlations are now supposed to happen on a scale, which is small compared to the scale of the Δ-hole fluctuations. Therefore one can set

$$g(x, x') = \widehat{g}\delta(x, x') \Longrightarrow g(\omega, p) = \widehat{g} = constant$$

and equation (2.4) becomes

$$P(\omega, p) = \frac{\Delta(\omega, p)}{1 - \widehat{g}\Delta(\omega, p)}. \tag{2.5}$$

The full pionic self energy $\Pi(\omega, p)$ is gained by multiplying $P(\omega, p)$ with the pionic vertex factors of figure 2.1. In the end one gets [EW88]

$$\Pi(\omega, p) = q^2 \left(\frac{f_\Delta}{m_\pi}\right)^2 \frac{\Delta(\omega, p)}{1 - \widehat{g}\Delta(\omega, p)}.$$

2.3 Pionic dispersion relation

The Δ-hole loop $\Delta(\omega, q)$ is evaluated explicitly in appendix C. There we made a zero-width approximation for the Δ and considered only Δ-hole loops. The result for symmetric nuclear matter is given in equation (C.5).

$$\Delta(\omega, p) = -\frac{8}{9}\rho \frac{\omega_\Delta}{\omega_\Delta^2 - \omega^2}$$

Here ω_Δ is the energy of a Δ-hole loop. In ordinary nuclei proton and neutron densities are different. In the appendix it is also shown, that in the simple Δ-hole framework the corrections due to this fact can be neglected (see figure C.3).

Therefore we are disregarding this effect and follow the symmetric prescription in this simple picture. According to section 1.2.4 one expects to find also a Lehmann representation for the pion. In the simple Δ-hole model it can actually be shown[2] analytically that

$$G_\pi(\omega,p) = \frac{1}{\omega^2 - p^2 - m_\pi^2 - \Pi(\omega,k)} = \frac{Z_1}{\omega^2 - \omega_1^2 + i\eta} + \frac{Z_2}{\omega^2 - \omega_2^2 + i\eta}$$

with

$$\begin{aligned} Z_1 &= \frac{1}{2}\left(1 - \frac{\widehat{E}^2 - E_{free}^2}{\sqrt{\left(\widehat{E}^2 - E_{free}^2\right)^2 + 4k^2 C\omega_\Delta}}\right) \\ Z_2 &= \frac{1}{2}\left(1 + \frac{\widehat{E}^2 - E_{free}^2}{\sqrt{\left(\widehat{E}^2 - E_{free}^2\right)^2 + 4k^2 C\omega_\Delta}}\right) \end{aligned} \tag{2.6}$$

where

$$\begin{aligned} C &= \frac{8}{9}\left(\frac{f_\Delta}{m_\pi}\right)^2 \rho \\ \widehat{E} &= \sqrt{\omega_\Delta^2 + g' C\omega_\Delta} \\ E_{free} &= \sqrt{p^2 + m_\pi^2} \\ \omega_{1,2}^2 &= \frac{1}{2}\left(\widehat{E}^2 + E_{free}^2 \pm \sqrt{\left(\widehat{E}^2 - E_{free}^2\right)^2 + 4k^2 C\omega_\Delta}\right). \end{aligned}$$

Therefore the pion in the nuclear medium has two clearly separated branches and the spectral density becomes

$$\rho(\omega,q) = Z_1\ \delta(\omega^2 - \omega_1^2) + Z_2\ \delta(\omega^2 - \omega_2^2).$$

The more energetic branch is called 'Δ-hole branch' while the less energetic one is called 'pion branch'. The dispersion relations and the strengths of the two branches are shown in figure 2.2.

If one considers a non-interacting Δ-hole state and a pion, then their dispersion relations are given by

$$\begin{aligned} \omega_\pi(p) &= \sqrt{p^2 + m_\pi^2} \\ \omega_{\Delta-hole}(p) &= m_\Delta - m_{nucleon} + \frac{p^2}{2\ m_\Delta}\ . \end{aligned}$$

[2] see appendix C.3.1 on page 127

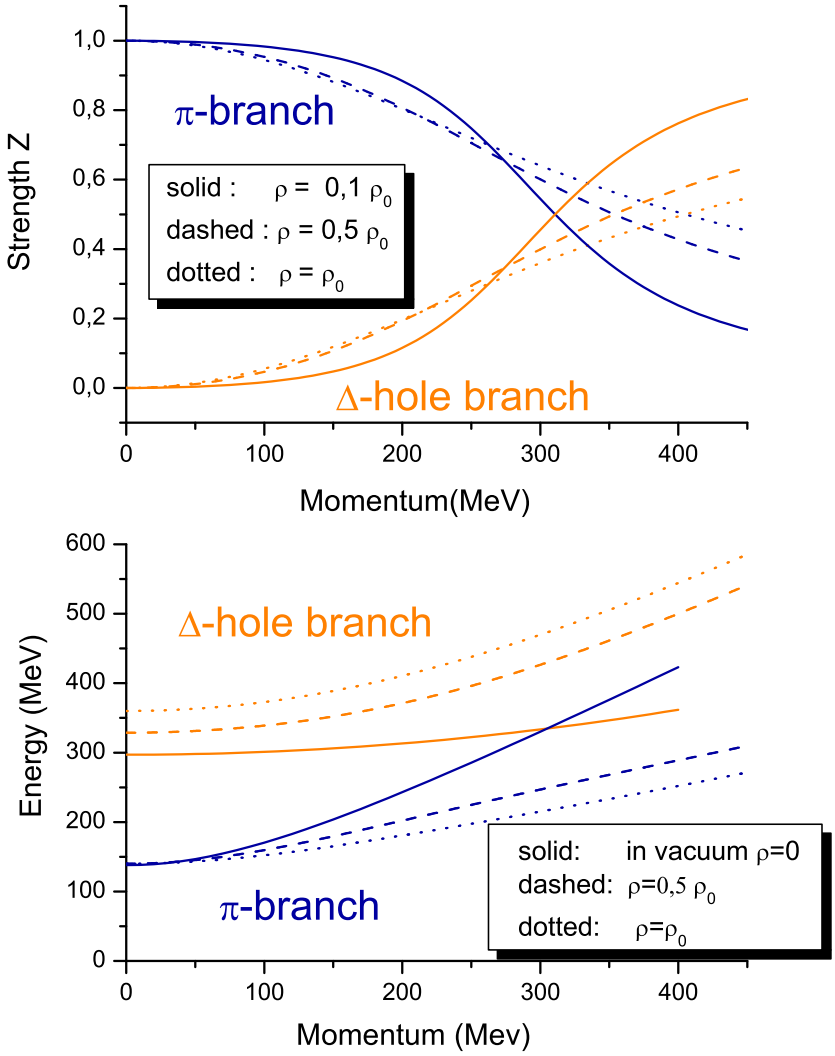

Figure 2.2: Dispersion relation for the two pion branches and strength distribution in the simple Δ-hole model.

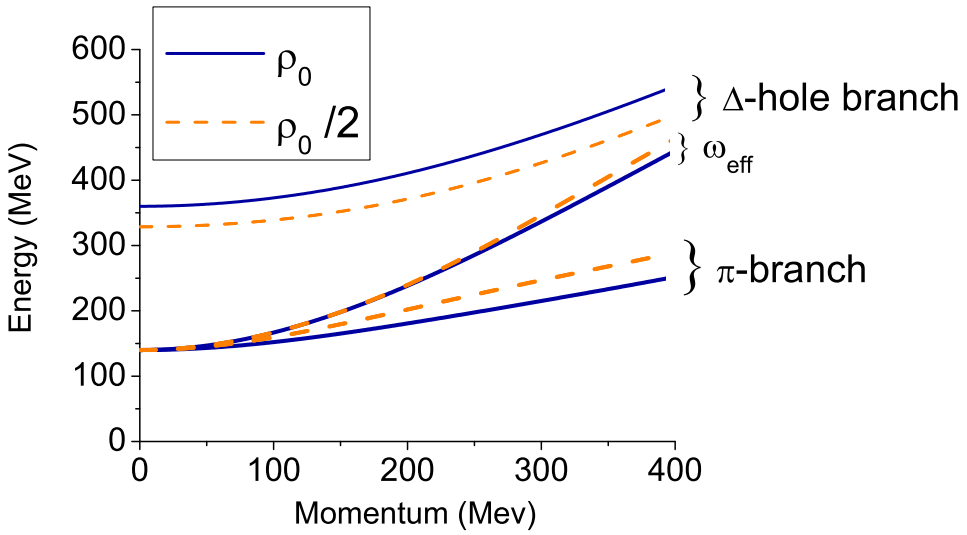

Figure 2.3: Dispersion relation for the two pion branches and the effective energy.

The dispersion relation for the free pion is identical to the dispersion relation of the pion branch at $\rho = 0$. And the dispersion relation of the free Δ-hole state corresponds to the Δ-branch at $\rho = 0$. Therefore one interprets strength of the pion in the Δ-hole branch as a pion which is fluctuating into a Δ-hole state.

At $\rho = 0$ the pion can not fluctuate into a Δ-hole state, equation (2.6) shows $Z_1 = 0$, $Z_2 = 1$ for all momenta. With increasing density the pion becomes a mixture of both states - it has strengths in both branches as can be seen in upper graph of figure 2.2. At momenta above 420 MeV at normal nuclear matter density the pion is most probably found in the Δ-hole branch.

In our semi-classical transport simulation we are propagating pions. We are actually not propagating the full spectral function of those pions, we are rather describing them as classical quasi particles in the nuclear medium with a well defined energy and lifetime. To describe the energy of those pions we can now define an effective pionic energy in the medium. This effective pionic energy is averaged over the spectral function by

$$\omega_{eff} = Z_1\omega_1 + Z_2\omega_2. \tag{2.7}$$

The effective energy can be found in figure 2.3. Now one can also define an optical potential for the pions by

$$\begin{aligned} \omega_{eff} &= \omega_{free} + V_{opt} \\ \Longrightarrow V_{opt} &= \omega_{eff} - \omega_{free} = \omega_{eff} - \sqrt{p^2 + m_\pi^2}. \end{aligned} \tag{2.8}$$

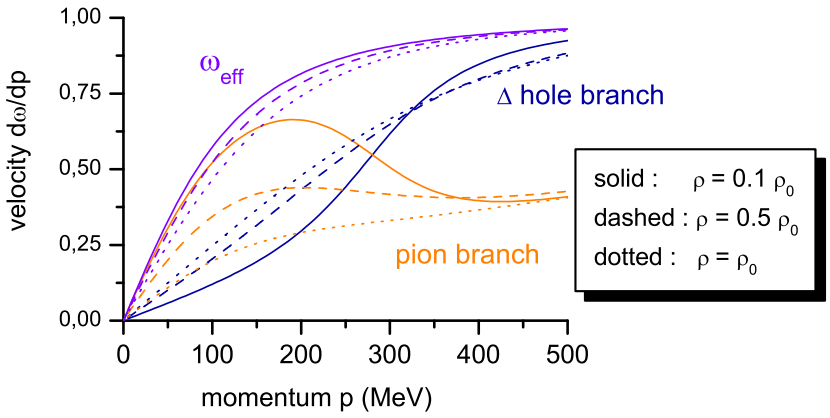

Figure 2.4: Specific velocities $\frac{d\omega}{dk}$ of the different pion branches.

The two pion branches show totally different behaviors concerning the specific velocities of the branches (see figure 2.4). Therefore it might be interesting to implement the full spectral function of the pion in the simulation and to use the dispersion relation of the branches to control the dynamics. Then one would use the interpretation of the Lehmann representation to propagate two distinct sorts of pions, each having its own mass and dynamics. This would be the unification of Ehehalt's and Larionov's ansatz. From the author's point of view the most severe problem of this ansatz might be, that one needs to redistribute the pionic testparticles according to their spectral function after each time step in a consistent way. The trivial fact

$$\frac{d\omega_{eff}}{dk} \neq Z_\pi \frac{d\omega_{\pi\ branch}}{dk} + Z_{\Delta-hole} \frac{d\omega_{\Delta-hole\ branch}}{dk}$$

is sometimes irritating, but this can be understood by the momentum dependence of the Z factors in $\omega_{eff} = Z_1\omega_1 + Z_2\omega_2$ which were used to average the energy over the spectral function. By averaging over the spectral function one seems to loose information on the dynamics of the distinct branches. This can be seen when comparing the velocities due to our ω_{eff} prescription to the 'real' velocities of the two branches in figure 2.4.

2.4 State-of-the-art low-energy calculation

J. Nieves and E. Oset presented in [NO93] a low energy optical potential for pions based on the Δ-hole model. They declare their potential to be valid up to kinetic pion energies around 60 MeV. This model includes besides first order diagrams as presented in appendix C also second order diagrams. On top of this they use

a Δ propagator, which has the Δ width included in the denominator:

$$G_\Delta(E,p) = \frac{1}{E - E_\Delta(p) + \frac{i}{2}\Gamma}.$$

For this reason their result has to be considered as a much more elaborate model than the simple picture of appendix C and we will use their results in the regime of $E_{kin} \leq 60MeV$. Due to the fact that at those low energies the Δ-branch is to be expected very weak, we only consider the pionic branch and approximate its dispersion relation by the vacuum solution. Details concerning those calculations and their implementations in the BUU simulation can be found in appendix D.

Chapter 3

The Optical Model

In the scattering of light off a diffractive and maybe also absorptive medium one constructs a potential for the electromagnetic waves which resembles this absorption and diffraction in the medium. This potential is called the 'optical potential'. The scattering of particles can also be described by such a method due to the duality of particles and waves.

The elastic scattering of pions off an atomic nucleus can be described by a pionic wavefunction being scattered off a potential $U(r)$, which has a far reaching Coulomb part and a short-range part due to strong nuclear forces.

This potential can be constructed by summing up all individual interactions of the numerous nucleons with the incoming pion. In analogy to the scattering of light it is well known in the literature as the optical potential.

When a pion is scattered off a nucleus, then there is on the one hand elastic scattering and on the other hand inelastic scattering. Inelastic processes include absorption processes and processes with energy loss of the incoming beam.

After a short introduction into the formalism of elastic scattering with Coulomb interaction we are going to describe inelastic scattering by complex potentials and their connection to the pion self energy.

3.1 Elastic scattering off a Coulomb potential

The stationary Schrödinger equation for the problem is

$$\left[-\frac{\hbar^2}{2\mu}\nabla^2 + U(r)\right]\Psi(\vec{r}) = E\Psi(\vec{r})$$

with

$$U(r) = \frac{Zq_\pi e^2}{r} \ .$$

A solution of this problem is[1]

$$\Psi(\vec{r})_{Coulomb} = \frac{1}{(2\pi)^{3/2}2kr}\sum_{l=0}^{\infty}(2l+1)i^l\left(H_l^-(k,r) + e^{2i\sigma_l}H_l^+(k,r)\right)P_l(cos(\theta))$$

with the Coulomb phase shifts

$$\sigma_l = Arg\left[\Gamma(l+1+i\gamma)\right]$$

and the irregular spherical Coulomb functions[2] $H_l^{\pm}$. The asymptotic behaviors of those functions are

$$\lim_{r\to\infty} H_l^{\pm}(r) = \mp ie^{\pm i\left(kr-\frac{l\pi}{2}-\gamma log(2kr)\right)}.$$

So one can see that the term proportional H_l^- is an incoming spherical wave, while the term proportional H_l^+ is an outgoing spherical wave for $r \to \infty$.

3.2 Short-range and Coulomb potential

3.2.1 Elastic Scattering

In the case that

$$U(r) = U_{\text{Coulomb}} + U_{\text{short-range}}$$

one knows that in the limit $r \to \infty$ the potential is dominated by the Coulomb term. Therefore the solution for $r \to \infty$ should be expressed in terms of the spherical Coulomb functions. One constructs

$$F_l(k,r) = \frac{1}{2}\left[H_l^+(k,r)e^{i\sigma_l} + H_l^-(k,r)e^{-i\sigma_l}\right] \tag{3.1}$$

$$G_l(k,r) = \frac{1}{2i}\left[H_l^+(k,r)e^{i\sigma_l} - H_l^-(k,r)e^{-i\sigma_l}\right] \tag{3.2}$$

and demands that the solution of the wave equation should be expressed as a linear combination of those two functions:

$$\lim_{r\to\infty}\Psi(\vec{r}) = \sum_{l=0}^{\infty}\xi_l(k,r)P_l(cos(\theta)) \tag{3.3}$$

with

$$\xi_l(k,r) = A_l\left[sin(\delta_l)F_l(r) + cos(\delta_l)G_l(r)\right].$$

[1] An extensive treatment of this topic can for example be found in [Joa75].

[2] details in [Mes76] Appendix B1

This can actually be recast as

$$\xi_l(k,r) = \widehat{A}_l \left(H_l^-(k,r) + e^{2i\Delta_l} H_l^+(k,r) \right)$$

with

$$\Delta_l = \sigma_l + \delta_l.$$

The full solution for the wavefunction in the asymptotic regime including the right normalization is given by

$$\begin{aligned} \lim_{r\to\infty} \Psi(\vec{r}) &= \frac{1}{(2\pi)^{-3/2} 2kr} \sum_{l=0}^{\infty} (2l+1) i^l \left(H_l^-(k,r) + e^{2i\Delta_l} H_l^+(k,r) \right) \\ &= \Psi(\vec{r})_{Coulomb} + \frac{1}{(2\pi)^{-3/2} 2kr} \sum_{l=0}^{\infty} (2l+1) i^l e^{2i\sigma_l} \left(e^{2i\delta_l} - 1 \right) H_l^+(k,r) \end{aligned}$$

which is a sum of the pure Coulomb wavefunction and a term which stems from the short-range potential. One can now rewrite the whole wavefunction as

$$\lim_{r\to\infty} \Psi(\vec{r}) = A \left(e^{ikz} + f(\theta) \frac{e^{ikr}}{r} \right) \tag{3.4}$$

to project on outgoing spherical waves and incoming plane waves. The scattering amplitude, which is associated with the outgoing spherical wave is given by

$$f(\theta) = f(\theta)_{\text{Coulomb}} + f(\theta)_{\text{short-range}}$$

with

$$\begin{aligned} f(\theta)_{\text{Coulomb}} &= -\gamma e^{2i\sigma_0} \frac{e^{-i\gamma log\left(sin^2(\theta/2)\right)}}{2ksin^2(\theta/2)} \\ f(\theta)_{\text{short-range}} &= \frac{1}{2ik} \sum_{l=0}^{\infty} (2l+1) e^{2i\sigma_l} \left(e^{2i\delta_l} - 1 \right) P_l\left(cos(\theta)\right). \end{aligned}$$

The phase δ_l is caused by the short-range potential. It is equal to zero in the case of a pure Coulomb potential.

Evaluating phase shifts

The problem can basically be divided into two regimes. One regime with $r < R_{max}$ is under influence of the nuclear and the Coulomb potential at the same time. For $r > R_{max}$ there is only the Coulomb potential and the solution is given by (3.3). In the case $r < R_{max}$ one normally has to solve the Schrödinger equation

numerically and match the result continuously to the solution of $r > R_{max}$ at R_{max}.

$$\begin{aligned} \Psi_{inside}(R_{max}) &= \Psi_{outside}(R_{max}) \\ \frac{\partial \Psi_{inside}(R_{max})}{\partial r} &= \frac{\partial \Psi_{outside}(R_{max})}{\partial r}. \end{aligned}$$

Defining the logarithmic derivative for each partial wave

$$\begin{aligned} \kappa_l &= \frac{\frac{\partial \xi_l^{inside}(R_{max})}{\partial r}}{\xi_l^{inside}(R_{max})} \\ &= \frac{\partial ln\left[\xi_l^{inside}(R_{max})\right]}{\partial r} = \frac{\partial ln\left[\xi_l^{outside}(R_{max})\right]}{\partial r} \\ &= \frac{\frac{\partial (sin(\delta_l)F_l(r)+cos(\delta_l)G_l(r))}{\partial r}}{sin(\delta_l)F_l(r)+cos(\delta_l)G_l(r)} \end{aligned}$$

one finally gets for the phase shifts

$$tan\delta_l = \frac{\frac{\partial F_l(k,r)}{\partial r} - \kappa_l F_l(k,r)}{\frac{\partial G_l(k,r)}{\partial r} - \kappa_l G_l(k,r)}. \tag{3.5}$$

The κ_l's are given by the numerical solution of the Schrödinger equation for $r < R_{max}$. The functions F_l and G_l are tabulated. Therefore δ_l can be calculated.

3.2.2 Inelastic scattering

Now we are dealing with processes which include energy loss and absorption due to the short-range potential. They lead to a reduction of the outgoing elastically scattered wave [3]. To model those processes one introduces a so-called optical potential, which is complex and destroys the hermitian nature of the Hamiltonian. The Hamiltonian is now given by

$$H(r) = T_{kin} + V(r) + iW(r)$$

with the real fields V(r) and W(r). This leads to a violation of the continuity equation by

$$\frac{\partial \rho(\vec{r},t)}{\partial t} + \nabla j = \frac{2}{\hbar}\rho(\vec{r},t)W(\vec{r})$$

with the probability density

$$\rho(\vec{r},t) = \psi^\star(\vec{r},t)\psi(\vec{r},t)$$

[3] for more details see [Mos]

of the elastic wave ψ and its probability current

$$j(\vec{r},t) = \frac{i\hbar}{2\mu}\nabla\left(\psi^{\star}(\vec{r},t)\psi(\vec{r},t)\right).$$

Assuming the scattering process to be stationary ($\frac{\partial\rho(\vec{r},t)}{\partial t} = 0$) one ends up with

$$\nabla j = \frac{2}{\hbar}\rho(\vec{r},t)W(\vec{r})$$

and one can interpret the term on the right-hand side as a sink or source of the elastic probability current. In the case of elastic scattering, the total flux through a given closed surface S is equal to zero. In this case the total flux

$$\oint_S \vec{j}d\vec{S} = \oint_S \left(j_{out} - j_{in}\right) dS = \frac{2}{\hbar}\int \rho(\vec{r},t)W(\vec{r})dV$$

is not equal to zero. Therefore the cross section for reaction - that means absorption, energy loss or energy gain - is given by

$$\begin{aligned}
\sigma_{reac} &= \frac{\text{absorbed particles of the elastic flux per time}}{\text{incoming flux}} \\
&= \frac{\oint_S \left(j_{in} - j_{out}\right) dS}{j_{in}} \\
&= -\frac{2}{\hbar v}\int \rho(\vec{r},t)W(\vec{r})dV
\end{aligned} \tag{3.6}$$

with v being the velocity of the incoming beam. Given the elastic wavefunction ψ one could evaluate the reaction cross section.

If the potential is not complex, then the equations for real and imaginary part of the wavefunction decouple and are identical. It is sufficient to match the real parts of the wavefunction at the boundary. The matching of the imaginary part is then fulfilled immediately.

If one introduces a complex potential, then one has to match both real and imaginary parts, because their differential equations do not decouple in the first place and are not identical. That means one has four equations on the boundary. Two equations are needed to fix the normalization and the other two are used to fulfill the boundary condition of the outgoing Coulomb wave functions. Allowing δ_l to be any complex number, one has now the two degrees of freedom to match the boundary conditions.

The technique is described in section 3.2.1. One only has to consider δ_l and κ_l to be complex in equation (3.5). By calculating the phase shifts one has full information about the elastic wavefunction and therefore one can calculate the elastic cross section and also the reaction cross section. However in the optical model it is not possible to split the reaction cross section up into a cross section for absorption and a cross section for energy loss/gain processes. Only the sum can be evaluated consistently. To do this splitting classical eikonal approximations are common, e.g. [NO93] [EW88].

3.3 The pion optical potential

After having discussed the effect of introducing a complex optical potential one now has to wonder how to calculate this potential for a pion in the first place. There are two different strategies:

1. Fit a potential to the scattering data and make predictions on binding energies and other observables

2. Evaluate the potential from many body field theoretical models (effective field theory) to describe scattering data.

Potentials of the first type are for example the Stricker, McManus & Carr potential [SMC79] or the newer version by L. J. Abu-Raddad [AR02]. By construction they describe very well scattering data. Actually we should be more interested in potentials of the second type which give deeper insight into the hadronic processes, which give rise to the scattering of pions and nucleons. Nevertheless phenomenological potentials of the first type are important benchmarks for potentials of the second type.

Potentials of the second type use effective field theory to derive the self energy of the incoming particle in the medium. An example for those potentials is given in appendix D. In the next section we will see the connection between the self energy and the optical potential.

3.3.1 Pion self energy and pionic optical potential

The self energy can be used to describe an optical potential. It can be calculated in the framework of effective field theories and we have shown in chapter 2 how to derive the pionic self energy. In the framework of [BW75] one defines

$$2\ E \times V_{opt}(E,k) = \Pi(E,k) \tag{3.7}$$

with energy E and self energy Π. Here V_{opt} defines the optical potential to use in the Schrödinger equation

$$\left(-\frac{\hbar^2}{2m}\nabla^2 + V_{opt}\right)\Psi = E\Psi.$$

In a relativistic ansatz one describes the pion by the Klein-Gordon equation which reads in vacuum

$$\left(p^2c^2 + m_\pi^2\right)\Psi = E^2\Psi$$

and is modified in the medium due to the strong nuclear potential and the electromagnetic forces. Therefore those influences are coupled minimally to the pion

$$\begin{aligned} E &\rightarrow E - V_C - V_{opt} \\ \vec{p} &\rightarrow \vec{p} - \frac{e}{c}\vec{A}\ . \end{aligned}$$

Here the electromagnetic interaction is represented by its four potential $(V_C, \vec{A})$ and the nuclear potential is assumed to have only a fourth component. Therefore one gets

$$\begin{aligned} E^2 &\rightarrow (E - V_C)^2 - V_{opt}^2 - 2(E - V_C)V_{opt} \\ &\simeq (E - V_C)^2 - 2E\ V_{opt} \end{aligned}$$

if one neglects $V_{opt}^2 + 2V_C V_{opt}$ due to the fact that those terms are small compared to $E \times V_{opt}$ in the limit $V_{opt} \ll E$. Assuming a purely electrostatic interaction one sets $\vec{A} = 0$. The result is

$$\begin{aligned} \left(p^2c^2 + m_\pi^2 + 2\ EV_{opt}\right)\Psi &= (E - V_C)^2\,\Psi \\ \Longleftrightarrow \left((-i\hbar c\nabla)^2 + m_\pi^2 + 2\ EV_{opt}\right)\Psi &= (E - V_C)^2\,\Psi. \end{aligned}$$

Finally in the last equation an additive mass term $(2\ E \times V_{opt})$ appears, which makes it plausible that $2\ E \times V_{opt} = \Pi$. In chapter 2 we have already seen that the self energy is an effective mass shift caused by the medium.

This Klein-Gordon equation can technically be solved like the static Schrödinger equation. It is also a second order differential equation in $\vec{r}$. So one uses the machinery explained in the previous sections of this chapter.

Part II

Transport Simulation

Chapter 4

Transport Theory

Transport processes are special cases of non-equilibrium processes. In classical statistical dynamics one describes such processes by the Boltzmann equation. Derivations of the Boltzmann equation can therefore be found in any standard textbook, e.g. [Fli99]. In the 1930's this equation was modified by Nordheim, Uehling and Uhlenbeck to incorporate also quantum mechanical effects of fermionic systems. The resulting equation is the so-called "Boltzmann-Uehling- Uhlenbeck equation" (BUU equation).

In the beginning 1980's BUU models started to replace the simpler Cascade models in heavy-ion collision simulations [BK84]. In the late 80's the theory group at the JLU Giessen started to use the BUU model to describe heavy-ion collisions and later on also photon induced processes. The present work is based upon the model version described in [Eff96] and [Eff99].

4.1 Vlasov equation

In [BG88] the authors give a historical overview concerning transport models. There they also derive the Vlasov equation as an approximation to time dependent Hartree-Fock theory (TDHF). The approximations which are done are the assumption of a local mean field potential and the assumption that this mean field and the distribution function of the considered particles vary slowly.

Classical derivation. To motivate the Vlasov equation we want to follow a classical derivation. The Vlasov equation is a transport equation for the one-particle distribution function $f_1(\vec{r}, \vec{p}, t)$ in phase space. It does not incorporate collisions between particles. In classical dynamics Liouville's theorem grants

$$\frac{df_1(\vec{r}, \vec{p}, t)}{dt} = 0$$

which states that the phase space density around a point which is moved according to the equations of motion remains constant. Now one can rewrite this statement

$$\frac{df_1}{dt} = \frac{\partial f_1(\vec{r},\vec{p},t)}{\partial t} + \sum_{i=1}^{3} \frac{\partial r_i}{\partial t}\frac{\partial f_1}{\partial r_i} + \frac{\partial p_i}{\partial t}\frac{\partial f_1}{\partial p_i} = 0.$$

Using classical Hamilton's equations

$$\begin{aligned} \frac{\partial r_i}{\partial t} &= \frac{\partial H}{\partial p_i} \\ \frac{\partial p_i}{\partial t} &= -\frac{\partial H}{\partial r_i} \end{aligned}$$

we end up with

$$\frac{\partial f_1(\vec{r},\vec{p},t)}{\partial t} + \sum_{i=1}^{3} \frac{\partial H}{\partial p_i}\frac{\partial f_1}{\partial r_i} - \frac{\partial H}{\partial r_i}\frac{\partial f_1}{\partial p_i} = 0.$$

This is also the final result for the quantum mechanical derivation starting from TDHF without collisions. An important consequence of the fact that the Vlasov equation respects Liouville's theorem, is that an initial state which is in agreement with Pauli blocking can never become a final state in disagreement with it. The reason for this is simply that the phase space density of a canonical moved point stays constant.

4.2 BUU equation

In the case of an ensemble of N identical particles, which interact among each other, the situation becomes more complicated. Here one has to consider the N-particle distribution function $f_N(\vec{r_1},\ldots,\vec{r_N},\vec{p_1},\ldots,\vec{p_N},t)$, which has all the information and correlations of the N different particle species encoded. The ansatz is

$$\frac{df_N}{dt} = I^N_{coll}(f_N).$$

The Bogoliubov-Born-Kirkwood-Green-Yvon (BBKGY) hierarchy connects the N-particle density with the one-particle density. An approximation to BBKGY is the ansatz

$$f_N(\vec{r_1},\ldots,\vec{r_N},\vec{p_1},\ldots,\vec{p_N},t) = \prod_{i=1}^{N} f_1(\vec{r_i},\vec{p_i},t).$$

With this ansatz one assumes that the N-particle distribution function factorizes into a product of one-particle distribution functions f_1 . This ansatz neglects all

correlations between the particles and is valid in the limit of a low density gas. The resulting equation for the one-particle distribution function is

$$\frac{\partial f_1(\vec{r},\vec{p},t)}{\partial t} + \frac{\partial H}{\partial \vec{p}}\frac{\partial f_1(\vec{r},\vec{p},t)}{\partial \vec{r}} - \frac{\partial H}{\partial \vec{r}}\frac{\partial f_1(\vec{r},\vec{p},t)}{\partial \vec{p}} = I_{coll}\left(f_1\left(\vec{r},\vec{p},t\right)\right) \tag{4.1}$$

with the one-body Hamilton function

$$H(\vec{r},\vec{p}) = \sqrt{\left(\vec{p}+\vec{A}(\vec{r},\vec{p})\right)^2 + m^2 + U(\vec{r},\vec{p})} + A^0(\vec{r},\vec{p}) \tag{4.2}$$

In this relativistic Hamiltonian $U(\vec{r},\vec{p})$ denotes a scalar potential and $A = (A^0, \vec{A})$ denotes a vector potential. The left-hand side of equation (4.1) is just the Vlasov equation. The term $I_{coll}\left(f_1\right)$ incorporates now all scattering processes of the particles.

4.2.1 The collision term

The collision term describes the possibility of scattering. The degeneracy due to internal degrees of freedom (spin, isospin, ...) of the considered particle species is g. Let us normalize the one-body distribution functions by

$$\int f_1(\vec{r},\vec{p})\frac{d^3p}{(2\pi)^3}\; d^3r = \frac{N}{g}.$$

This normalization is important for the f blocking in the following equations. Now we have

$$g\; f_1(\vec{r},\vec{p})\; \frac{d^3p\; d^3r}{(2\pi)^3} = \begin{array}{l}\text{Number of particles in phase space cell of size}\\ d^3p\; d^3r \text{ centered around } (\vec{r},\vec{p})\end{array} .$$

Considering only scattering processes with two particles in initial and final state, let us denote the initial particles by A,B and the final states by a,b.

$$A(\vec{p_A})\; B(\vec{p_B}) \longrightarrow a(\vec{p_a})\; b(\vec{p_b})$$

If such a scattering event occurs at point $\vec{r}$, then the phase space around $(\vec{r},\vec{p_A})$ and $(\vec{r},\vec{p_B})$ loses particle density while the phase space gains particle density in $(\vec{r},\vec{p_a})$ and $(\vec{r},\vec{p_b})$. Therefore we introduce for each phase space point a gain term due to particles which are scattered into this phase space point and a loss term due to particles which are scattered out of this phase space point.

$$\begin{aligned}&\frac{df_1(\vec{r},\vec{p_A},t)}{dt} =\\ &= \int \frac{d^3p_B}{(2\pi)^3}\;\frac{d^3p_a}{(2\pi)^3}\;\frac{d^3p_b}{(2\pi)^3}\end{aligned} \tag{4.3}$$

$$\begin{aligned}
&\underbrace{(W(p_a,p_b\rightarrow p_A,p_B)f_1(\vec{r},\vec{p_a},t)_1(\vec{r},\vec{p_b},t)(1\pm f_1(\vec{r},\vec{p}_A,t))(1\pm f_1(\vec{r},\vec{p_B},t))}_{\text{gain term}}\\
&\underbrace{-W(p_A,p_B\rightarrow p_a,p_b)f_1(\vec{r},\vec{p_A},t)\ f_1(\vec{r},\vec{p_B},t)(1\pm f_1(\vec{r},\vec{p_a},t))(1\pm f_1(\vec{r},\vec{p_b},t)))}_{\text{loss term}}\\
=\ & I_{coll}\left(f_1\left(\vec{r},\vec{p_A},t\right)\right).
\end{aligned}$$

Here we denote by $W(p_A,p_B\rightarrow p_a,p_b)$ the probability of a scattering

$$A(\vec{p_A})\ B(\vec{p_B})\longrightarrow a(\vec{p_a})\ b(\vec{p_b})$$

and by $W(p_a,p_b\rightarrow p_A,p_B)$ the probability of a scattering

$$a(\vec{p_a})\ b(\vec{p_b})\longrightarrow A(\vec{p_A})\ B(\vec{p_B}).$$

The terms $(1\pm f_1)$ implement Pauli blocking $(-)$ or Bose enhancement $(+)$ in the final states. This depends on the identity of the final state particles. Using the cross sections for the scattering events one can transform equation (4.3) into

$$\begin{aligned}
&\frac{df_1(\vec{r},\vec{p_A},t)}{dt}\\
=\ &\int d^3p_B\ d^3p_a\ d\Omega\left(\measuredangle\left[\vec{p}_a,\vec{p}_b\right]\right)\frac{d\sigma}{d\Omega\left(\measuredangle\left[\vec{p}_a,\vec{p}_b\right]\right)}\\
&(f_1(\vec{r},\vec{p_a},t)f_1(\vec{r},\vec{p_b},t)(1\pm f_1(\vec{r},\vec{p_A},t))(1\pm f_1(\vec{r},\vec{p_B},t))\\
&-f_1(\vec{r},\vec{p_A},t)\ f_1(\vec{r},\vec{p_B},t)(1\pm f_1(\vec{r},\vec{p_a},t))(1\pm f_1(\vec{r},\vec{p_b},t)))\\
=\ & I_{coll}\left(f_1\left(\vec{r},\vec{p_A},t\right)\right).
\end{aligned}\tag{4.4}$$

4.3 BUU with more than one particle species

In our simulation we consider not only nucleons, but also all sorts baryons and mesons. For each species of particles one gets a distinct transport equation. It is important to note that each species has a different Hamilton function $H(\vec{r},\vec{p})$ because the masses and potentials are different. The potentials of one species of particles can depend on another one. The pionic potential is for example a function of the density of nucleons, which itself is the integral in momentum space over the nucleon distribution function. Therefore the pionic distribution function is coupled to the distribution function of the nucleons already by its potential. This holds for several distinct distribution functions which are already coupled on the level of potentials.

On top all distribution functions are explicitly coupled via the collision term. In the last paragraph we allowed only for scattering where the identity of the particle does not change. But in the same spirit one can also set up a collision term, which includes all possible channels of scattering. This is the so-called coupled-channel method.

All together we obtain several integral-differential equations, all coupled explicitly by the collision term and implicitly by the potentials.

$$\begin{aligned}
\frac{df_1^{nucleon}(\vec{r},\vec{p},t)}{dt} &= I_{coll}\left(f_1^{nucleon}\left(\vec{r},\vec{p},t\right), f_1^{\Delta}\left(\vec{r},\vec{p},t\right), f_1^{\pi}\left(\vec{r},\vec{p},t\right), \ldots\right) \\
&\vdots \\
\frac{df_1^{\Delta}(\vec{r},\vec{p},t)}{dt} &= I_{coll}\left(f_1^{nucleon}\left(\vec{r},\vec{p},t\right), f_1^{\Delta}\left(\vec{r},\vec{p},t\right), f_1^{\pi}\left(\vec{r},\vec{p},t\right), \ldots\right) \\
&\vdots
\end{aligned}$$

Chapter 5

The BUU transport code

5.1 Overview

In the investigated energy range of this diploma thesis there are only those particles of interest, which are built out of up- and down quarks. But besides those particles the BUU code also includes strange and charmed particles. Details concerning all particles implemented in the code can be found in [Eff99].

For low energy problems the most important particles are the nucleon itself, the Δ and the light mesons. Their properties are summarized in table 5.1.

particle	M_0 in MeV	Γ_0 in MeV
N(938)	938	0
$P_{33}(1232)$	1232	118
$P_{11}(1440)$	1462	391
π	138	0
η	547	10^{-3}
ρ	770	151
σ	800	800

Table 5.1: Important particles and their mass and decay width on the resonance pole according to [MS$^+$92].

Due to the fact that strong decays occur on a much smaller time scale than electroweak decays, the electroweak decays are not implemented in the code. An exception is the short living η-meson which is allowed to decay into electroweak decay channels.

The parameters of the resonances in the code are based on an analysis done by Manley and Saleski [MS$^+$92] and the Particle Data Group for the strange and charmed particle sector.

There is no spin dependence in the code. All cross sections and results are spin averaged.

5.2 Numerical Implementation

The BUU equation is solved with a so-called test particle ansatz. Let us assume that there is a number of n particles of one species. Then the distribution function of this species is represented by $N \times n$ test particles and one defines

$$f_1 = \frac{(2\pi)^3}{g} \frac{1}{N} \sum_{i=1}^{n \times N} \delta(\vec{r} - \vec{r_i}) \; \delta(\vec{p} - \vec{p_i}) \tag{5.1}$$

with the $\vec{r_i}, \vec{p_i}$ denoting the momenta and positions of the test particles. In our simulation we are using the so-called "parallel ensemble method". Using N test particles per real particle we split all test particles up into N ensembles. Only members of the same ensemble are allowed to scatter. This corresponds to N reactions which occur at the same time. The densities, which are needed for the potentials, are calculated by averaging over all ensembles to eliminate big fluctuations. In the parallel ensemble method the test particles have exactly the same properties as the real particles. Therefore they scatter also like real particles. In the limit $N \to \infty$ this method simulates the flux of all distribution functions in phase space.

In contrast to the parallel ensemble method it is also possible to use a "full ensemble method". The full ensemble method does really split up one real particle into N test particles. Therefore each test particle carries only $\frac{1}{N}$ of the charge, mass, ... of the real particle. In [Eff99] both methods are compared. In γ induced reactions both methods gave the same results. In contrast to this the results of π-induced processes showed an influence on the choice of the method. But this problem should be solved due to a modification of the collision criterion which was highly non-local in the earlier versions of the code. For details concerning the modification see section 5.2.2. Nevertheless renewed investigations of this topic with the new collision criterion might be an interesting topic for the future.

5.2.1 The propagation

The differential equations of the transport equations are now split into two distinct pieces: The propagation and the collisions. The propagation is therefore done by solving Vlasov's equation where $I_{coll} = 0$. Inserting the test particle ansatz into the BUU equation with $I_{coll} = 0$ leads to the following equations of motion:

$$\begin{aligned} \frac{d\vec{r_i}}{dt} &= \frac{\partial H}{\partial \vec{p_i}} \\ \frac{d\vec{p_i}}{dt} &= -\frac{\partial H}{\partial \vec{r_i}} \; . \end{aligned}$$

These are just the classical Hamilton equations. For all test particles we use a predictor-corrector scheme to evaluate the time stepping of the test particles.

The gradients of the Hamiltonian are evaluated on a grid with finite difference discretization [Eff99].

5.2.2 The collisions

After having accounted for the Vlasov equation of a non-interacting gas, one also has to account for the collisions. Here we will describe collisions with less than three particles in the initial state which are the most important processes in the model. The channel $\pi\ N\ N \rightarrow N\ N$ will be described later on. We choose for simplification all angle distributions in the collisions to be isotropic.

Collision probability for $A\ B \rightarrow a\ b\ \ldots$

To decide whether two test particles A and B scatter or not we use the geometrical interpretation of the cross section. Defining the impact parameter by

$$b = dist(A, B)$$

we can write down our first criterion for scattering as

$$b \leq \sqrt{\frac{\sigma_{tot}}{\pi}}$$

with $\sigma_{tot} = \sigma(AB \rightarrow anything)$. On top of this criterion we define a cut off for the cross sections to account for shadowing effects inside the medium [Eff99]. The cut off is a maximal cross section σ_{max} which two particles can have. The maximal impact parameter follows by $b_{max} = \sqrt{\frac{\sigma_{max}}{\pi}}$. For the different initial states the following cut offs are used:

collision partners	b_{max}
nucleon,nucleon	1.32 fm
baryon,baryon	1.6 fm
baryon, meson	2.52 fm
meson, meson	2 fm .

All together the probability for a scattering event will be

$$p(b) = \Theta(b_{max} - b)\ \ \Theta\left(\sqrt{\frac{\sigma_{tot}}{\pi}} - b\right). \tag{5.2}$$

The actual time point for the scattering event is chosen by an algorithm proposed by Kodama et al. [Kod84]. After this the individual channel for the collision is chosen in a Monte Carlo decision. Here the individual probabilities are proportional to the cross sections of each individual channel:

$$p_{AB \rightarrow X} = \frac{\sigma(AB \rightarrow X)}{\sigma_{tot}}.$$

Having chosen the individual channel one also determines the final state momenta by Monte Carlo decisions.

The old version of the collision probability. In previous versions of the BUU simulation [Eff99] the collision probability was defined to be

$$p(b) = \Theta(b_{max} - b)\ \min\left(\frac{\sigma_{tot}}{\pi b_{max}^2}, 1\right). \tag{5.3}$$

This equation allows particles to scatter whose distance is actually bigger than $\sqrt{\frac{\sigma_{tot}}{\pi}}$ which is not allowed anymore by the new probability defined in equation (5.2). Therefore the old prescription was less local than the new one. Besides this fact there is also another problem with the old collision probability. Let us consider a fixed target experiment with a single particle as a target. Then the rate R of reaction events will be given by

$$R = \int \Phi(b)\ p(b)\ 2\pi\ b\ db$$

with the incoming flux of particles $\Phi(b)$ and the probability $p(b)$ to interact with such a particle which has impact parameter b. Both collision probabilities should yield the same rate of reactions. Therefore follows

$$\begin{aligned} &\int \Phi(b)\ \Theta(b_{max} - b)\ \min\left(\frac{\sigma_{tot}}{\pi b_{max}^2}, 1\right) 2\pi\ b\ db \\ \stackrel{!}{=} &\int \Phi(b)\ \Theta(b_{max} - b)\ \ \Theta\left(\sqrt{\frac{\sigma_{tot}}{\pi}} - b\right) 2\pi\ b\ db \end{aligned}$$

Now let us suppose $\sigma_{tot} < \pi b_{max}^2$

$$\int_0^{b_{max}} \Phi(b) \frac{\sigma_{tot}}{\pi b_{max}^2}\ b\ db \stackrel{!}{=} \int_0^{\sqrt{\frac{\sigma_{tot}}{\pi}}} \Phi(b)\ b\ db \tag{5.4}$$

and consider two different cases:

- Suppose the flux is homogeneous $\Phi(b) = const.$ Here both integrals of equation (5.4) give the same result and the equation (5.4) is true. Therefore both collision probabilities yield the same result as long as the flux is homogeneous.

- Now suppose the flux is inhomogeneous. Then the left hand side and the right hand side of equation (5.4) have different results in the general case and the equation is wrong. Therefore the two different collision probabilities yield different results on reaction rates, which means that one of them must be faulty. Since the new collision criterion satisfies the intuitive interpretation of a cross section, the old one must have been less accurate.

Decay probability for $R \rightarrow a\ b\ \ldots$

For resonance decays one defines

$$p(b) = 1 - e^{-\frac{\Gamma}{\gamma}\Delta t}$$

as decay probability. Δt is the time step size in the calculation frame, Γ is the decay width in the rest frame of the resonance and γ is the Lorentz factor to go from the calculation frame to the rest frame of the decaying resonance.

Pauli blocking

For the nucleons in the final states we check for Pauli blocking. Because all other distribution functions are expected to be rather small, one neglects Pauli blocking or Bose enhancement for the other final state particle species.

If one of the final state particles is Pauli blocked then the whole collision is dismissed. In low-energy photon- and pion-induced reactions one expects the nucleus to remain close to its ground state. Therefore it is not necessary to define a dynamical Pauli blocking probability based on the actual test-particle densities. Rather one defines

$$p_{\text{Pauli blocking}} = \theta(p - p_{fermi}(\rho(r)))$$

to decide on Pauli blocking for each final state. Here is no Monte Carlo decision necessary. A dynamical description of Pauli blocking is described in [Eff99].

Potentials in the collisions

For a collision with N particles in the initial state we define [Eff99] [Ehe92]

$$\sqrt{s_{free}} = \sum_{i=1}^{N} \sqrt{m_i^2 + \vec{p}_i^{\,cm\ 2}}$$

with the center of mass momenta $\vec{p}_i^{\,cm}$. All cross sections for the decision on the collisions are evaluated at the point $s = s_{free}$. This prescription is a tribute to the fact that the experimental cross sections, which serve as an input to the simulation, are elementary cross sections measured in the vacuum. Then we determine in a Monte-Carlo decision the outgoing momenta $\vec{p}_i{}'^{\,cm}$ in the CM-frame, such that $\sqrt{s_{free}}$ is conserved. Here we choose $\sqrt{s_{free}}$ to be conserved, because it is easier to perform the Monte-Carlo decision for the momenta without having to account for the momentum-dependend potentials. In the next step we now need to be concerned how to conserve $\sqrt{s}$.

To conserve energy in the collision it is also necessary to account for the potentials of the particles which are defined in the local rest frame [1]. Therefore

[1] Frame where the total flux of nucleons is zero.

we need to look at the real $\sqrt{s}$ in the local rest frame[2]:

$$\sqrt{s} = \sqrt{\left(\sum_{i=1}^{N} E_i^{lrf}\right)^2 - \left(\sum_{i=1}^{N} p_i^{lrf}\right)^2}$$

with

$$E_i^{lrf} = \sqrt{m_i^2 + \vec{p}_i^{\,lrf\ 2}} + V_i\left(\vec{r}, \vec{p}_i^{\,lrf}\right).$$

We now demand that $\sqrt{s}$ is conserved in the scattering process. This is achieved by rescaling all center of mass momenta after the collision with the same parameter x such that $\sqrt{s}$ is conserved:

$$\vec{p}_i'^{\ cm} \rightarrow x\ \vec{p}_i'^{\ cm} \text{for all i.}$$

Momentum conservation is guaranteed, since all momenta are rescaled with the same parameter in the CM-frame. Summarizing the algorithm:

1. Evaluate $\sqrt{s}$ of the initial state in the local rest frame.
2. Boost all particles to CM-frame.
3. Evaluate $\sqrt{s_{free}}$ and determine cross section at $\sqrt{s} = \sqrt{s_{free}}$.
4. Decide on final state momenta by a Monte-Carlo decision such that $\sqrt{s_{free}}$ is conserved in CM-frame.
5. Boost all particles back to local rest frame.
6. Evaluate $\sqrt{s}$ of the final state in local rest frame.
7. Scale final state momenta in CM-frame such that $\sqrt{s}$ is conserved.

With this algorithm we achieve full energy and momentum conservation in the scattering process and take into account that we are using vacuum data as input.

5.3 Hadronic potentials in the simulation

In high energy transport simulations it is often not necessary to implement any mesonic or electromagnetic potential. These potentials are often much less energetic than the general energy scale. In the case of low-energetic pion absorption and γ-induced 2π production with γ-energies between 400 and 460 MeV, this is clearly not the case.

[2]The potentials are only well defined in the local rest frame.

For technical reasons we define in the simulation for all particles a potential V such that

$$\sqrt{\vec{p}^2 + m^2} + V(\vec{p}, \vec{r}) = \sqrt{\left(\vec{p} + \vec{A}(\vec{r}, \vec{p})\right)^2 + m^2 + U(\vec{r}, \vec{p})} + A^0(\vec{r}, \vec{p})$$

where the right-hand-side is the general one-body Hamiltonian of equation (4.2). Let us now investigate the vector and scalar potentials U, A we want to consider in our simulation.

5.3.1 The nucleon potential

The potential is a mean field potential suggested by Welke et al. [WPK+88]. One defines a local rest frame by demanding the vanishing of the total flux of nuclear matter in this frame. In our case this is normally the laboratory frame since we are investigating nuclei in their groundstate resting in the laboratory. Even if those nuclei are hit by a photon or pion, they will not be accelerated in a sizeable manner. Therefore the local rest frame is always nearly identical with the laboratory frame. The potential in the local rest frame is defined to be

$$W(\vec{r}, \vec{p}) = A\ \frac{\rho(\vec{r})}{\rho_0} + B\ \left(\frac{\rho(\vec{r})}{\rho_0}\right)^{\tau} + \frac{2\ C\ g}{\rho_0} \int \frac{d^3p'}{(2\pi)^3} \frac{f(\vec{r}, \vec{p}')}{1 + \left(\frac{\vec{p} - \vec{p}'}{\Lambda}\right)^2}$$

The calculations in this thesis are all done with the so-called "medium momentum dependent" parameter set of [Eff99]. The potential defined above is inserted into the Hamiltonian as the zeroth component of a vector potential [Eff99], hence $V_{nucleon} = W$.

5.3.2 The Δ-potential

Phenomenology tells us that Δ potential has to be $-30\ MeV$ deep at ρ_0 [EW88] (pages 248-249). Comparing to a momentum independent nucleon potential, which is roughly 50 MeV strong, the Δ-potential is therefore assumed to be

$$V_\Delta = \frac{2}{3}\ V_{nucleon}. \tag{5.5}$$

Consequently the Δ potential has the same shape as the nucleon potential, but is scaled to match the phenomenologic value at ρ_0.

5.3.3 The pion potential

For the pion potential we will use a low-energy potential according to Oset et al. [NO93] which is declared valid up to 60 MeV kinetic energy. But we also

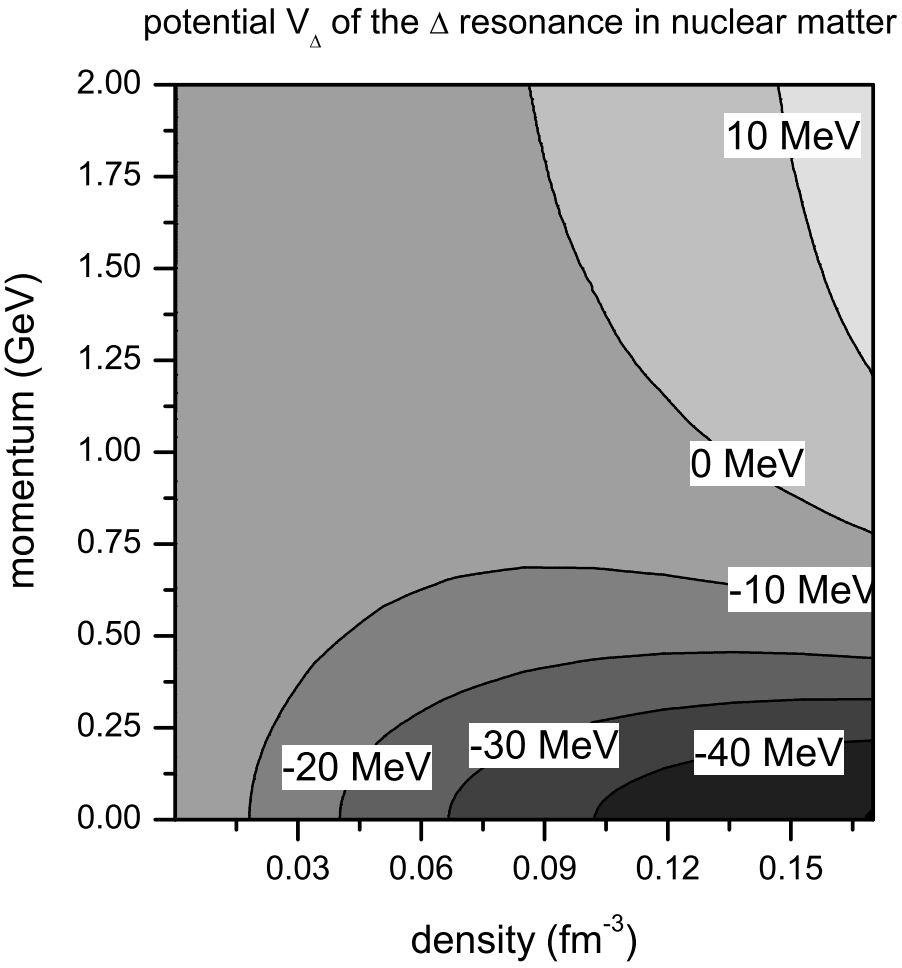

Figure 5.1: Potential of the Δ-resonance.

want to describe more energetic pions. Therefore we exploit for higher energies the results of the simple Δ-hole model derived in section 2.3. But we have to demand that the potential for the pion is differentiable according to momentum at the point where we match the high-energy to the low-energy prescription - otherwise the velocity $v = \frac{\partial H}{\partial p}$ would be discontinuous.

Low energies.

In the low energy regime of $p_\pi \leq 80\ MeV$ the results by Oset et al. are exploited (details in appendix D). Oset et al. are deriving with field theoretical means a self energy Π for the pion, which can be rewritten as $\Pi(\omega, \vec{p}) = 2\omega\ V_{Oset}(\omega, \vec{p})$. With this self energy the energy of the pion is obtained by

$$\omega = \sqrt{m^2 + p^2 + \Re\left(\Pi(\omega, \vec{p})\right)} = \sqrt{m^2 + p^2 + \Re\left(2\omega\ V_{Oset}(\omega, \vec{p})\right)} \tag{5.6}$$

introducing the self energy as a scalar potential. We do not solve the dispersion relation of equation (5.6) because this would cause large numerical cost since we need the dispersion relation at a larger number of grid points in phase space to evaluate the derivatives of $\omega(p)$ in a sensible manner.

Rather we remind ourselves that at very low energies in the simple Δ-hole model the pion is most probably found in the pion branch according to the upper graph of figure 2.2, and according to the lower graph of the same figure the dispersion relation for the π-branch does not differ much compared to the free dispersion of the π-branch for $p_\pi \leq 100\ MeV$. Therefore we assume in a first step for the dispersion relation at low energies the vacuum approximation of the π-branch, which is just the dispersion relation of a free pion:

$$\omega^2 = p^2 + m^2.$$

Now we insert this rough approximation into the right-hand-side of equation (5.6) to gain a reliable result for ω :

$$\begin{aligned} \omega(p) &= \sqrt{m^2 + p^2 + \Re\left(\Pi(\sqrt{p^2 + m^2}, \vec{p})\right)} \\ &= \sqrt{m^2 + p^2 + \Re\left(2\sqrt{p^2 + m^2}\ V_{Oset}(\sqrt{p^2 + m^2}, \vec{p})\right)}\ . \end{aligned} \tag{5.7}$$

High energies.

For higher energies we use the dispersion relation derived in equation (2.7):

$$\omega(p) = \omega_{eff} = Z_1\omega_1 + Z_2\omega_2 \tag{5.8}$$

Medium energies.

Now we define for technical reasons the hadronic potential V_π for the pion such that

$$\omega(p) = \sqrt{p^2 + m^2} + V_\pi(p) \; .$$

Using the results for $\omega(p)$ of equations (5.7) and (5.8) we get a well defined potential in both the high energy regime

$$V_{high} = \omega_{eff} - \sqrt{p^2 + m^2}$$

and the low energy regime

$$V_{low} = \sqrt{m^2 + p^2 + \Re\left(2\sqrt{p^2+m^2}\; V_{Oset}(\sqrt{p^2+m^2}, \vec{p})\right)} - \sqrt{p^2+m^2} \; .$$

But it would be discontinuous at $p = 80\ MeV$ which is our upper limit for the low-energy regime.

Therefore we now match both potentials in the regime of $80\ MeV \leq p \leq 140\ MeV$ by a interpolating spline to gain a continuous derivative and therefore a continuous velocity of the pion. We demand that the first derivative of the potential should be continuous at the boundaries of this interval. Using a spline ansatz with

$$V_{matching}(\vec{r}, \vec{p}) = a(\vec{r})\; x^3 + b(\vec{r})\; x^2 + c(\vec{r})\; x + d \text{ with } x = |\vec{p}| - 80\ MeV$$

we demand therefore

$$\begin{aligned}
V_{matching} \quad (|\vec{p}| = 80\ MeV, \vec{r}) &= V_{low}\ (|\vec{p}| = 80\ MeV, \vec{r}) \\
V_{matching} \quad (|\vec{p}| = 140\ MeV, \vec{r}) &= V_{high}\ (|\vec{p}| = 140\ MeV, \vec{r}) \\
\frac{\partial}{\partial p} V_{matching} \quad (|\vec{p}| = 80\ MeV, \vec{r}) &= \frac{\partial}{\partial p} V_{low}\ (|\vec{p}| = 80\ MeV, \vec{r}) \\
\frac{\partial}{\partial p} V_{matching} \quad (|\vec{p}| = 140\ MeV, \vec{r}) &= \frac{\partial}{\partial p} V_{high}\ (|\vec{p}| = 140\ MeV, \vec{r})
\end{aligned}$$

This is solved by

$$\begin{aligned}
a(\vec{r}) &= -\frac{2(V_{high}(p_2, \vec{r}) - V_{low}(p_1, \vec{r})) - \Delta \frac{\partial}{\partial p}\left(V_{high}(p_2, \vec{r}) + V_{low}(p_1, \vec{r})\right)}{\Delta^3} \\
b(\vec{r}) &= \frac{3\Delta(V_{high}(p_2, \vec{r}) - V_{low}(p_1, \vec{r})) - \Delta^2 \frac{\partial}{\partial p}\left(V_{high}(p_2, \vec{r}) - 2V_{low}(p_1, \vec{r})\right)}{\Delta^3} \\
c(\vec{r}) &= \frac{\partial}{\partial p} V_{low}(p_1, \vec{r}) \\
d(\vec{r}) &= V_{low}(p_1, \vec{r})
\end{aligned}$$

with $p_1 = 80\ MeV$, $p_2 = 140\ MeV$ and $\Delta = p_2 - p_1 = 60\ MeV$.

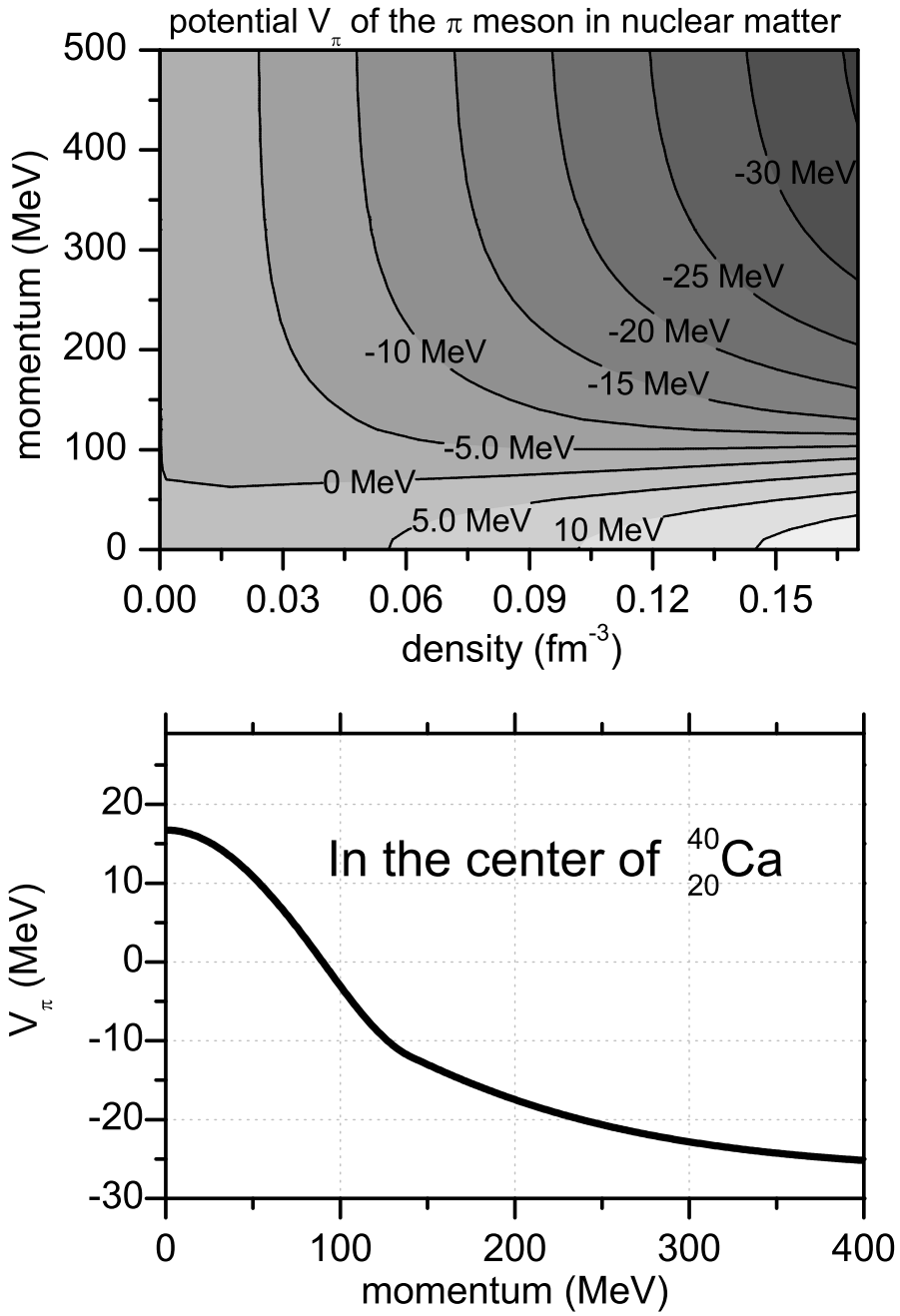

Figure 5.2: Hadronic potential for the pion. The upper plot shows the overall shape of the potential dependent on momentum and density. In the lower plot we see the strength of the potential in the center of a $^{40}_{20}Ca$ nucleus.

Definition of the potential. Summarizing, we define

$$\begin{aligned} V_\pi(\vec{p}) &= \Theta\left(80\ MeV - |\vec{p}|\right) V_{low}(\vec{p}) \\ &\quad + \Theta\left(140\ MeV - |\vec{p}|\right) \Theta\left(|\vec{p}| - 80\ MeV\right) V_{Matching} \\ &\quad + \Theta\left(|\vec{p}| - 140\ MeV\right) V_{high}(\vec{p}) \end{aligned} \tag{5.9}$$

and now the Hamiltonian for the pion is well defined

$$H = \sqrt{p^2 + m_\pi^2} + V_\pi \ .$$

The potential for the pion is shown in figure 5.2. It is repulsive for nearly all densities and all momenta below 100 MeV. For higher momenta it turns attractive. The repulsion is caused by a nearly momentum independent s-wave term, while the attraction is caused by the momentum dependent p-wave term. The p-wave term vanishes at zero momentum and gains strength with increasing momentum. At constant density the potential is therefore continously decreasing with momentum.

Latest experimental results.

In latest experiments at GSI concerning $^{208}Pb(d,^3He)$ reactions [G$^+$02] and at MAMI observing $^3He(e,e'\pi^+)^3H$ reactions [K$^+$01] new results on the pionic self energy at threshold were obtained. The results hint at a value of about $V_\pi(p = 0) \simeq 25\ MeV$. The potential by Oset et al. amounts to some lower values of about 18 MeV in symmetric nuclear matter at normal matter density (see figure D.1). But one has to consider also large experimental uncertainties. Results at low densities and finite momenta need to be extrapolated to higher densities and zero momentum. The result by Oset et al. [NO93] is therefore still our model of choice at low energies. But one should be aware of the fact that a larger potential at threshold seems to be favored by experiment.

5.4 The Coulomb potential

The Coulomb potential was introduced in the BUU simulation in a fully relativistic manner [Tei96]. To save computation time it is useful at low energies to use just the static Coulomb term.

$$V_{Coulomb}(\vec{r}) = \frac{1}{4\pi\epsilon_0} \int \frac{\rho(\vec{r}\,')}{|\vec{r} - \vec{r}\,'|} d^3r'$$

5.5 Cross sections

The cross sections of the BUU simulation are described in [Eff99] and [Leh03]. The most important channels at low energies are

$$N\ N \ \rightarrow \ N\ N$$

$$
\begin{aligned}
N\ N\ \pi &\leftrightarrow N\ N \\
N\ N &\leftrightarrow N\ Resonance \\
N\ N &\leftrightarrow \Delta\ \Delta \\
N\ Resonance_A &\leftrightarrow N\ Resonance_B \\
Meson\ Baryon &\leftrightarrow Resonance \\
\pi\ N &\leftrightarrow \pi\ N \\
\pi\ N &\rightarrow \pi\ \pi\ N \\
\pi\ N &\leftrightarrow \eta\ N
\end{aligned}
$$

Many additional reaction channels are described in the mentioned references. Here we want to concentrate on the improvements which became necessary to describe also low energy pion scattering. The improved channels are on the one hand the channel $\pi\ N \leftrightarrow \pi\ N$ and on the other hand the channel $N\ N\ \pi \leftrightarrow N\ N$, the latter being the most important for pion absorption at low energies.

We describe the absorption of the pion by explicit collisions of the pion with either one or two nucleons. Especially, we do not implement the imaginary part of the self energy to define a absorption rate for the pion.

A pion hitting a nucleon can produce an intermediate Δ resonance state. This Δ resonance experiences medium-modifications in our simulation. In section 5.3.2 we defined already a potential which modifies the dynamics of the Δ resonance. On top we consider a modification of its lifetime. Martin Effenberger introduced in [Eff99] a spreading potential exploiting results of Oset and Salcedo [OS87]. Their spreading potential accounts for in-medium decay channels for the Δ, e.g. $N\Delta \rightarrow NN$. These decay channels lead to a modified lifetime compared to the lifetime based solely on the vacuum $\Delta \rightarrow N\pi$ processes. As a standard we are implementing this spreading potential [3].

5.5.1 Quasielastic $\pi\ N \rightarrow \pi\ N$ scattering

In the region around the Δ resonance the cross section for $\pi\ N \rightarrow \pi\ N$ scattering is well described by Δ formation and decay. The process is then described by $\pi\ N \rightarrow \Delta \rightarrow \pi\ N$. But this is not a good description of the data in the low energy tail regions of the Δ.

All different events in pion nucleon scattering can now be categorized into four channels:

$$
\begin{aligned}
C_1 &= \sigma_{\pi^-\ n\rightarrow\pi^-\ n} = \sigma_{\pi^+\ p\rightarrow\pi^+\ p} \\
C_2 &= \sigma_{\pi^-\ p\rightarrow\pi^0\ n} = \sigma_{\pi^0\ n\rightarrow\pi^-\ p} = \sigma_{\pi^+\ n\rightarrow\pi^0\ p} = \sigma_{\pi^0\ p\rightarrow\pi^+\ n} \\
C_3 &= \sigma_{\pi^-\ p\rightarrow\pi^-\ p} = \sigma_{\pi^+\ n\rightarrow\pi^+\ n}
\end{aligned}
$$

[3] Details in [Eff99] pages 248-249.

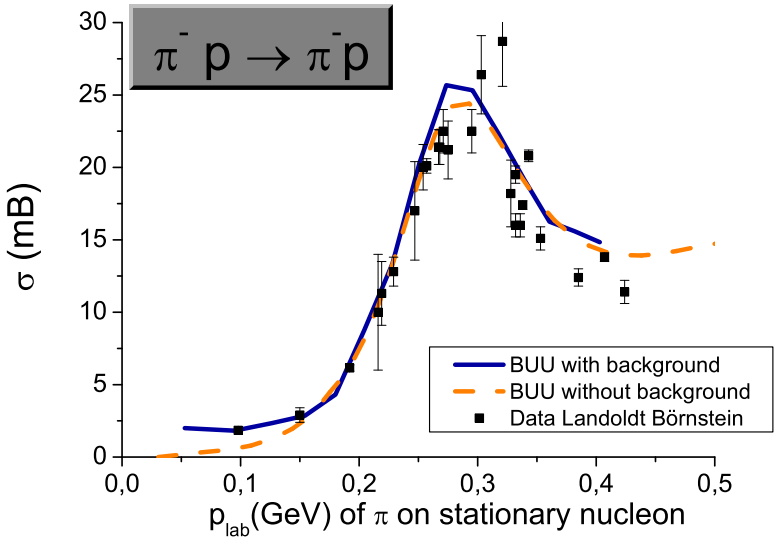

Figure 5.3: Elastic background. The data are taken out of [LB88].

$$C_4 \quad = \quad \sigma_{\pi^0\ n\to\pi^0\ n} = \sigma_{\pi^0\ p\to\pi^0\ p}.$$

The cross sections in the individual cross sections are either connected by time reversal or isospin symmetry. The pion and nucleon scatter either through an Isospin $I = \frac{3}{2}$ or $I = \frac{1}{2}$ state.

$$\begin{array}{ccc} & \nearrow\ I = 3/2\ \searrow & \\ \pi\ N & & \pi\ N \\ & \searrow\ I = 1/2\ \nearrow & \end{array}$$

Channel 1 is a full $I = \frac{3}{2}$ scattering process. The other three channels are mixtures of both channels. The cross section for $\sigma_{\pi\ N\to\Delta\to\pi\ N}$ is given explicitly in [Eff99]. This channel represents the P_{33} amplitude of pion nucleon scattering according to Manley and Saleski [MS+92]. As expected, channel 1 is well described solely by a Δ-resonance-scattering amplitude in the $I = \frac{3}{2}$ channel, therefore we neglect a background term in this channel. In channels 2 and 3 there are good data sets for

$$\pi^- p \to \pi^-\ p$$
$$\pi^- p \to \pi^0\ n.$$

We are using a background term to describe those channels in a better way:

$$\sigma_{\text{background}} = \sigma_{\text{data fit}} - \sigma_{\Delta}\ .$$

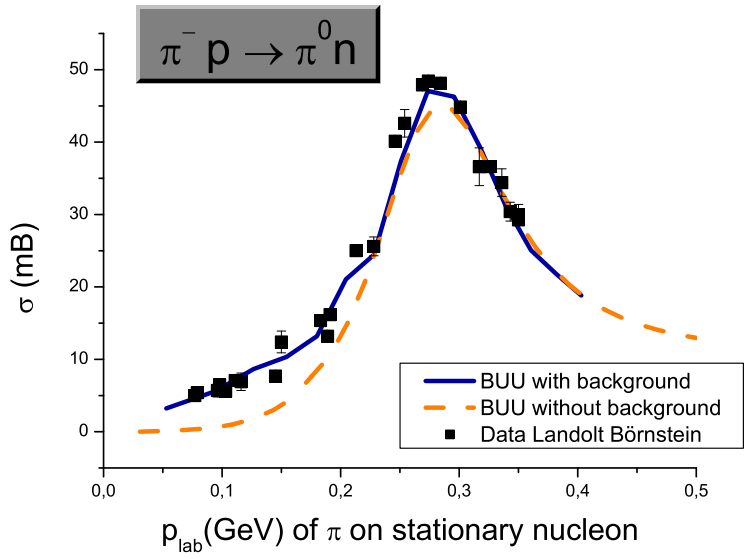

Figure 5.4: Charge exchange background. The data are taken out of [LB88].

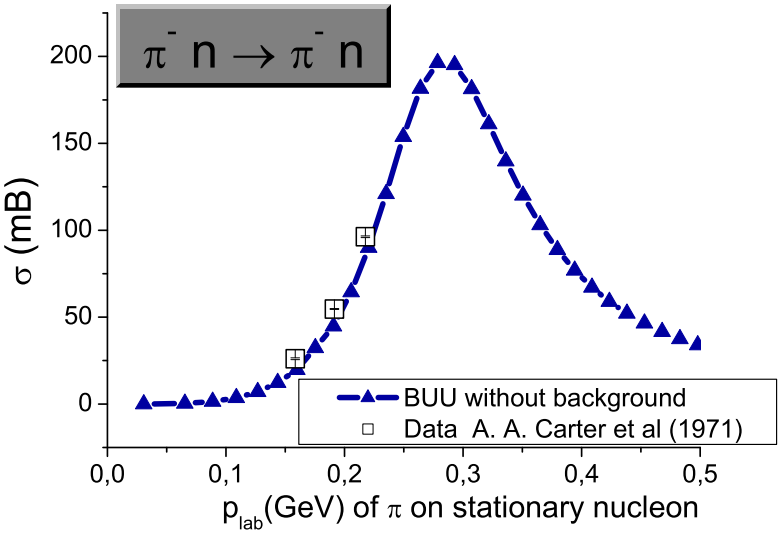

Figure 5.5: Channel 1 with Isospin $I = \frac{3}{2}$. The data are taken out of [CWB$^+$71]

The influence of the background is shown in figures 5.3 and 5.4. Channel 4 is completely inaccessible for experiment. Therefore we can not introduce any background term and we have to admit uncertainties in this channel.

5.5.2 The process $N\ N \to N\ N\ \pi$

Already in [Eff96] a background for the process $N\ N \to N\ N\ \pi$ was presented. This background cross section is defined to be

$$\sigma^{bg}_{N\ N \to N\ N\ \pi} = \sigma^{data}_{N\ N \to N\ N\ \pi} - \sigma^{resonance\ contribution}_{N\ N \to N\ N\ \pi} \ . \tag{5.10}$$

In this process we have the following four different channels

$$\begin{aligned} p\ p &\to p\ p\ \pi^0 \\ p\ p &\to p\ n\ \pi^+ \\ p\ n &\to p\ p\ \pi^- \\ p\ n &\to p\ n\ \pi^0 \ . \end{aligned}$$

All other processes are related to these channels by charge conjugation. Refinements to the work of [Eff96] became necessary because the earlier work concentrated on higher energies, therefore missing some strengths in the fit of the low energy regime. The older work was also done before newer data points were published. A comparison of the old and new fit prescriptions can be found in figures 5.6, 5.7, 5.8 and 5.9.

5.5.3 The process $N\ N\ \pi \to N\ N$

Following the same path as [Eff96] (section 3.4) we use detailed balance to derive the cross sections for the $N\ N\ \pi \to N\ N$ background out of the $N\ N \to N\ N\ \pi$ background. The cross section for $N\ N \to N\ N\ \pi$ is given by

$$\begin{aligned} & \sigma_{N_a\ N_b \to N_A\ N_B\ \pi} \\ = \ & S_{AB} \int \frac{(2\pi)^4}{4 p_{ab} \sqrt{s}}\ \delta^4 \left(p_a + p_b - p_A - p_B - p_\pi\right) \\ & |M_{N_a\ N_b \to N_A\ N_B\ \pi}|^2 \frac{d^3 p_A}{(2\pi)^3\ 2\ E_A}\ \frac{d^3 p_B}{(2\pi)^3\ 2\ E_B}\ \frac{d^3 p_\pi}{(2\pi)^3\ 2\ E_\pi} \\ = \ & S_{AB} \frac{1}{(2\pi)^3 64 p_{ab} \sqrt{s^3}}\ |M(\sqrt{s})_{\ N_a\ N_b \to N_A\ N_B\ \pi}|^2 \int dm^2_{AB} dm^2_{A\pi} \end{aligned} \tag{5.11}$$

with

$$m^2_{xy} = (p_x + p_y)^2$$

and

$$S_{AB} = \begin{cases} \frac{1}{2} & \text{if particles A and B are identical} \\ 1 & \text{otherwise} \end{cases}$$

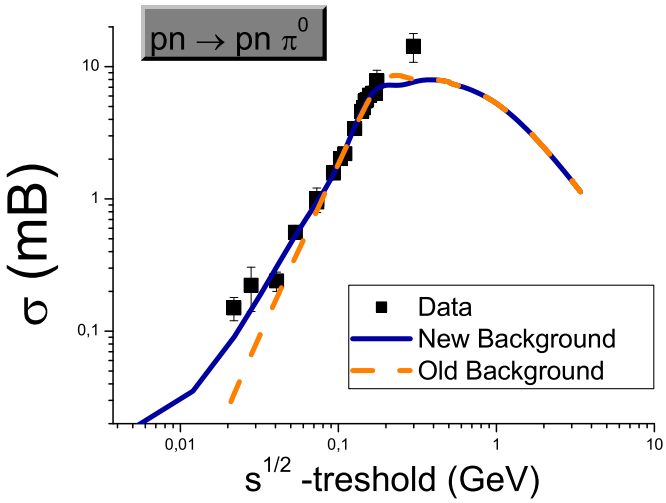

Figure 5.6: New background for $p\ n \leftrightarrow p\ n\ \pi^0$. The data are taken out of [LB88].

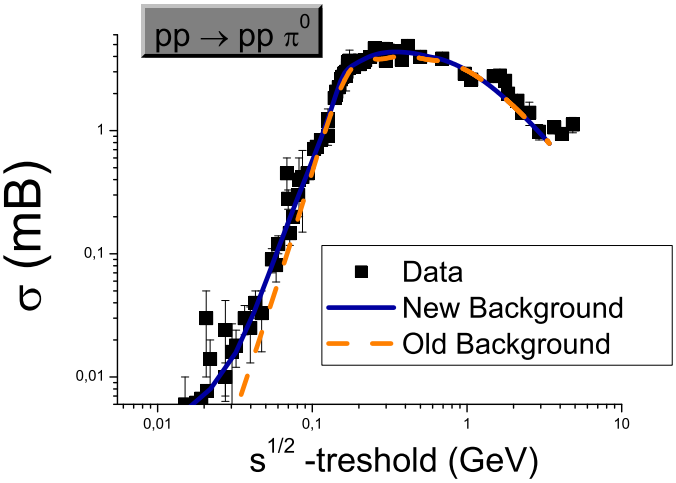

Figure 5.7: New background for $N\ N \leftrightarrow p\ p\ \pi^0$. The data are taken out of [LB88],[B$^+$95],[M$^+$92],[S$^+$82] and [A$^+$88].

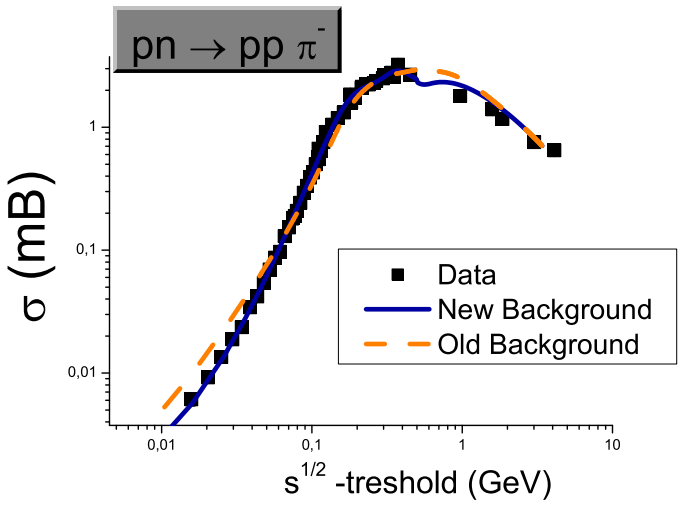

Figure 5.8: New background for $p\ n \leftrightarrow p\ p\ \pi^-$. The data are taken out of [LB88],[D$^+$01] and [T$^+$88].

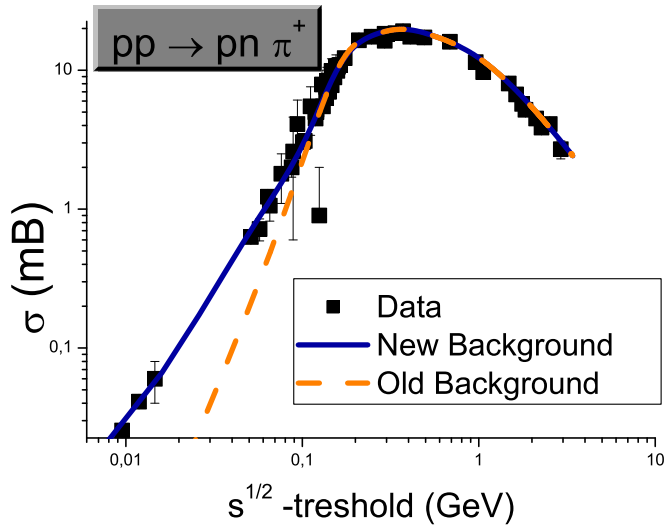

Figure 5.9: New background for $p\ p \leftrightarrow p\ n\ \pi^+$. The data are taken out of [LB88],[H$^+$95] and [S$^+$82].

as symmetry factor. The momentum p_{ab} denotes the momentum of the particles a and b in their center of mass frame. Equation (5.11) holds under the assumption that the matrix element is independent of the outgoing momenta. Demanding detailed balance we get

$$|M| = |M_{\ N_a\ N_b \to N_A\ N_B\ \pi}| = |M_{N_A\ N_B\ \pi \to N_a\ N_b}|$$

Therefore one can define a pion absorption rate

$$\Gamma_{N_A\ N_B\ \pi \to N_a\ N_b} = S_{ab} S_{AB} \frac{p_{ab}}{4\pi\sqrt{s}} |M|^2 \frac{1}{2E_\pi} \frac{\rho_{N_A}}{2E_A} \frac{\rho_{N_B}}{2E_B} \tag{5.12}$$

$$\text{with symmetry factor} \qquad S_{ab} = \begin{cases} \frac{1}{2} & \text{if particles a and b are identical} \\ 1 & \text{otherwise} \end{cases} .$$

This rate depends on the densities ρ_{N_A} and ρ_{N_B} of the nucleons in the initial state. The matrix element $|M|^2$ can be calculated from equation (5.11)

$$|M(\sqrt{s})_{\ N_a\ N_b \to N_A\ N_B\ \pi}|^2 = \left(S_{AB} \frac{1}{64(2\pi)^3 p_{ab}\sqrt{s}^3} \int dm_{AB}^2 dm_{A\pi}^2 \right)^{-1} \sigma_{\ N_a\ N_b \to N_A\ N_B\ \pi}$$

and it shows that $\Gamma_{N_A\ N_B\ \pi \to N_a\ N_b}$ depends linearly on $\sigma_{\ N_a\ N_b \to N_A\ N_B\ \pi}$. This cross section $\sigma_{\ N_a\ N_b \to N_A\ N_B\ \pi}$ is according to equation (5.10) a sum of two contributions:

$$\sigma_{\ N\ N \to N\ N\ \pi} = \sigma^{bg}_{\ N\ N \to N\ N\ \pi} + \sigma^{resonance\ contribution}_{\ N\ N \to N\ N\ \pi}$$

since we needed to introduce a background cross section in this channel to fit the $N\,N \to N\,N\,\pi$ data. Therefore $\Gamma_{N_A\ N_B\ \pi \to N_a\ N_b}$ can also be split in a resonance and a background contribution:

$$\Gamma_{N_A\ N_B\ \pi \to N_a\ N_b} = \Gamma^{bg}_{N_A\ N_B\ \pi \to N_a\ N_b} + \Gamma^{resonances}_{N_A\ N_B\ \pi \to N_a\ N_b}$$

with

$$\begin{aligned} \Gamma^{bg}_{N_A\ N_B\ \pi \to N_a N_b} &\sim \sigma^{bg}_{\ N\ N \to N\ N\ \pi} \\ \Gamma^{resonances}_{N_A\ N_B\ \pi \to N_a\ N_b} &\sim \sigma^{resonance\ contribution}_{\ N\ N \to N\ N\ \pi} . \end{aligned}$$

Details concerning this absorption rate can be found in [Eff96] and [Eff99]. The resonance absorption rate is included in the code by the explicit propagation of the resonances. The background absorption rate $\Gamma^{bg}_{N_A\ N_B\ \pi \to N_a\ N_b}$ is introduced to fulfill detailed balance of the $NN \longleftrightarrow NN\pi$ process.

Isospin symmetry

Let us study the isospin symmetry of the full absorption rate defined by equation (5.12). Therefore we assume symmetric nuclear matter.

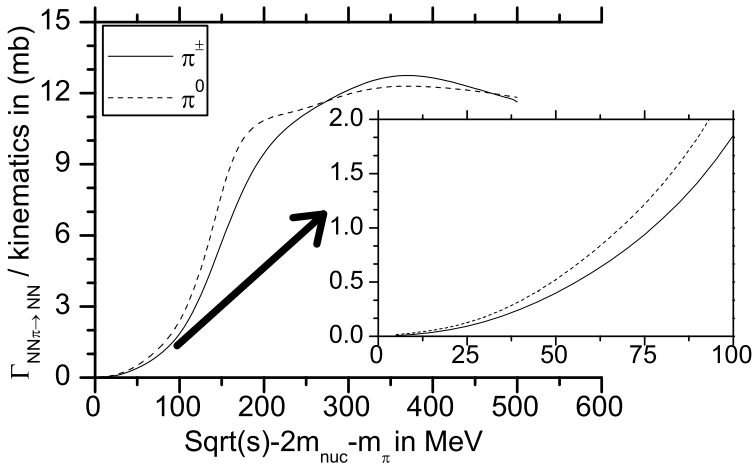

Figure 5.10: Decay rates based on the $NN\pi \to NN$ process in units of mb/K assuming Isospin symmetric nuclear matter. K is defined in equation 5.13.

The pions and nucleons have all the same mass in our simulation. For a given $\sqrt{s}$ of the initial πNN state the kinematical factors are therefore identical for all processes. Let us abbreviate the kinematical factors by K

$$K = \frac{p_{ab}}{4\pi\sqrt{s}} \frac{1}{2E_\pi} \frac{\rho}{2E_A} \frac{\rho}{2E_B} \left(\frac{1}{64(2\pi)^3 p_{ab}\sqrt{s}^3} \int dm_{AB}^2 dm_{A\pi}^2 \right)^{-1} . \qquad (5.13)$$

With this notation and the accurate symmetry factors follows

$$\begin{aligned}
\Gamma_{\pi^- NN} &= \Gamma_{\pi^- np} + \Gamma_{\pi^- pp} = K \left(\frac{1}{2}\sigma_{pp\to\pi^- np} + \sigma_{np\to\pi^- pp} \right) \\
\Gamma_{\pi^+ NN} &= \Gamma_{\pi^+ np} + \Gamma_{\pi^+ nn} = K \left(\frac{1}{2}\sigma_{nn\to\pi^+ np} + \sigma_{np\to\pi^+ nn} \right) \\
\Gamma_{\pi^0 NN} &= \Gamma_{\pi^0 np} + \Gamma_{\pi^0 pp} + \Gamma_{\pi^0 nn} = K \left(\sigma_{np\to\pi^0 np} + \frac{1}{2}\sigma_{pp\to\pi^0 pp} + \frac{1}{2}\sigma_{nn\to\pi^0 nn} \right) .
\end{aligned}$$

In the simulation we assume

$$\begin{aligned}
\sigma_{pn\to\pi^- pp} &= \sigma_{np\to\pi^+ nn} \qquad (5.14) \\
\sigma_{nn\to\pi^+ pn} &= \sigma_{pp\to\pi^- pn} \\
\sigma_{pp\to\pi^0 pp} &= \sigma_{nn\to\pi^0 nn}
\end{aligned}$$

therefore the decay rates for the charged pions based on the $NN\pi \to NN$ processes are identical. These decay rates are shown in figure 5.10 in units of mb/K. We see that Isospin symmetry is not exactly fulfilled. The fits to the data of

$NN \to NN\pi$ shown in figures 5.6 ref 5.9 lead to higher absorption rates at low energies for the neutral pion than for the charged pion.

At very low energies there might be an influence of the different masses of the charged and neutral pions. The lighter mass of the π^0 might lead to higher production rates in the $NN \to NN\pi^0$ processes at threshold. Therefore the reaction probability in the reversed $NN\pi^0 \to NN$ channel is larger. Another open problem are experiments investigating neutrons in the incoming channel of the $NN \to NN\pi$ process. They suffer from the problem that such experiments must actually be done with deuterium since the neutron is not stable in vacuum. This leads to uncertainties in the $NN \to NN\pi$ cross sections, which might show up in the asymmetry of the data at low energies.

The background absorption rate Γ^{bg}

The background absorption rate

$$\begin{aligned} \Gamma_{\pi^{\pm}NN} &= K\left(\frac{1}{2}\sigma^{bg}_{pp\to\pi^- np} + \sigma^{bg}_{np\to\pi^- pp}\right) \\ \Gamma_{\pi^0 NN} &= K\left(\sigma^{bg}_{np\to\pi^0 np} + \sigma^{bg}_{pp\to\pi^0 pp}\right) \end{aligned} \tag{5.15}$$

is explicitly included into BUU. Here we have already introduced the assumptions of equation (5.14). With this absorption rate we define an absorption probability

$$p_{abs} = 1 - e^{-\Gamma^{bg}\Delta t}$$

to absorb the pion in a time step of size Δt. If we decide in a Monte-Carlo decision to absorb the pion in some special time step, then the energy and momentum of the pion is distributed among two randomly chosen nucleons in its neighborhood. If these nucleons are not Pauli blocked then the absorption takes place in the simulation, otherwise the absorption process is dismissed. The background absorption rate including the kinematical factors is shown in figure 5.11. There we assumed the initial nucleons to be at rest.

According to its contruction it depends in symmetric matter on the following sizes

$$\Gamma^{bg} \sim \rho^2 \frac{\Phi_2^{NN}}{\Phi_3^{\pi NN}} \sigma^{bg} \ .$$

Due to its dependence on the inverse of the three-body phase-space Φ_3 it is exploding for low $\sqrt{s}$ because $\Phi_3 \to 0$ for $\sqrt{s} \to 0$. This would be a problem if there was no Pauli blocking. Those nucleons which would be produced at such low $\sqrt{s}$ are very probable to be Pauli blocked, therefore the real absorption rate does not blow up for $\sqrt{s} \to 0$. This will be shown in the next chapter where we analyze the full width of the pion in a full BUU simulation which includes also Pauli blocking of the final states.

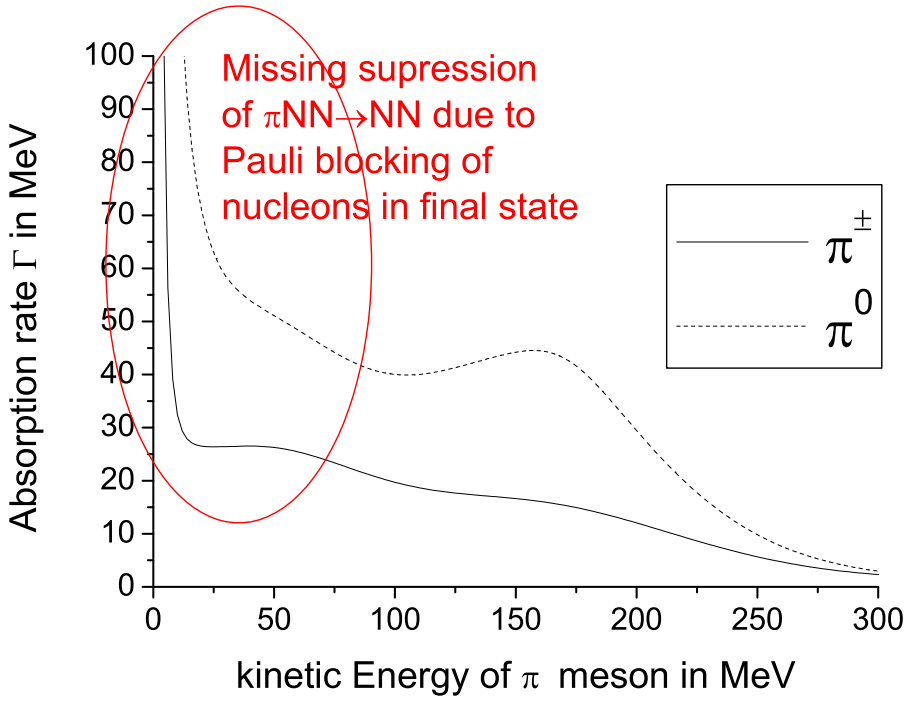

Figure 5.11: Absorption rate $\Gamma^{bg}_{NN\pi\to NN}$ according to equation (5.15) in symmetric matter $\rho_p = \rho_n = \rho_0/2$ assuming the initial nucleons to be at rest. In a full calculation one also has to consider Pauli blocking of the final states, this is not done here. Therefore we overestimate the effect of this absorption rate at low $\sqrt{s}$ where the three-body phase-space Φ_3 vanishes ($\Gamma^{bg}_{NN\pi\to NN} \sim \Phi_3^{-1}$).

5.6 Initialization

5.6.1 Nucleons

The nucleons are initialized according to a Wood-Saxon distribution in coordinate space and a Fermi-Gas- distribution in the momentum space. Details (e.g. numerical stability of this ground state) can be found in [Eff99].

5.6.2 Reactions induced by pions

Especially for pion induced reactions it is illustrative to study the effects of the Coulomb potential. Therefore we want to have a look at the distortion of the incoming pion trajectory which is also shown in figure 5.12. The pionic test particle is in the beginning totally characterized by its impact parameter b, its distance to the center of the nucleus r_{dist} and its momentum p. After initialization the test particle is propagated according to Hamilton's equation with

$$H = \sqrt{p^2 + m^2} + V_{Coulomb}(r) + V_{hadronic}$$

The question is the following: What is the maximum impact parameter for a test particle to make hadronic interactions? The hadronic potential and interactions are negligible outside a sphere with radius $r = 2r_{nucleus}$. Therefore we want to look for the maximum impact parameter b_{max} for a test particle to enter the sphere with radius $r = 2r_{nucleus}$ around the origin of the nucleus. As an example I treat the ${}^{40}_{20}Ca$ nucleus. The differential equations

$$\frac{\partial r_i}{\partial t} = \frac{\partial H}{\partial p_i}$$
$$\frac{\partial p_i}{\partial t} = -\frac{\partial H}{\partial r_i}$$

with $H = \sqrt{p^2 + m^2} + V_{Coulomb}(r)$ are solved numerically with a predictor-corrector scheme[4].

The results for the b_{max} parameter, which depends on the distance at initialization, are given in figure 5.13. It can be seen that for pions with $E_{kin} \geq 10MeV$ it is sufficient to initialize the simulation at $70fm$ distance from the nucleus. Although the Coulomb force has long range, the b_{max} parameter saturates very nicely. The parameter b_{max} is important, because in case of a black disc scattering the cross section would be proportional to b^2_{max}.

In practice the pions are initialized at $r_{dist} = 80fm$. In the first step of the simulation solely the pions are propagated until they reach $r_{dist} \simeq 2r_{nucleus}$. Then

[4]Since we are considering a relativistic Hamiltonian we can not exploit the trivial solutions for the Coulomb trajectories derived in classical electrodynamics. Therefore we solve the differential equation numerically.

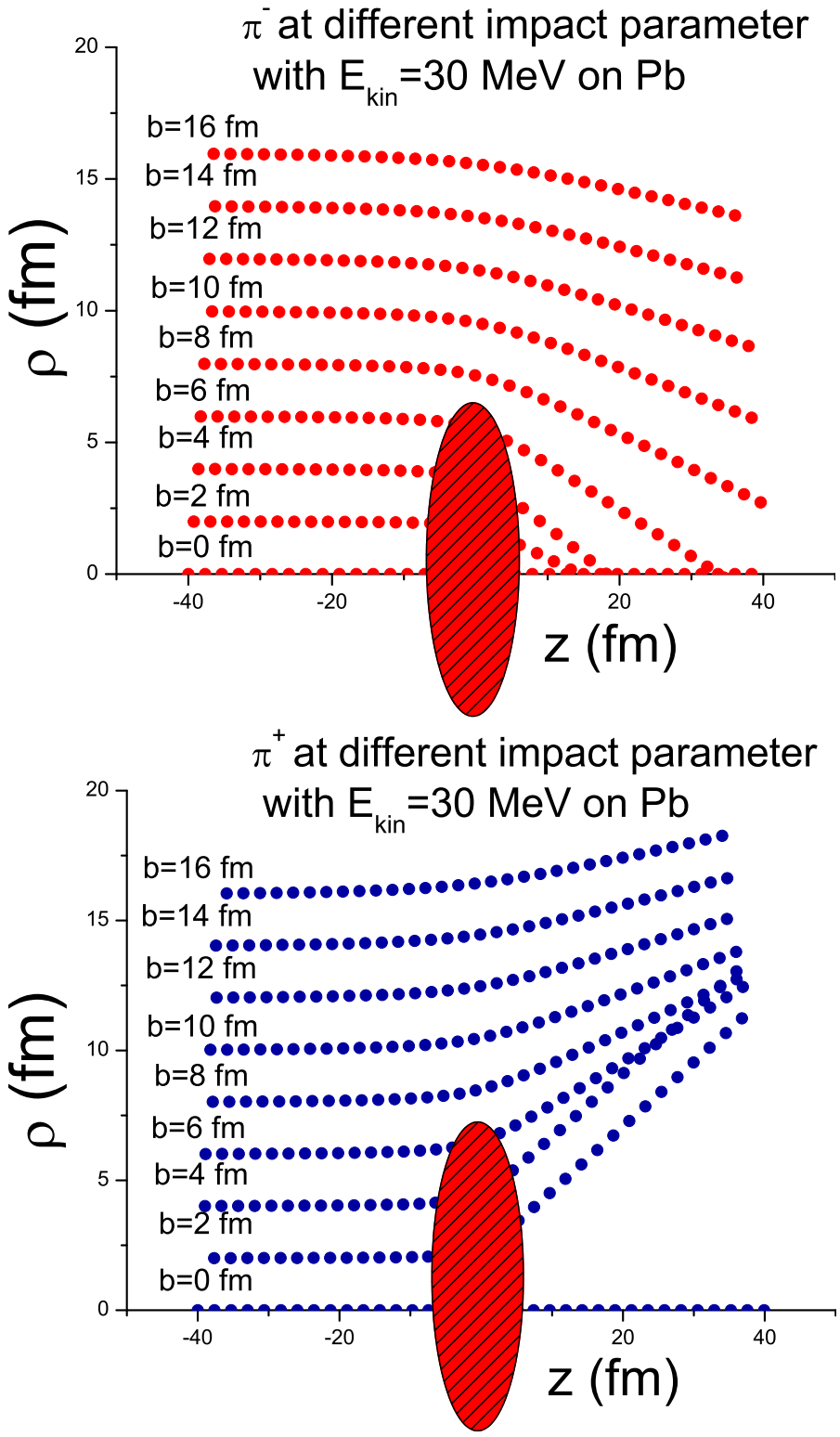

Figure 5.12: Trajectories due to the electromagnetic forces in cylindrical coordinates (z,ρ) and different impact parameters b. The incoming pions have kinetic energies of $30MeV$. The target is a $^{207}_{82}Pb$ nucleus.

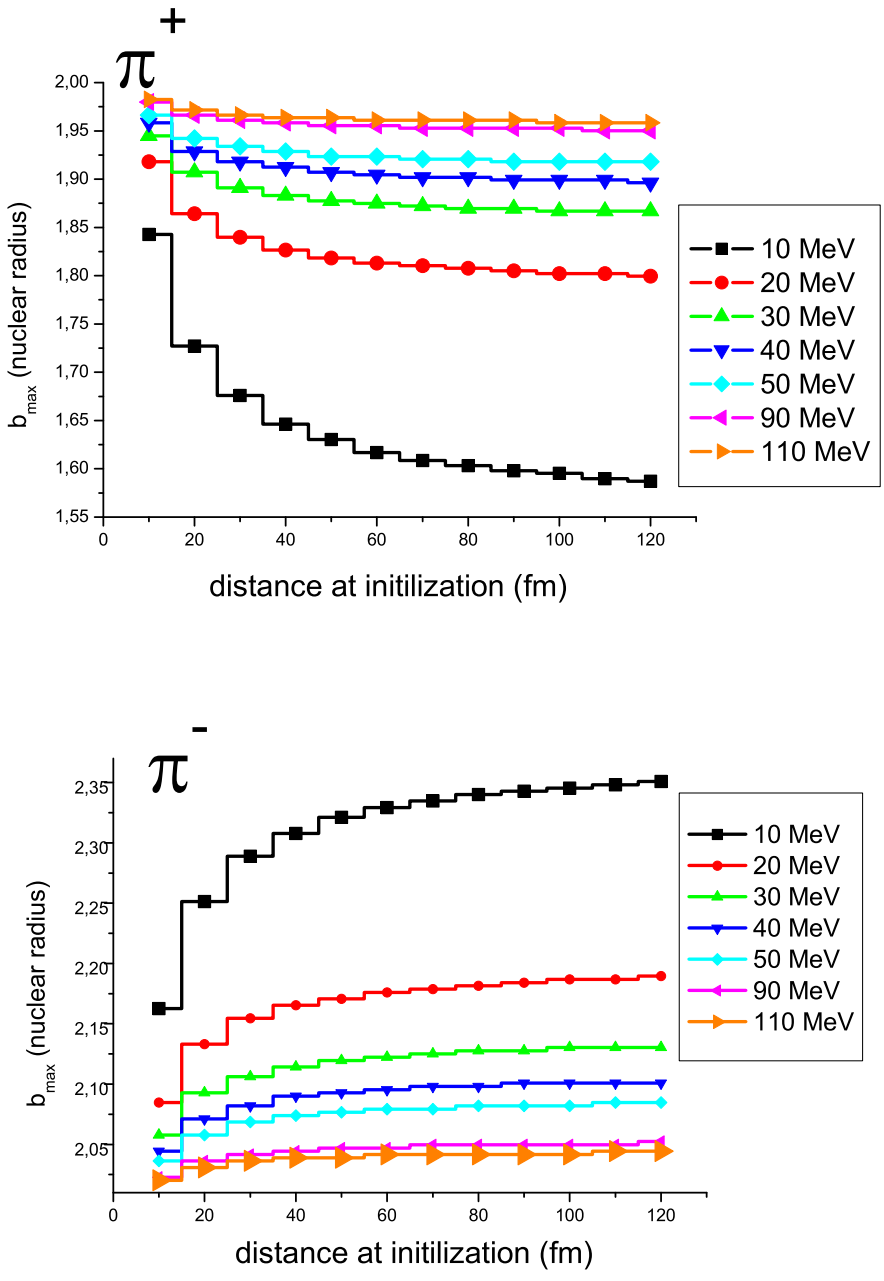

Figure 5.13: b_{max} for $^{40}_{20}Ca$ at different kinetic energies.

in the next step the full BUU simulation with all particles in it starts. If one started the full BUU code with pions at 80 fm, then it would take too long until the pions reached the nucleus and the ground state of the nucleus could have become unstable due to the long time period.

5.6.3 Reactions induced by photons

The initialization of γ induced reactions is treated extensively in [Eff99] and [Eff96]. The only modification to this treatment can be found in the $\gamma N \rightarrow N\pi\pi$ reactions. Here we established full energy conservation with the algorithm described in section 5.2.2. In the previous version of the code this algorithm was only used for two-body final states.

Part III

Results

Chapter 6

Properties of pions inside a nucleus

Before we proceed with absorption and reaction cross sections of pions on nuclei, we will first have a look at the properties of pions inside the nuclear medium. In this section we choose the calcium nucleus to examine the absorption rates and mean free path of the pion inside this nucleus. The calcium nucleus is symmetric in proton and neutron number and therefore we can compare in the end to earlier works on the mean free path of the pions which assumed symmetric nuclear matter as well.

We especially investigate the influence of a hadronic pion potential on the following parameters:

Full width. The number $N(t)$ of pions which did not interact with the medium by absorption or elastic scattering processes is expected to follow a

$$N(t) \sim \exp\left(-\Gamma(E_{kin})\ t\right) \tag{6.1}$$

description[1]. The parameter Γ denotes the full width of the pion, also called collisional width. It includes scattering processes as well as absorptive processes.

Mean free path. Here we consider the number of undisturbed pions in the beam depending on their traveled distance

$$N(z) \sim \exp\left(-\frac{z}{\lambda}\right). \tag{6.2}$$

The parameter λ is the so-called mean free path. Analytically the mean free path is also given by

$$\lambda = \frac{v}{\Gamma}$$

where v denotes the velocity of the pions.

[1]Derivation in section 1.2.3.

6.1 Numerical procedure

We initialize the pions in the center of a ${}^{40}_{20}Ca$ nucleus with a given total energy. Their momentum p is calculated in the medium such that

$$\begin{aligned} E_{total} &= E_{kin}^{Vacuum} + m_\pi \\ &= \sqrt{p^2 + m_\pi^2} + V_\pi(p, r = 0) + V_{Coulomb}(r = 0) \end{aligned}$$

with the hadronic potential V_π of the pion which is defined in equation (5.9). After each time step i of the simulation we extract the number of undisturbed pions $N(t = i\Delta t)$ and their position z(t). The simulation stops before the pions leave the region of central density. Therefore all results are obtained at central density.

According to equation (6.1) we fit $N(t)$ by a exponential decay ansatz and extract the full width Γ. We also fit $N\left(z(t)\right)$ according to equation (6.2) and extract the mean free path λ.

6.2 The accuracy of isospin symmetry in the model

First we want to investigate results of the BUU simulation without utilizing any potentials. In the simulation we use for all pions identical masses of $m_\pi = 138\ MeV$ and neglect therefore Isospin breaking on the level of the masses. Neglecting the Coulomb potential as well we expect full isospin symmetry in the ${}^{40}_{20}Ca$ -nucleus. In conclusion the three different pions should have the same velocity and width.

In figure 6.1 we see that all pions do actually have the same velocities but not the same width. The time stepping algorithm is the same for all pions if there is no potential included, therefore the result on the velocities had to be expected. In contrast to this the widths are different for the charged and uncharged pions, which yields also different mean free paths in both channels. But the difference is quite small except for very low energies.

The reason for this can be found in the implementation of the absorption and scattering processes. As discussed in section 5.5, we are using vacuum data for the elementary processes. The absorptive width of the charged pions is fixed by the elementary reactions

$$\begin{aligned} p\ p &\rightarrow p\ n\ \pi^+ \\ p\ n &\rightarrow p\ p\ \pi^- \end{aligned}$$

and the absorptive width of the π^0 is determined by

$$\begin{aligned} p\ p &\rightarrow p\ p\ \pi^0 \\ p\ n &\rightarrow p\ n\ \pi^0 \end{aligned}$$

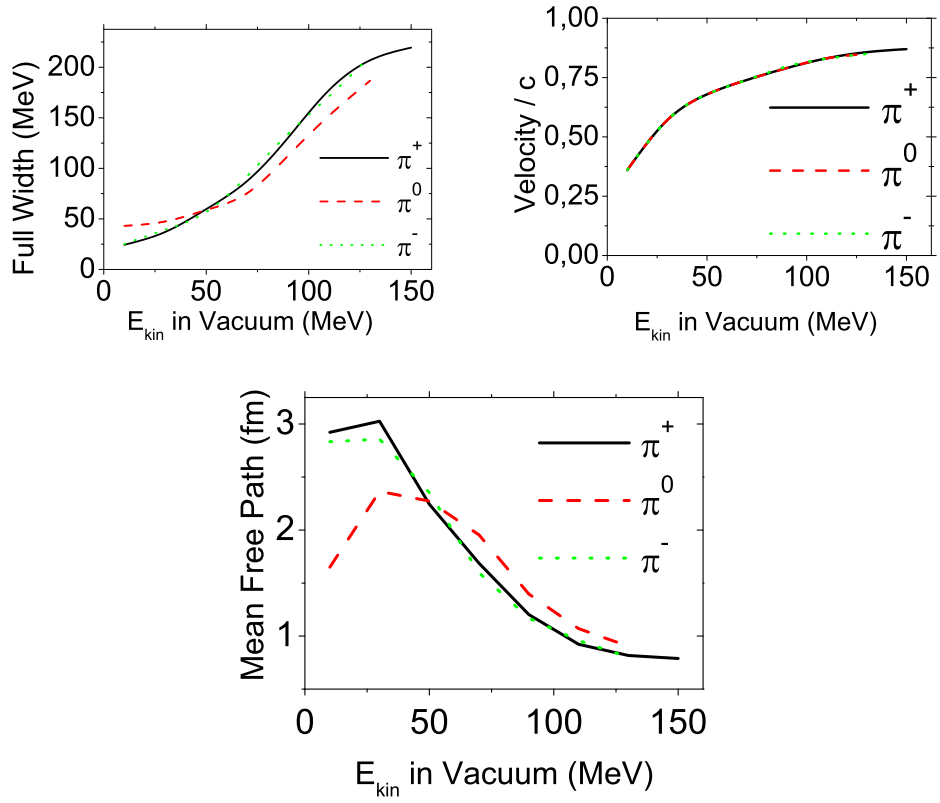

Figure 6.1: BUU results without Coulomb and hadronic potential inside a ${}^{40}_{20}Ca$ nucleus. Isospin symmetry is explicitly broken for very low energies. The central density is $\rho = 0.159 fm^{-3}$, $\rho_p = \rho_n = \frac{\rho}{2}$.

exploiting detailed balance for the $NN\pi \rightarrow NN$ process. For this channel we have already shown in section 5.5.3 that there exist problems with Isospin symmetry due to the elementary $NN \rightarrow NN\pi$ data sets which serve as an input for the detailed balance prescription. There we have seen that the decay rate for the neutral pion is at low energies higher than for the charged one. This explains the larger width of the π^0 near threshold.

In the scattering processes we also treat the charged and the uncharged pions differently. Since there are no data in the channel

$$\pi^0 n \rightarrow \pi^0 n$$

we were not able to implement a background cross section in this channel. This might explain missing strength in the π^0 width at larger energies where the quasi-elastic scattering becomes more important. At threshold this can be neglected due to Pauli blocking.

For the charged pions we are actually always using the same data sets as input and relate the processes of the charged pions by Isospin symmetry, e.g.

$\pi^+ n \to \pi^+ n$ receives the same cross section as $\pi^- p \to \pi^- p$. As a result of this prescription we conserve the symmetry among the charged pions.

The problem of isospin breaking is connected with the elementary data sets which are used as an input for the simulation. This could be solved by a theoretical model for the scattering processes based on an effective model for QCD which demands isospin symmetry.

6.3 Energy shift in the medium

Now we want to study medium modifications due to the potentials. The pions in the medium experience the following dispersion relation:

$$E = \sqrt{p^2 + m^2} + V_{hadronic}(p, r) + V_C(r)$$

The upper graph of Figure 6.2 gives a good impression of the modified dynamics inside the medium. We show the kinetic energy which a pion would have in the vacuum versus its kinetic energy in the medium. The Coulomb energy inside the calcium nucleus amounts 8.9 MeV, which is rather small compared to approximately 20 MeV in a lead nucleus. The two full curves without hadronic potentials for the charged pions are just shifted by two times 8.9 MeV.

Introducing also hadronic potentials leads to strongly modified kinetic energies in the medium. The potential for the pion was shown in figure 5.2. We have seen that it is repulsive for small energies and turns attractive for large energies.

In the lower part of figure 6.2 we see the difference between the kinetic energy in the medium and in the vacuum. At low values of E_{kin}^{Vacuum} the kinetic energies in the medium are decreased by the repulsive hadronic potential. At higher values of E_{kin}^{Vacuum} the kinetic energies in the medium are enhanced due to the attractive behavior of the hadronic potential at large momentum. The point where $E_{kin}^{vacuum} = E_{kin}^{medium}$ differs for all three pions, this difference is basically a shift due to the Coulomb potential.

6.4 Collisional width in the medium

In the following sections we will show curves with the following meaning:

- BUU. We propagate the pion in an electromagnetic and hadronic potential.
- BUU without hadronic potential. Here we include just the Coulomb potential.
- BUU without Coulomb and hadronic potential. Here we do not include any potentials.

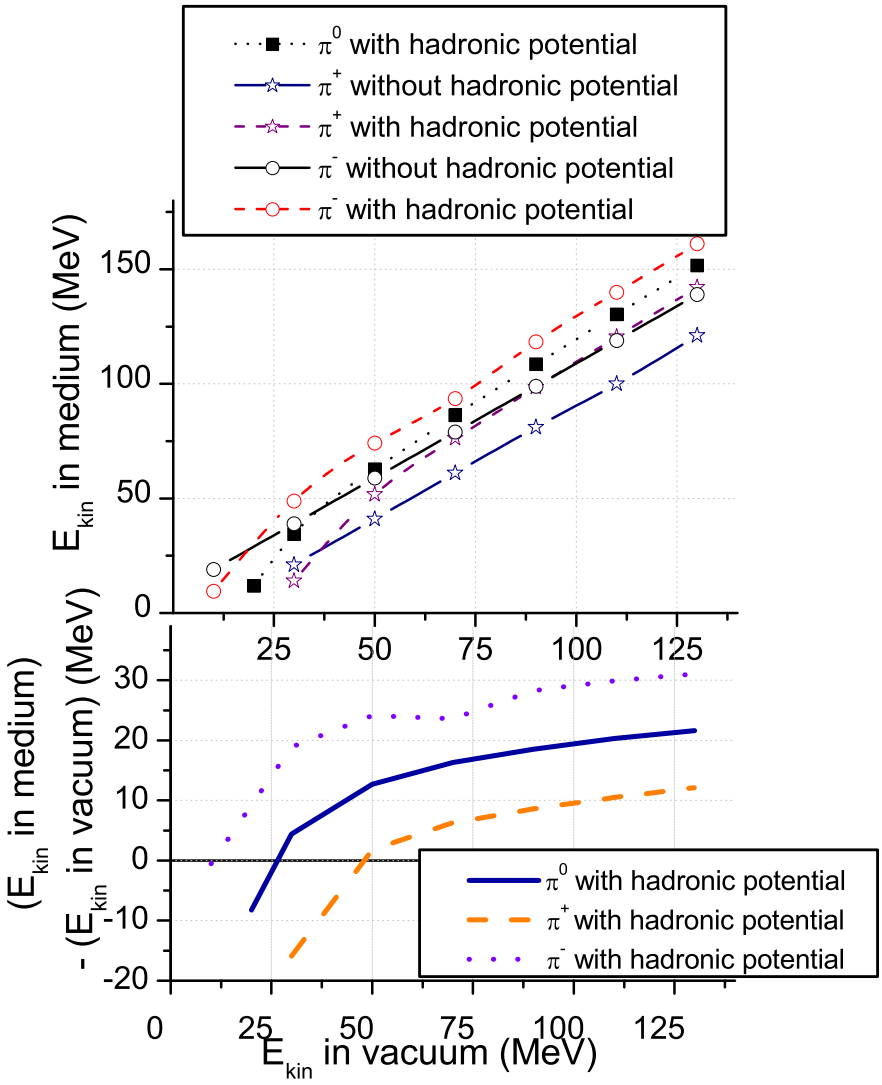

Figure 6.2: Shift of the kinetic energy of the pion in the center of a $^{40}_{20}Ca$ nucleus. Central density: $\rho = 0.159 fm^{-3}$, $\rho_p = \rho_n = \frac{\rho}{2}$.

6.4.1 Results for the π^0 meson

The result for the π^0 meson is shown in figure 6.3. At low energies there is practically no difference between the simulation with and without hadronic potential for the π^0. Due to the fact that there is basically no resonance contribution in this energy regime, the width of the pion is dominated by its absorption via the $N\ N\pi \rightarrow N\ N$ background. At higher energies a difference between both scenarios occurs. Here the decay width is smaller if the hadronic potential is included.

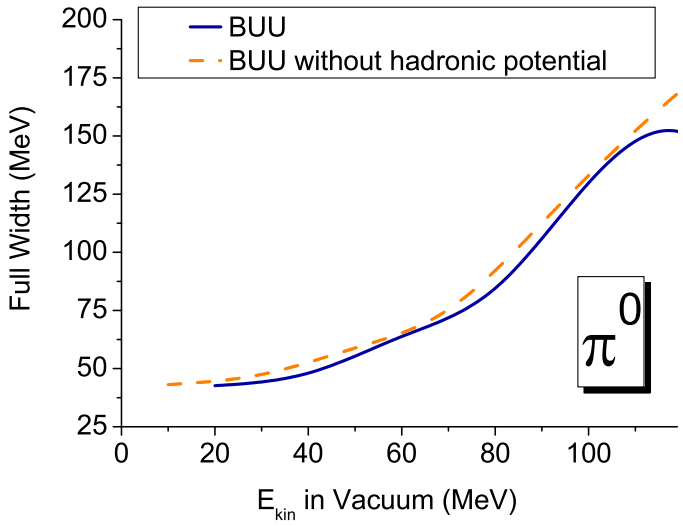

Figure 6.3: Full width of the π^0 in the medium. Central density: $\rho = 0.159 fm^{-3}$, $\rho_p = \rho_n = \frac{\rho}{2}$.

These deviations can be understood by investigating the resonance production process $N\ \pi \rightarrow \Delta$. The mass $\mu^\star$ of the Δ is fixed by

$$\mu^\star = \sqrt{s} = \sqrt{(E_\pi + E_N)^2 - (\vec{p}_\pi + \vec{p}_N)^2}$$

and its momentum is given by

$$\vec{p}_\Delta = \vec{p}_\pi + \vec{p}_N.$$

If we include the hadronic potential then E_{kin}^{medium} increases compared to the case where we have no hadronic potential, as we have seen in figure 6.2. Therefore also the pionic momentum increases and as a consequence the average value of $|\vec{p}_\Delta|$ increases as well. The momentum dependent potential of the Δ resonance is given in equation (5.5) and shown in figure 5.1. For $|\vec{p}_\Delta| \leq 400 MeV$ at $\rho = \rho_0$ it is negative, but continuously rising.

The mass of the Δ resonance in its rest frame is given by

$$\sqrt{s} = \mu^\star = \mu + V(\vec{p}_\Delta).$$

The variable μ is the off-shell mass of the resonance and $V(\vec{p}_\Delta)$ is its scalar potential. We now consider $\sqrt{s}$ fixed. Then an increase in $|\vec{p}_\Delta|$ leads to a decrease in μ which is in the considered energy regime always smaller than the peak mass of the Δ resonance. Therefore an increase in $|\vec{p}_\Delta|$ leads to a Δ resonance which is more off shell. The production of a resonance is more probable if it is produced close to its peak mass.

Therefore the increase in $|\vec{p}_\Delta|$ - caused by the potential - leads to a decrease of the production probability. Therefore the process $N\ \pi \rightarrow \Delta$ is less probable and the width of the pion decreases.

6.4.2 Results for the charged π-mesons

For the charged pions, the results are a little bit harder to interpret due to the influence of electromagnetic forces. We have seen in figure 6.1 that in the case of no potentials both charged pions have the same width. Figure 6.4 shows that the curves for the two charged pions are shifted by approximately 18.9 MeV which is just the difference in the Coulomb potential of a positively and negatively charged pion in the center of a ${}^{40}_{20}Ca$ nucleus. After shifting the curve for the π^+ it is nearly identical to the curve for the π^-.

The full result for the charged pions is shown in figure 6.5. In the scattering processes we neglect for numerical simplification the Coulomb energies since electromagnetic energy conservation is automatically fulfilled because of charge conservation. However, positively charged particles will have smaller momentum in the Coulomb field of the nucleus compared to the vacuum and negatively charged particles vice versa.

For the full width of the pion the processes $NN\pi \rightarrow NN$ are most important.

For the π^- meson the possibility for absorption on a $n-p$ state is more probable than on a $p-p$ state as can be seen in figures 5.8 and 5.9. Therefore here the Coulomb effects in the initial state of the scattering process cancel because the overall charge in the scattering process is very probable to be zero.

For the π^+ meson we will also have a $p-n$ state as the preferred scattering partner. Here the sum of all charges is $q_{tot} = +2$. Therefore the width for the π^+ is decreased because the momenta of the scattering partners in the incoming channel are decreased due to the Coulomb potential.

At high energies we see also for the charged pion the same effect of a decreasing width at high energies due to the hadronic potential.

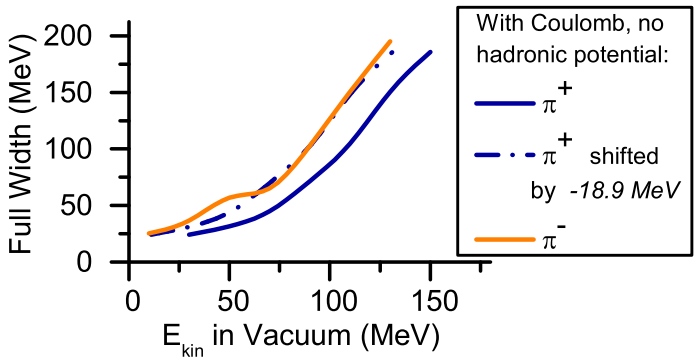

Figure 6.4: Influence of the Coulomb potential on the width of the charged pions. No hadronic potential for the pion is utilized. Central density: $\rho = 0.159 fm^{-3}$, $\rho_p = \rho_n = \frac{\rho}{2}$.

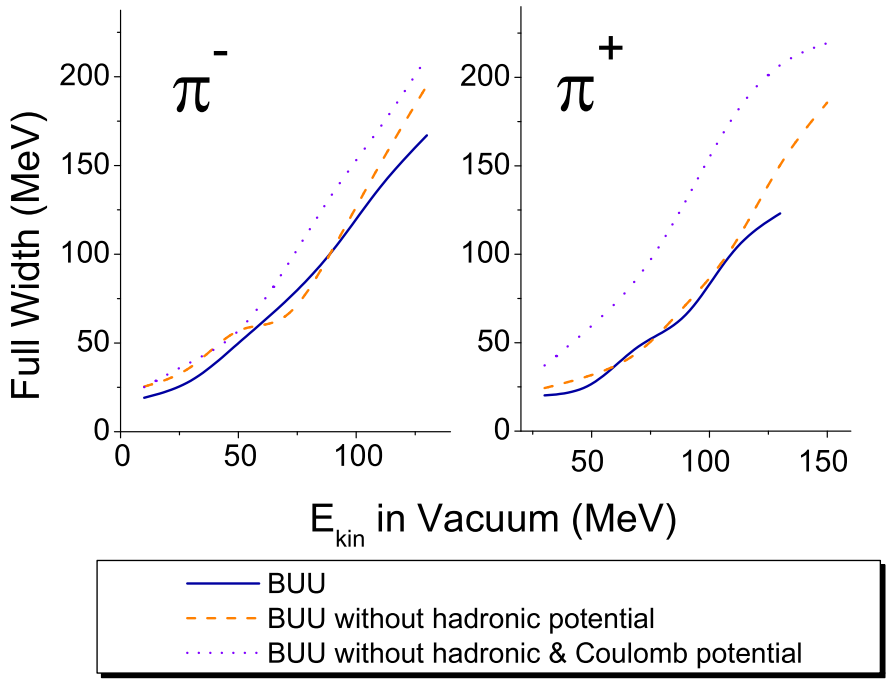

Figure 6.5: Full width of the charged π-mesons in a ${}^{40}_{20}Ca$ nucleus. Central density: $\rho = 0.159 fm^{-3}$, $\rho_p = \rho_n = \frac{\rho}{2}$.

6.5 Velocity of the π mesons in the medium

The velocity of the test particles is given by Hamilton's equation

$$\begin{aligned}\frac{\partial r_i}{\partial t} &= \frac{\partial H}{\partial p_i} = \frac{\partial\left(\sqrt{p^2+m^2}+V_{hadronic}+V_{Coul}\right)}{\partial p_i} \\ &= \frac{p_i}{\sqrt{p^2+m^2}} + \frac{\partial V_{hadronic}}{\partial p_i}.\end{aligned}$$

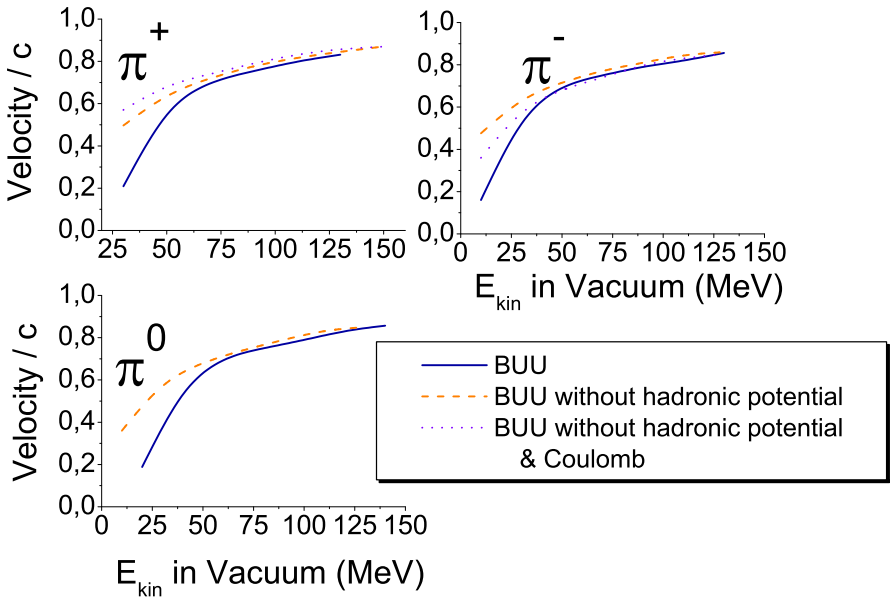

Figure 6.6: Velocity of the π-mesons in center of a ${}^{40}_{20}Ca$ nucleus. Central density: $\rho = 0.159 fm^{-3}$, $\rho_p = \rho_n = \frac{\rho}{2}$.

Neglecting the hadronic potential we expect the positively charged pion to be slowed down in the Coulomb potential and the negatively charged pion to be accelerated compared to the vacuum velocity. This behavior is also shown in figure 6.6.

If we also include the hadronic potential then the velocity is decreased, especially at low energies. The hadronic potential is repulsive for low values of E_{kin}^{vacuum}. Therefore the kinetic energy in the medium is very small and the velocity is slowed down. The term $\frac{\partial V_{hadronic}}{\partial p}$ is always negative: Large in absolute magnitude for low energies and small for energies greater than 80 MeV and leads to an overall reduction of the velocities.

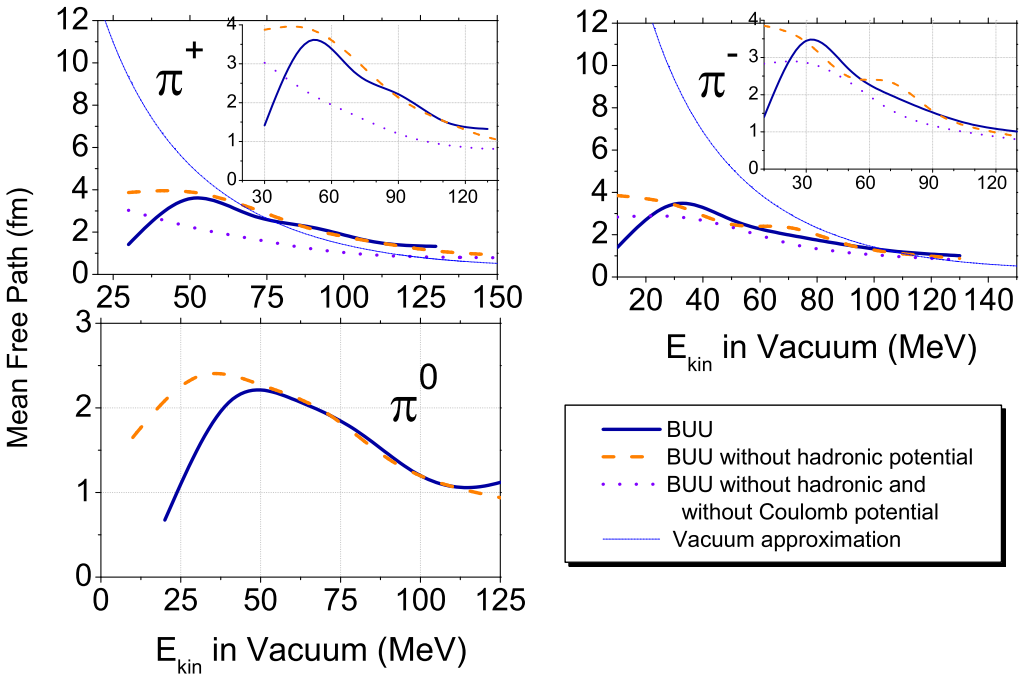

Figure 6.7: Mean free path of the pion in the central density region of a $^{40}_{20}Ca$ nucleus. Central density: $\rho = 0.159 fm^{-3}$, $\rho_p = \rho_n = \frac{\rho}{2}$. The curves denoted 'vacuum approximation' are explained in section 6.6.1.

6.6 Mean free path

We extract the mean free path directly from our numerical simulation, but analytically the mean free path is also given by $\lambda = \frac{v}{\Gamma}$. Therefore we now need to consider the two effects discussed earlier to understand the changes in the mean free path:

- Modification of the decay width Γ due to the potentials.
- Modification of the velocity v due to the potentials.

Especially at very low energies the effect of including the hadronic potential becomes visible in figure 6.7. In the standard simulation the mean free path drops rapidly at low energies compared to the simulation without hadronic potential. This sharp decrease of the mean free path stems from the velocity decrease at low energies when including the hadronic potential (see figure 6.6). At larger values of the kinetic energy the effect of decreasing width and decreasing velocity just cancel for the charged pions. For the neutral pion we see an increase of the mean free path due to the decreasing width above 120 MeV (see figure 6.3).

The most important effect of the hadronic potential is the large decrease of the mean free path at very low energies.

6.6.1 The vacuum approximation

An approximation which is often used by experimental physicists is the eikonal vacuum approximation [EW88] [CMMN90] to make a scientific guess on the mean free path of the pion in the medium. The dispersion relation

$$E^2 = p^2 + m^2 + \Pi(E,p)$$

leads to

$$p = \sqrt{E^2 - \Pi(E,p) - m^2}.$$

In the eikonal approximation one assumes the wave function to be a plane wave

$$\Psi(z) = e^{ipz}.$$

The probability density is therefore

$$\rho(z) = \Psi(z)^\dagger \Psi(z) = e^{-\frac{z}{\lambda}}$$

with

$$\lambda = \frac{1}{2\ \Im(p)} \tag{6.3}$$

being the mean free path. To first order in density, the self energy is approximated by

$$\Pi(E,p) = -4\pi\ F(E,p)\ \rho.$$

Here $F(E,p)$ denotes the forward scattering amplitude of the pion. In the vacuum approximation we make use of the optical theorem

$$\Im\left[F(E,p)\right] = \sigma_{Vacuum}\ \frac{p}{4\pi}\ .$$

Expanding p for low ρ we obtain [EW88]

$$\lambda = \frac{1}{\rho\ \sigma_{Vacuum}}.$$

Using actual data from the PDG data group [H$^+$02b] which are shown in figure 6.8, we can now evaluate the mean free path. We assume

$$\begin{aligned} \sigma_{\pi^- n \to X} &= \sigma_{\pi^+ p \to X} \\ \sigma_{\pi^+ n \to X} &= \sigma_{\pi^- p \to X}\ . \end{aligned}$$

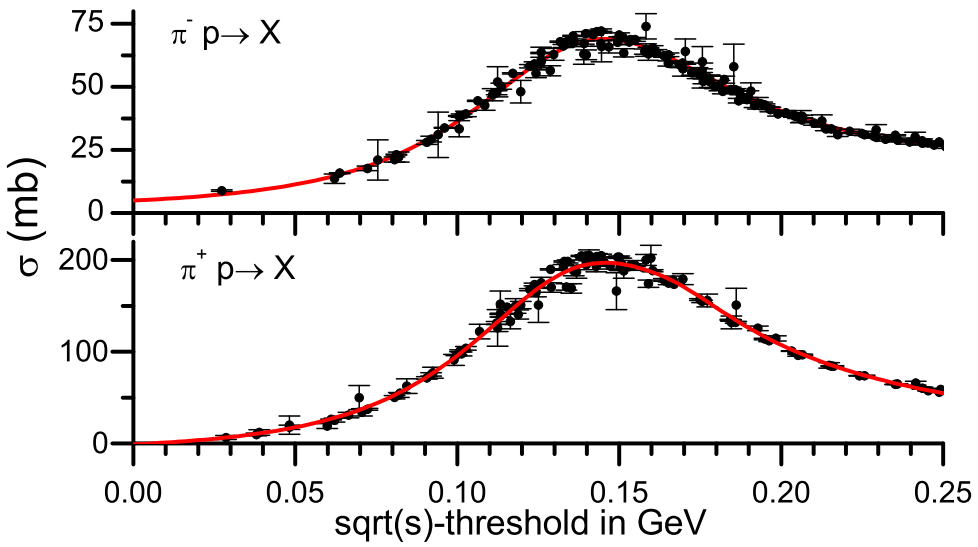

Figure 6.8: Total cross sections for π-proton collisions. Data are taken out of [H$^+$02b]. The red curve is our fit to the data. At low $\sqrt{s}$ this fit is rather vague in the upper graph.

because there exist no data for πn scattering since the neutron is not stable in the vacuum.

We calculate σ_{Vacuum} for the π^+ and π^- by averaging over the neutron and proton contribution to the cross section:

$$\begin{aligned} \sigma^{\pm}_{Vacuum} &= \frac{1}{2}\sigma_{\pi^{\pm}n\to X} + \sigma_{\pi^{\pm}p\to X} \\ &= \frac{1}{2}\sigma_{\pi^{+}p\to X} + \sigma_{\pi^{-}p\to X} \ . \end{aligned}$$

We get the same results for both pions. For the charged pions this approximation is shown in figure 6.7 compared to full BUU calculations which consider as well the Pauli blocking of the final states, the Fermi motion of the initial states and the energy shift due to the electromagnetic interaction.

We see large deviations from the vacuum approximation. The vacuum approximation does not consider any kind of multi-body interactions at low energy. Only the two body πN interaction is allowed. We have seen in section 5.5.2 that we were forced by detailed balance to introduce a $NN\pi \to NN$ cross section to explain the $NN \to NN\pi$ scattering data. Such a three body $NN\pi$ interaction is not included in the vacuum approximation. This seems to be the reason why it is overestimating the mean free path at low energies.

We have to conclude that the vacuum approximation is qualitatively and quantitatively not reliable in our energy regime where the multi-body collisions are important.

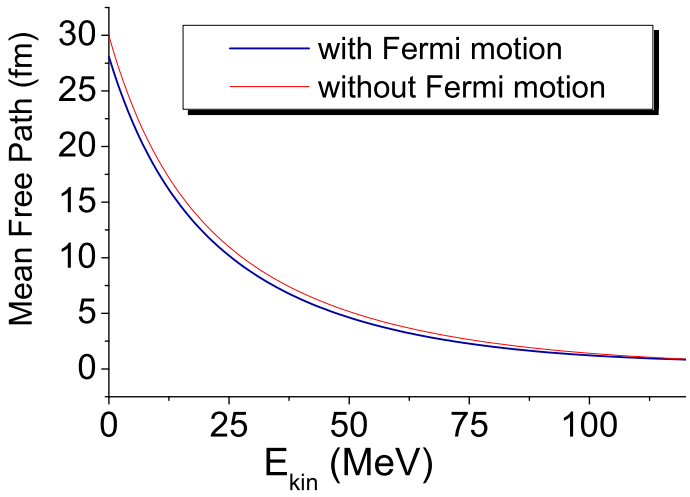

Figure 6.9: Mean free path in the vacuum approximation.The red curve is calculated by $\lambda = \frac{1}{\rho\ \sigma_{Vacuum}}$.

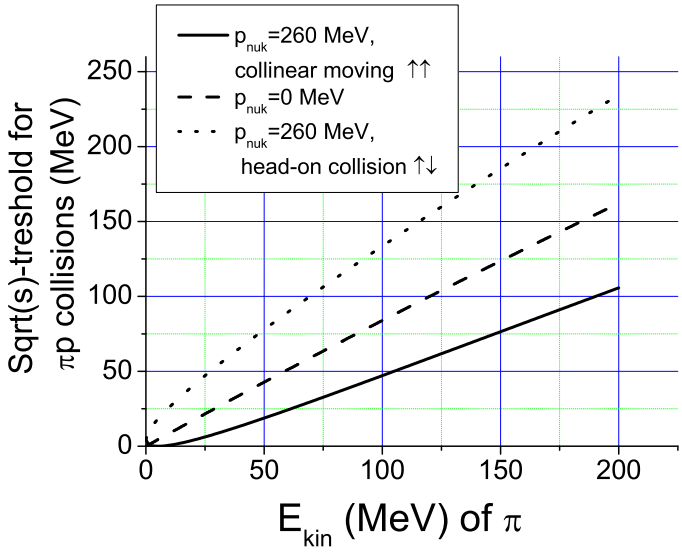

Figure 6.10: $\sqrt{s} - threshold$ for πp collision. We consider a resting nucleon p_{nuk}=0, a nucleon with $p_{nuk} = 260\ MeV$ colliding head-on with the pion and a nucleon with $p_{nuk} = 260\ MeV$ moving in the same direction as the pion. The momentum of 260 MeV reflects the typical Fermi momentum in nuclei.

We also investigated the influence of Fermi-motion and modified

$$\lambda = \frac{1}{\rho \ \sigma_{Vacuum}}$$

to

$$\lambda = \frac{1}{4 \ \int \sigma_{Vacuum}(\sqrt{s}) \ \frac{d^3p}{(2\pi)^3}} \tag{6.4}$$

and calculated the mean free path by summing over the interactions in the Fermi sea. The Fermi momentum was assumed to be 260 MeV and the fit of the $\sigma_{Vacuum}(\sqrt{s})$ data can be found in figure 6.8. The factor 4 stems from spin and isospin degeneracy.

The result of this considerations can be seen in figure 6.9. The modifications of the mean free path due to the Fermi motion in the vacuum approximation are very small.

In figure 6.10 we show the modification of $\sqrt{s}$ due to the Fermi motion. At low kinetic energies of the pion the Fermi motion is not sufficient to increase $\sqrt{s}$ in such a way that the averaged cross section is much enhanced. We see also that in collisions where the pion and nucleon are moving in the same direction the $\sqrt{s}$ is very low. Therefore one becomes sensitive to the insecurities in fitting the π^- channel of figure 6.8 at low $\sqrt{s}$. Hence we can not attribute the small differences in figure 6.9 to any physical effect.

6.6.2 Comparison to optical model results

Calculations by Patrick Hecking [Hec81]

In [Hec81] Patrick Hecking presents calculations concerning the mean free path of the pion. He is using two different types of phenomenological optical potentials. The first parameter set for an optical potential is taken out of Stricker's analysis [SMC79], the second one is calculated by Chai and Riska [CR79]. Starting from equation (6.3) one can calculate the imaginary part of the momentum using the dispersion relation

$$p^2 = E^2 - \left(m^2 + 2E \ V_{opt}(p, E)\right). \tag{6.5}$$

One has to solve the real and imaginary part of the dispersion relation. But instead, Hecking approximates the real part by the vacuum solution

$$\Re\left[p^2\right] = E^2 - m^2 \tag{6.6}$$

and uses this approximation in the equation for the imaginary part

$$\Im\left[p^2\right] = -\Im\left[2E \ V_{opt}(p, E = \sqrt{p^2 + m^2})\right]. \tag{6.7}$$

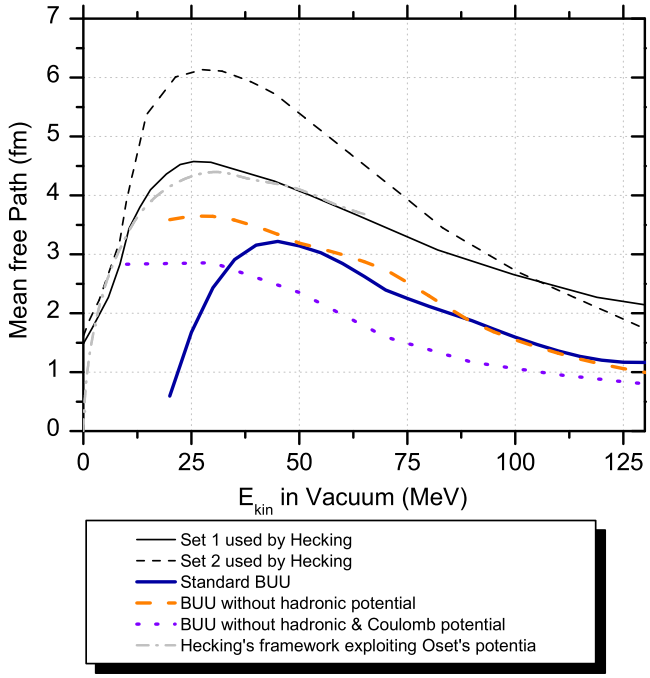

Figure 6.11: Averaged mean free path of the charged pions in the medium $\lambda_{avg} = \frac{1}{2}(\lambda_{\pi^+} + \lambda_{\pi^-})$, BUU versus optical model. Set 1 denotes the Stricker parameterization, set 2 denotes the parameter set by Chai and Riska. The BUU results are obtained with density $\rho = 0.159 fm^{-3}$, $\rho_p = \rho_n = \frac{\rho}{2}$.

This last equation now defines also $\Im[p]$ to be used in equation (6.3). He is not considering Coulomb effects. Rather he is defining an averaged mean free path by

$$\lambda_{avg} = \frac{1}{2}(\lambda_{\pi^+} + \lambda_{\pi^-})$$

and claims that this cancels all Coulomb effects for $E_{kin} > 15 MeV$. To compare to his results we also averaged the results for the charged pions. In figure 6.11 the comparison is shown, let us investigate the single BUU curves:

Standard BUU. We solve the complete dispersion relation of equation (6.5) for the pion and propagate the pion in an electromagnetic and hadronic potential. This curve is the most realistic one.

BUU without hadronic potential. Here we include just the Coulomb potential which shifts the π^+/π^- energies. We see that there are differences to the first curve, which raises doubts about Hecking's claim concerning the cancellation of the Coulomb effects.

BUU without Coulomb and hadronic potential. Here we calculated the mean free path without any potentials. This includes the same physics as Hecking's results.

The last curve is much too low compared to Hecking's results. Only in the case where we include only the Coulomb potential we come closer to his predictions. Before discussing the importance of the latter differences let us have a look at the results of Mehrem, Radi and Rasmussen [MRR84].

Exploiting [NO93] with vacuum approximations Exploiting the potential derived by Oset et al. in [NO93] we can also for this potential introduce vacuum approximations and evaluate a mean free path. Exploiting

$$\Im\left[p^2\right] \simeq -\Im\left[2E\ V_{opt}(p, E=\sqrt{p^2+m^2})\right]$$

we get for the mean free path

$$\begin{aligned}\lambda &= \frac{1}{2\Im\left[p\right]} = \frac{\Re\left[p\right]}{\Im\left[p^2\right]} \\ &\simeq -\frac{p}{\Im\left[2\sqrt{p^2+m_\pi^2}V_{opt}(p, E=\sqrt{p^2+m^2})\right]}\end{aligned}$$

parameterizationpproximation. This result is also shown in figure 6.11. It is compatible with Hecking's results with the Stricker parametrization and the same vacuum approximations.

Calculations by Mehrem, Radi and Rasmussen [MRR84]

Mehrem, Radi and Rasmussen [MRR84] criticize in their work the results of Hecking [Hec81]. They solve the full dispersion relation and report a mean free path of the pion which is much smaller compared to Hecking's results. They are using an optical potential calculated by J. A. Carr[2] who also helped to calculate the parameter set denoted 'Stricker' in Hecking's work. In their work this large difference is attributed to Hecking's approximations described in equations (6.6) and (6.7). Their result for the mean free path is shown in figure 6.12 in comparison to our result obtained with the BUU simulation. At very low energies the mean free path in the BUU simulation without the hadronic potential corresponds very well to the result by Mehrem, Radi and Rasmussen.

Including the hadronic potential we notice that the mean free path breaks down at low kinetic energies of the pion. At low kinetic energies the hadronic potential becomes repulsive. In classical mechanics particles can not propagate in regions where $E_{kin} < V$. This is also true for our BUU simulation which

[2]Parameters are given in [MRR84].

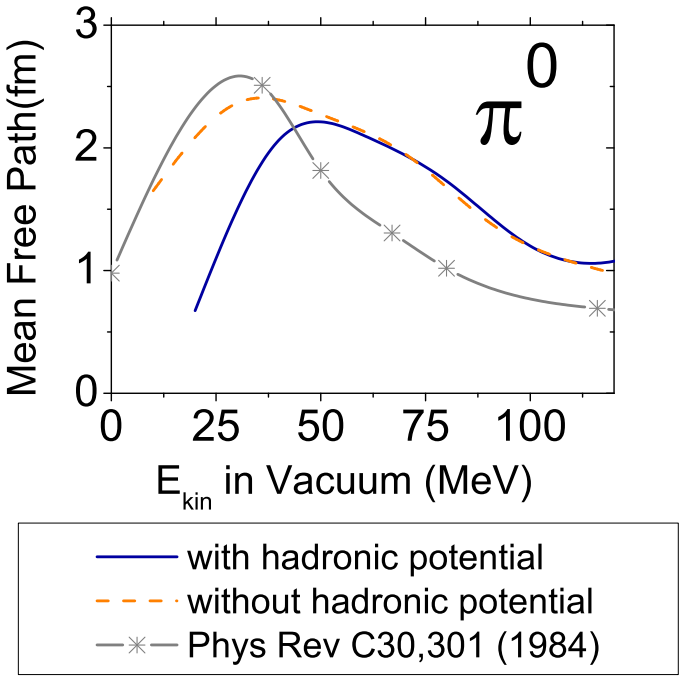

Figure 6.12: Mean free path of the π^0 meson. Results of the BUU simulation versus a quantum mechanical analysis carried out by Mehrem, Radi & Rasmussen [MRR84]. The stars denote the quantum mechanical results. The spline connecting the quantum mechanical results is just meant to guide the eye.

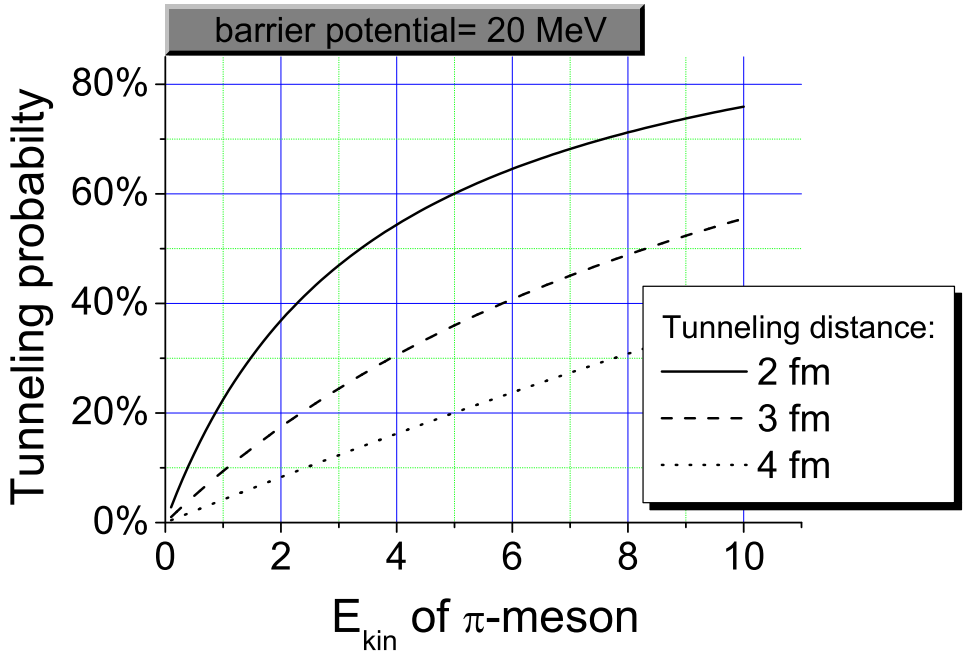

Figure 6.13: Tunneling probability for a pion through a potential barrier of height 20 MeV.

uses classical trajectories for the test particles. In contrast to classical mechanics, quantum mechanics allows for tunneling into such forbidden regions where $E_{kin} < V$. Therefore the classical interpretation underestimates the mean free path at low energies where the tunneling effect becomes important.

We can estimate the importance of this tunneling effect, using the standard formula[3] for the tunneling probability $T(E)$ for a particle with kinetic energy E_{kin} through a potential barrier of width L and height V :

$$T(E) = \frac{4x^2}{4x^2 + (1+x^2)^2 \sinh(L\kappa)}$$

with $\kappa = x\sqrt{2mE_{kin}}$ and $x = \sqrt{\frac{V-E_{kin}}{E_{kin}}}$. Inserting $m = m_\pi$ and a sensible scenario of $V = 20\ MeV$ for the hadronic potential at low kinetic energies we get the results shown in figure 6.13. The rather large tunneling probabilities show the importance of the tunneling concept. This effect can not be accounted for in our semi-classical theory based on classical trajectories for the pions.

[3] e.g. [Nol97],pages 257-258.

At higher energies Mehrem, Radi and Rasmussen report a lower mean free path than the results of our simulation. All together the result without the hadronic potential agrees best with the quantum mechanical result of those three authors.

The large differences of the BUU results and Hecking's results should not be taken too serious because Mehrem, Radi and Rasmussen claim that his approximations were not appropriate. Nevertheless the disagreement between Hecking and his critics shows that the question for the mean free path of the pion does not have a trivial answer.

Finally it is an open question whether we implemented a reasonable mean free path for the pion. This can only be answered by experiment. A test for our assumptions and our model will therefore be absorption and reaction cross sections which will be addressed in the next chapter.

Chapter 7

Pion induced events

7.1 Quantum mechanical results

With a given optical potential for the pion we can calculate with the techniques of chapter 3 reaction cross sections for pion-nucleus scattering. The results are obtained with a numerical routine [Shy] which solves the Klein-Gordon equation for the pion and deduces thereby its distorted wave-function. The boundary conditions for the pionic wave-function are described in section 3.2.

7.1.1 Implementation of the Oset potential

In [NO93] J. Nieves and E.Oset presented a model for low energy pion nucleus scattering which is described in appendix D. This complex model contains a lot of different contributions. An important check is whether we can reproduce their results with the optical potential out of their paper while using our own code to solve the Klein-Gordon equation.

Oset and Nieves included small terms in their potential which were obtained by a best-fit-procedure to scattering data. These terms denoted by δP_3 and δV_3 in [NO93] we did not include because they do not have a clear microscopic interpretation.

Our results are shown in figure 7.1 together with the results reported in [NO93]. Comparing our curves with the curves reported in [NO93], we see small differences on the level of 5% for a calcium target and on the level of 10% for a Carbon target. Actually we expected such small differences due to the missing terms and the presumably different numerical procedure to calculate the distorted wave. The overall agreement is good and therefore we claim that we have implemented the potential in the right way.

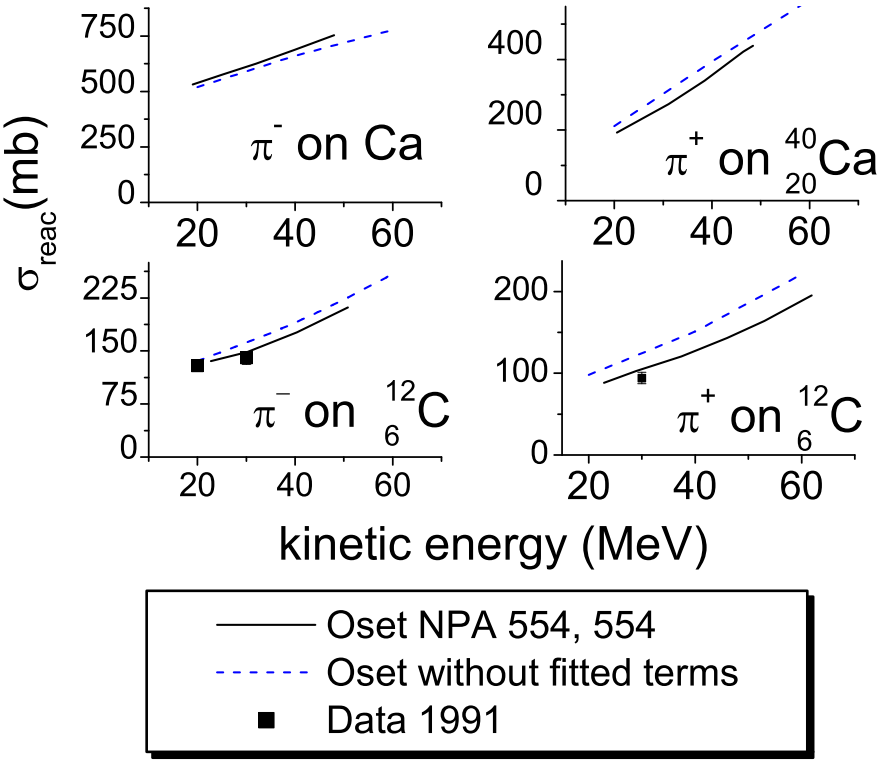

Figure 7.1: Implementation of the Oset potential [NO93]. Data are taken out of [F$^+$91]. The dashed curve is our result without the fitted terms of the potential.

7.1.2 Dependence on the real part of the optical potential

To investigate the importance of the real part of the optical potential we consider on the one hand the microscopic model by Nieves and Oset and on the other hand the standard phenomenological model by Stricker, McManus and Carr [SMC79].

Figure 7.2 clearly shows that both models make different predictions on reaction cross sections. Considering π^+ on Lead we see large discrepancies. However, data does not exist to judge the quality of these potentials.

We calculate the reaction cross section once with the full optical potential and once without the real part of the optical potential. We see a huge impact of the real part of the optical potential on the cross section for both models and all nuclei under consideration. There is a decrease of up to 50% if we do not include the real part. At higher energies the effect is much more pronounced. In the next section we will study whether there is a comparable effect in the semi-classical BUU model.

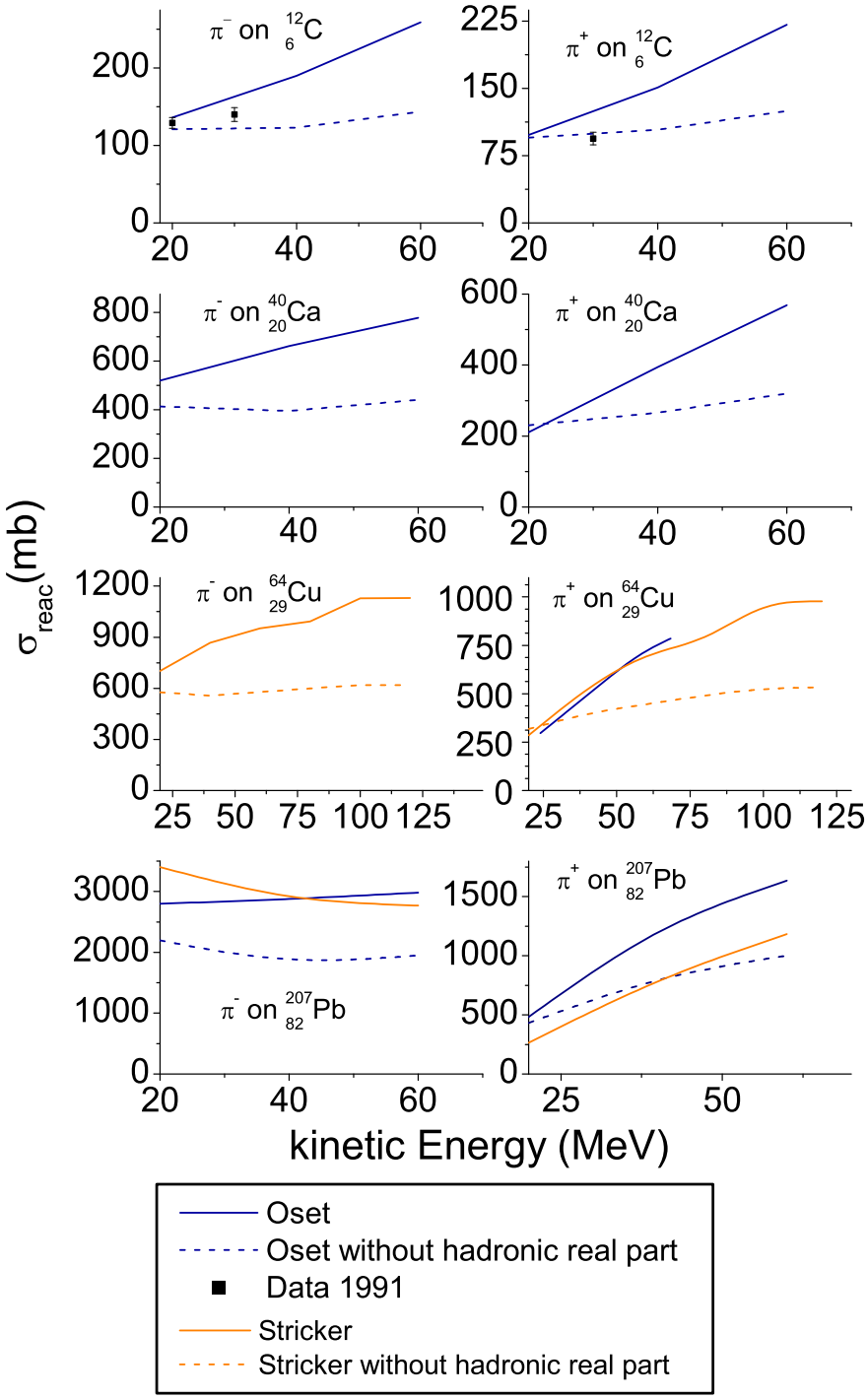

Figure 7.2: Reaction cross sections in quantum mechanical calculations. The calculations denoted by 'Stricker' are carried with V_{opt} according to [SMC79], those denoted by 'Oset' are carried out with V_{opt} according to [NO93]

7.2 Evaluating cross sections in the BUU model

The cross sections for some arbitrary process is gained by an integration over the possible impact parameters of the pions:

$$\sigma_{process} = 2\pi \int_0^\infty p(b)\ b\ db. \tag{7.1}$$

The function $p(b)$ denotes the probability for such a process for a pion incoming with the impact parameter b. Since $p(b)$ is vanishing for large b we can cut off the integral at some b_{max} without making a sizeable error. This probability is given by

$$p(b) = \frac{N_{process}(b)}{N_{init}(b)}.$$

where $N_{init}(b)$ is the distribution of the initialized pions and $N_{process}(b)$ denotes the number of pions which were initialized with some b and then caused the regarded process. We initialize the pions according to the following distribution

$$N_{init}(b) = C\,b\ \forall\ b \leq b_{max} \tag{7.2}$$

continously in the parameter b. The parameter b_{max} is chosen such that the result is insensitive to an increase in b_{max}. For π-induced experiments we choose for example $b_{max} = 1.5\ r_{nucleus} + 2.52fm$ with $2.52\ fm = \sqrt{\sigma_{max}/\pi}$. σ_{max} denotes the maximal experimental cross section in the elementary $\pi\ N$ collisions. Let N be the total number of initialized pions. The parameter C is then determined to be $C = \frac{2N}{b_{max}^2}$ to fulfill the normalization

$$N = \int_0^{b_{max}} N_{init}(b)db.$$

Finally we get

$$\begin{aligned} \sigma_{process} &= 2\pi \int_0^{b_{max}} \frac{N_{process}(b)}{N_{init}(b)}\ b\ db \\ &= \pi\ b_{max}^2\ \frac{\int_0^{b_{max}} N_{process}(b)db}{N}. \end{aligned}$$

The term $\int_0^{b_{max}} N_{process}(b)db$ is simply the sum of all initialized pions which caused the regarded process in the simulation.

7.3 Comparison between BUU simulations and quantum mechanical results

For the BUU simulations we distinguish three cases:

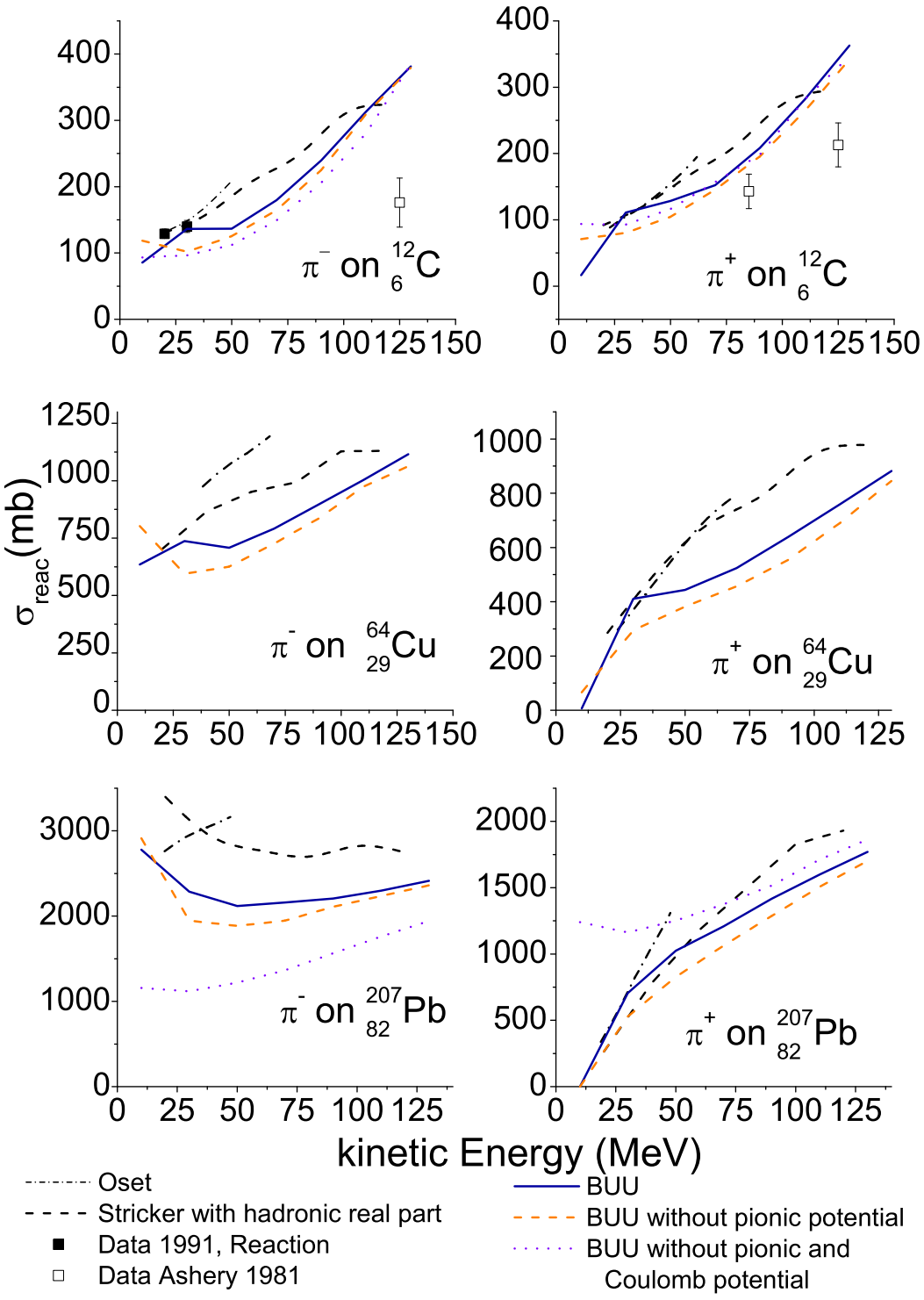

Figure 7.3: Reaction cross sections. BUU versus quantum mechanical calculations by Stricker et al. [SMC79] and Oset et al. [NO93]. Data points are taken out of [A+81] and [F+91].

BUU. Here we use both the Coulomb and the hadronic potential stemming from the self energy of the pion.

BUU without hadronic potential. Here we use only the Coulomb potential and no hadronic potential for the pion.

BUU without hadronic and Coulomb potential. Here we implement no potentials for the pion.

In figure 7.3 the results of the BUU calculations are compared to the results of the quantum mechanical models. First we want to compare the curves denoted 'BUU' to the quantum mechanical results.

For the light Carbon nucleus we achieve nice agreement with the quantum mechanical calculations. But the comparison to the data measured by Ashery et al. [A$^+$81] is not satisfying. Here both the semi-classical BUU model and the model by Stricker et al. overestimate the reaction data.

In the case of the more massive Copper and Lead nuclei we achieve qualitatively a good agreement to the results by Stricker et al.. However, their results predict much higher reaction cross sections at large energies. The curves by Oset et al. could especially for the Lead nucleus not be reproduced by the BUU model. Here we have discrepancies in the shape and height of the curves.

Considering the BUU simulations without hadronic potential for the pion, we do not see a large difference compared to the calculations with the hadronic potential. This is quite astonishing since we have seen such a huge effect for both quantum mechanical models.

In quantum mechanics also the imaginary part of the potential leads to a deformation of the elastic wave and not only to its absorption. In our semi-classical simulation only the real part of the potential creates a deformation of the trajectory of the pion. One could speculate that there are cancellations occurring in the quantum mechanical picture which are not realized in the BUU model.

Comparing the curves in figure 7.3 of the simulation carried out without any potential with the curves in the same figure exploiting the Coulomb potential, we see that the Coulomb potential is very important at such low energies. Its long range leads to a deformation of the trajectories already before the pions reach the nucleus. Therefore the negative pions can interact with the nucleus even if the have large impact parameter while the positive pions are deflected. We have already seen this in figure 5.13 where we studied the influence of the Coulomb potential. In the case of the Lead nucleus it is the most important ingredient in the model. Including the Coulomb potential we see a reduction of the cross section for the π^+ and a large increase of the cross section for the π^-. Since the nucleus is positively charged, it is attracting the negatively charged pion and repelling the positively charged one. Hence the cross section for the π^- meson is always bigger than the cross section for the π^+ meson.

Once the pion enters the nucleus it feels the hadronic potential which amounts 20 to -40 MeV as well as the Coulomb potential which amounts to roughly 10 MeV in a medium size nucleus and to roughly 20 MeV in the case of a Lead nucleus. At very low energies the two potentials nearly cancel for the negatively charged pion, while the add up to a strongly repulsive potential in the case of a π^+.

In the cross sections for Carbon and Copper we see small kinks in figure 7.3 at roughly 30 MeV kinetic energy for the curves implementing a hadronic potential. We will investigate the origin of these kinks in the context of absorption cross sections.

Unfortunately there exist only a few data points for reaction cross sections on complex nuclei. This process is therefore not suited to judge on the quality of a theoretical model.

7.4 Absorption cross sections in the BUU simulation

In a quantum mechanical calculation one cannot calculate absorption cross sections without any ambiguities. As mentioned earlier in chapter 3, one has to split the reaction cross section into an inelastic-scattering and an absorptive part. In the BUU simulation the calculation of an absorption cross section is an easy task due to the semi-classical treatment.

Absorption cross sections are very interesting to us because there exist some data points to compare our theoretical predictions to. This is the most reasonable possibility to evaluate the quality of our model with pion induced experiments. For pion induced experiments the initial state is trivial. Therefore the results are directly related to the interaction of the pion with the nuclear medium.

There are also a lot of data points obtained by photon induced experiments. The simulation of those reactions consists of two distinct parts. First one needs a good model for the γ-nucleon reactions which produce the pions inside the nuclear medium. Here medium modifications might play a role and already the initialization of the initial state is therefore model dependent. Then one needs a good model for the final- state interactions of the pions. If there are discrepancies between the theoretical model and the experimental data, then it might be difficult to distinguish between shortcomings in the initial and the final state. Hence those experiments are a benchmark to evaluate the quality of our final-state model for the pions, but the π-induced experiment is better suited in our energy regime.

7.4.1 Qualitative understanding

To get a qualitative understanding of the absorption process, we first want to study where the absorption takes place in position space. The figures 7.4 and 7.5 give a qualitative impression at different kinetic energies of the incoming negatively charged pion.

In figure 7.4 we see where the absorption takes place in the nucleus if we introduce a hadronic potential for the pion. The figure 7.5 shows the same for the simulation without hadronic potential. We count the number of pions $N_{prod}(b, z)$ which were produced with impact parameter b and coordinate in beam direction z. In the same way we determine $N_{abs}(b, z)$ as the number of absorbed pions at (b,z). Then we evaluate

$$N_{eff\ abs}(b, z) = \frac{N_{abs}(b, z) - N_{prod}(b, z)}{N_{init}(b)}$$

which is the effective number of pions absorbed at b, z. We divide by $N_{init}(b)$ in equation (7.2) to cancel the geometrical effect that there are more pions initialized with large b values than with low ones. In the end we perform those evaluations for a set of different kinetic energies of the pion.

The coding of the colors is chosen to be the same for all plots:

- Black denotes the place where the maximal production rate is encountered.
- In regions which are colored navy blue, there is no effective absorption taking place - either no processes are taking place or there are occurring as much absorption processes as production processes.
- Going down the color scheme to red, the effective absorption is increasing. In red regions the effective absorption is maximal.

Let us investigate the graphs of figure 7.4 and 7.5:

10 MeV. Here the hadronic potential shows its full strength. For the standard simulation all the absorption takes place on the surface of the Lead nucleus. In the simulation without the hadronic potential the absorption takes place all over in the nucleus which means that the pion can penetrate deeply into the nucleus. We have seen in figure 6.7 that the mean free path drops rapidly at low energies if we include the hadronic potential. This can also be seen in those plots.

40 MeV. We have seen in figure 5.2 that the potential is nearly vanishing at this energy for nearly all densities. Therefore it easy to understand why we do not see a difference between both types of simulations. Around 40 MeV the mean free path of the pion is maximal. Therefore the pions are penetrating the whole nucleus before being absorbed.

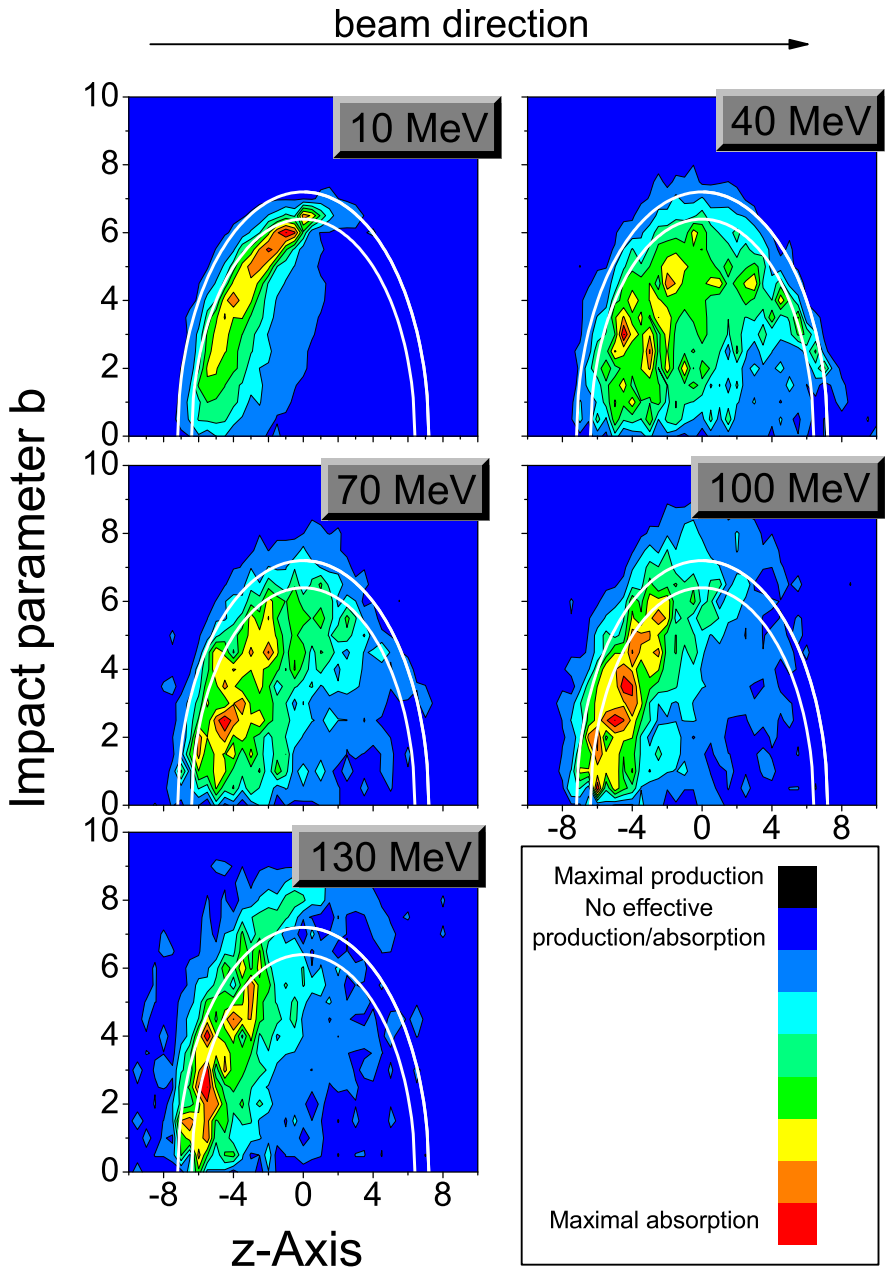

Figure 7.4: Qualitative picture of the effective π^- absorption on Lead in the standard BUU simulation at different kinetic energies. The two white shades show the $radius \pm surface$ of the nucleus.

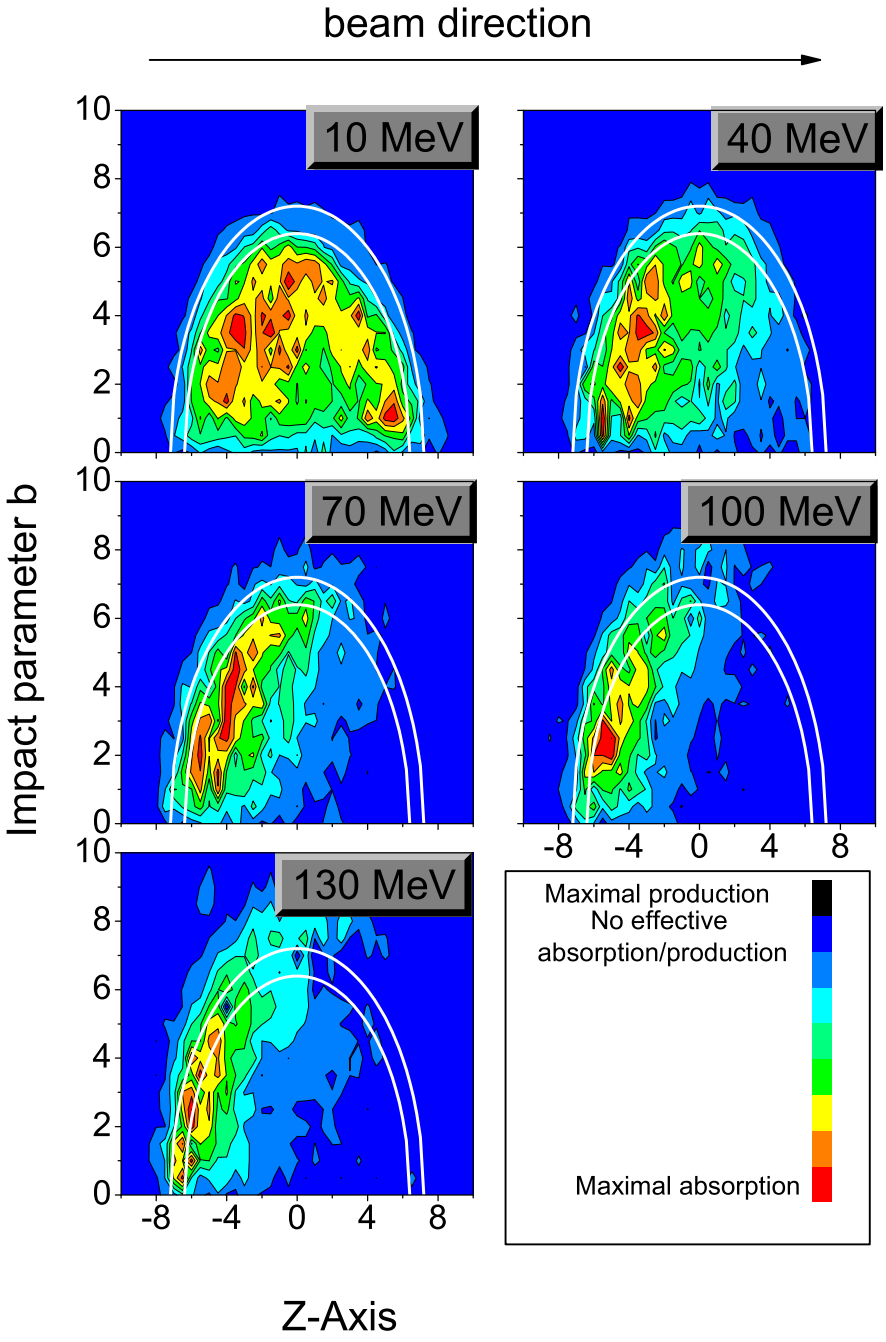

Figure 7.5: Qualitative picture of the π^- absorption on Lead without the hadronic potential at different kinetic energies. The two white shades show the $radius \pm surface$ of the nucleus.

70 MeV and 100 MeV. We see in both figures a slight enhancement of absorption processes inside the nucleus. For 70 MeV the mean free path amounts 2.5 fm according to figure 6.7 in the bulk medium. This allows for a deep penetration of the nuclear medium. At $100MeV$ we see that the mean free path decreases - for both types of simulations the penetration decreases.

130 MeV. According to figure 6.7 the mean free path has now dropped to 1.5 fm. The main absorption is now occurring at the surface again. The penetration is in both cases rather low although it seems to be a little enhanced for the standard simulation with the attractive hadronic potential included.

7.4.2 Quantitative results

Now we want to compare quantitative results of the BUU simulation to absorption data. In figures 7.6, 7.7 and 7.8 we show calculations for different nuclei. The results of the BUU simulation are labeled in the same way as for the reaction cross sections. In figure 7.6 we see good agreement with the data. The very old Carbon data of 1951 should not be taken too serious. Both nuclei of figure 7.6 are rather light.

Interpretation of the kink at 30 MeV. The small kink at 30 MeV in the graphs denoted 'BUU', which was already noticed in the reaction data, can be explained by two effects which work in opposite directions. The probability for the pions to get absorbed depends on two parameters:

- The distance which they have to travel inside the nuclear medium.
- The mean free path inside this medium.

We have seen in figure 6.7 that the mean free path breaks down at very low energies if we implement a hadronic potential. Hence the absorption cross section should increase due to the decrease of the mean free path if we go to lower values of the kinetic energy.

But on the other hand the repulsive hadronic potential pushes such low energetic pions easily out of the nucleus and the distance they have to travel inside the medium decreases. Below the kink at 30 MeV the effect of the repulsion is more important and the absorption cross section decreases. Above the kink we see the effect of decreasing mean free path coming into play because here the slope of the absorption cross section is negative. However, in the data points we do not see such a kink. The kink is thus a remnant of the semi-classical approximation. Already in section 6.6.2 we have seen that the classical trajectories do overestimate the influence of the hadronic potential on the mean free path at very low energies.

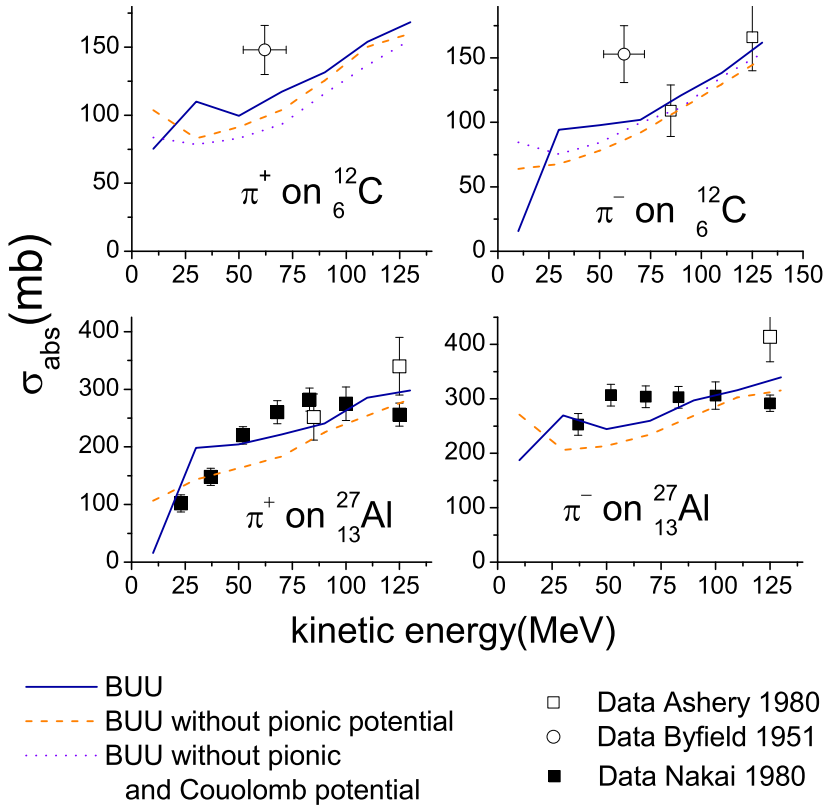

Figure 7.6: Absorption on light nuclei depending on the choice of potentials for the pion. Data points are taken out of [BKL+52],[A+81] and [N+80].

The overall agreement is slightly better if the hadronic potential is included.

Figure 7.7 shows the cross sections for Copper and Tin. Regarding the curve labeled 'BUU', we see rather good agreement with the data for the Tin nucleus. The results for the Copper nucleus are rather poor. Both nuclei are of medium size, therefore it is hard to understand why the model works for one nucleus and not for the other.

The overall agreement to data is much better if the hadronic potential is included. The importance of the Coulomb potential can be see in the Tin graphs. Here the Coulomb force is mainly responsible for the shape of the cross section. Also for these nuclei a kink in the 'BUU' curve at 30 MeV can be noticed.

Figure 7.8 shows results for massive nuclei. For the Gold nucleus the agreement to data is excellent if we include the hadronic potential. In the case of the Lead nucleus we see some agreement with the absorption cross sections reported by Oset et al. [NO93]. The kink at 30 MeV has disappeared. For those nuclei the Coulomb potentials are more pronounced and overwhelm at lower energies

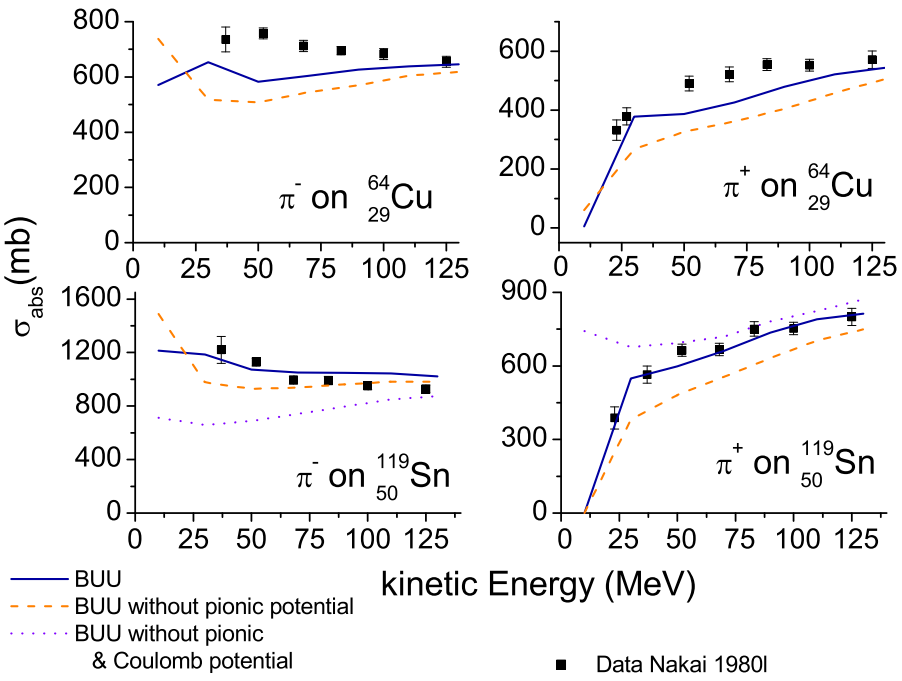

Figure 7.7: Absorption on medium-sized nuclei depending on the choice of potentials for the pion. Data points are taken out of [N+80].

the effect of the decreasing mean free path for the curve labeled 'BUU'. The agreement to data is much better if the hadronic potential is included.

Short summary. In contrast to the reaction cross section, the absorption cross section is more sensitive to the hadronic potential of the pion. At kinetic energies of the incoming pion above 30 MeV we observe an increase in the absorption cross sections due to the hadronic potential.

In terms of the mean free path alone one cannot explain the difference. We have already seen in figure 6.7 that the mean free path is quite insensitive to the hadronic potential. Only at very low energies the mean free path is affected and becomes much smaller when the hadronic potential is included. This effect can actually be seen in figures 7.6 and 7.7 where we noticed the small kinks at roughly 30 MeV. Since we do not observe such a kink in the data sets we must conclude that we really do overestimate the effect of the potential on the mean free path as suspected in section 6.6.2 where we compared our mean free path to the quantum mechanical analysis carried out by by Mehrem, Radi and Rasmussen [MRR84].

Since the mean free path is mainly unaffected by the hadronic potential above 30 MeV we conclude that rather the modification of the dynamics of the pion is the main effect of the hadronic potential. In its repulsive regime the hadronic potential pushes the pion outwards and the overall path of the pion in the nu-

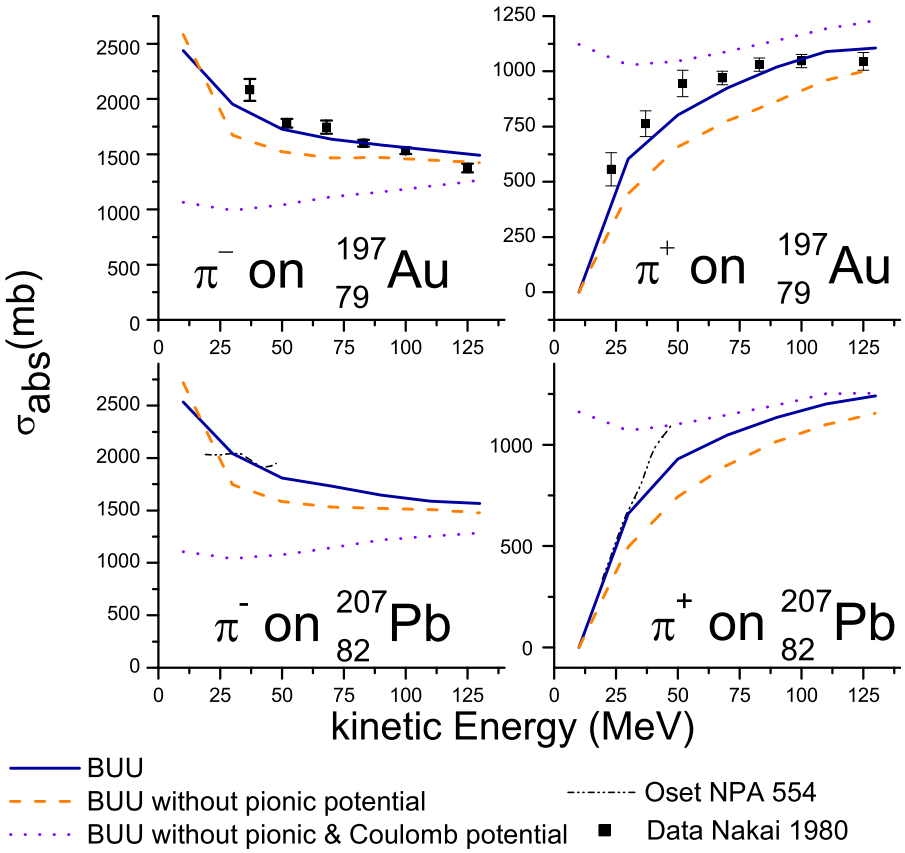

Figure 7.8: Absorption on heavy nuclei depending on the choice of potentials for the pion. Data points are taken out of [N+80].

cleus becomes shorter. Therefore the probability of absorption is decreased. The attractive behavior at larger energies causes an extended distance which the pion has to travel inside the nucleus. Thus the probability of absorption is enhanced.

Minor comments on the data sets. The data sets themselves already include some theoretical assumptions by the experimentalists: For example assumptions on angular distributions of the pions, assumptions on the ratio of charge exchange and absorption. The disagreement to the very old data sets of 1951 [BKL+52] should not be considered too important. Nevertheless one would wish to compare to a different newer data set to have a better feeling for the experimental uncertainties.

Conclusions. The overall agreement to the data is very satisfying. Considering the fact that the pions have very large wave lengths at such low energies, the success of our semi-classical BUU model is quite astonishing. Due to the

large wave length one expects also multi-particle collisions to be important. But actually we have only $2 \rightarrow 2$ and $2 \leftrightarrow 3$ processes implemented explicitly in the simulation.

The overall agreement to the data is much better with the hadronic potential included. Introducing this potential, one accounts also for multi-particle interactions for the pion. These interactions are hidden in the mean field potential, but show up explicitly when one is calculating the self energy. The upper picture of figure 2.1 visualizes those multi-particle interactions which are included in the self energy. In the self energy we consider contributions where the pion scatters several times into a Δ-hole loop or even more complicated intermediate states which are included in the calculations by Oset and Nieves [NO93]. In our simulation we add such interactions as a mean field to the explicit two-body and three-body interactions and finally achieve better agreement to the data.

One has to conclude that the mean field of the pion is an important ingredient for transport simulations at such low energies.

7.5 Dependence on the Δ-potential

We have already seen that it is quite important to describe the pion with a mean field in the medium. Actually, one of the most important absorption processes for the pion is the process

$$N\ N\ \pi \rightarrow \Delta N \rightarrow NN.$$

The potential for the nucleon is rather well established. But we need to ask for the Δ-potential. There are three choices of potential we want to study:

Potential 1. The standard potential in our BUU simulation is fixed by phenomenology to $V_\Delta = \frac{2}{3}\ V_{Nucleon}$ as described in section 5.3.2.

Potential 2. In this ansatz we describe then Δ-resonance and the nucleons with the same potential $V_\Delta = V_{Nucleon}$.

Potential 3. According to Ehehalt [Ehe92] we define also an effective Δ-hole energy on basis of the simple Δ-hole model, which was discussed in section 2.3. We define in analogy to equation (2.7)

$$\omega_{eff}^{\Delta-hole} = (1 - Z_1)\ \omega_1 + (1 - Z_2)\ \omega_2$$

and interpret in nonrelativistic approximation the following term as the energy of a Δ-hole state:

$$\omega^{\Delta-hole}(p) = \frac{p^2}{2m_\Delta} + m_\Delta + V_\Delta - m_N - V_N.$$

Demanding $\omega^{\Delta-hole} = \omega_{eff}^{\Delta-hole}$ we end up with an equation for the potential of the Δ-resonance

$$V_\Delta = (1 - Z_1)\omega_1 + (1 - Z_2)\omega_2 - \frac{p^2}{2m_\Delta} - m_\Delta + m_N + V_N \,.$$

In figure 7.9 the influence of the different choices for the Δ-potential is shown. Although the potentials 1 and 3 differ quite a lot in the overall shape, both potentials nearly give the same results on absorption. Only at very low energies the differences become visible.

The potential 2 is much more attractive than the standard potential 1. Therefore we expect the Δ's, which are produced in $N\,\pi \rightarrow \Delta$ events, to be accelerated towards the center of the nucleus.

Pions can only be absorbed by such $\pi\, N \rightarrow \Delta$ processes where the Δ's collide thereafter with a nucleon to scatter into a two-nucleon state. In the vacuum, the Δ would decay into a π meson and a nucleon again. Expecially in the very light nuclei we see a big influence of the Δ potential. In those nuclei the probability for the Δ to decay inside is reduced because the nuclear radius is small. Including now a more attractive potential enhances this probability dramatically because the Δ is pulled inside the nuclear medium.

Wolfram Peters showed in [Pet98] explicitly that the phenomenological value of 30 MeV is a sensible value for the shift of the Δ energy in the medium. Utilizing the distorted wave impulse approximation he compared photon-nucleus scattering data to experiment. To describe the scattering data he needed to introduce such a mass shift for the Δ. This mass shift of 30 MeV is the reason why we favor the 'potential 1' prescription for our simulation.

All absorption and reaction cross section shown in previous sections have been calculated with the 'potential 1' prescription. But it is interesting to see in figure 7.9 that we could fit the absorption data for Copper and the absorption data for π^- on Carbon better by a more attractive Δ potential. Nevertheless all other absorption results favor the 'potential 1' prescription.

It is interesting to see, that the results in this work depend moderately on the explicit value of this mass shift. Therefore a more exact statement concerning the mass shift would be interesting - e.g. how much one might change this value without losing the consistence in the γ-nucleus experiments.

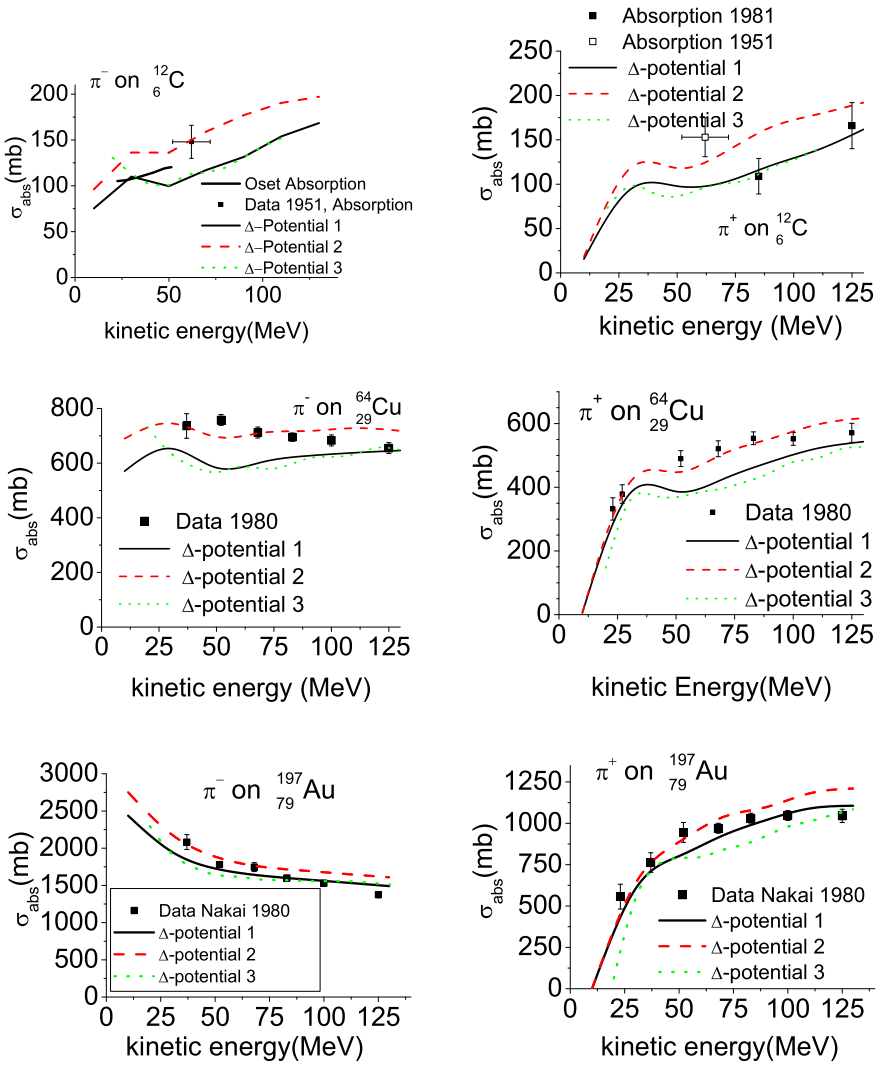

Figure 7.9: Dependence of the absorption cross section on the choice of the Δ potential. All calculations include the hadronic potential of the pion. The solid line represents the calculation with the standard Δ potential in the BUU model. Data points are taken out of [BKL⁺52],[A⁺81] and [N⁺80].

Chapter 8

Photon induced $\pi\pi$ production

According to present knowledge the world we are living in has a spontaneously broken symmetry. This chiral symmetry is expected to be restored in a medium of higher temperature or respectively higher density. The order parameter of this symmetry breaking is the so-called quark condensate $\langle q\overline{q}\rangle$. If this quark condensate vanishes, than the symmetry is fully restored. Models like [BW96] make predictions for $\langle q\overline{q}\rangle$ to decrease by about 30% already at nuclear matter densities. This decrease should have an influence on the hadrons, and their properties should be modified inside a nucleus due to this partial restauration of the chiral symmetry.

The so-called σ-meson or σ-state ($J^P = 0^+$) is in the context of quantum chromodynamics (QCD) the chiral partner of the π-meson ($J^P = 0^-$). One expects both to be mass degenerate in a phase which is chiral symmetric. Since the pions are the Goldstone bosons of the symmetry, one does not expect them to become much more massive in the unbroken phase. Hence the mass of the sigma meson ($m_\sigma \simeq 400 - 1200\ MeV$ in vacuum) is expected to drop to lower values with increasing density of the medium.

In this chapter we will investigate $\gamma A \to \pi\pi A$ processes at photon energies between 400 and 460 MeV. Those processes are well suited to investigate the σ's mass inside a nucleus. The crucial point is, that the process $\gamma A \to \pi^0\pi^0 A$ can also occur via a two step process

$$\gamma A \to \sigma A \to \pi^0\pi^0 A\ .$$

In contrast the channels

$$\gamma A \to \pi^0\pi^\pm A$$

do not allow a σ in the intermediate state. Therefore one expects a shift of the invariant mass of the $\pi^0\pi^0$ final state, if there is some mass shift of the σ in the medium. Whereas one might not expect this mass shift in the $\pi^0\pi^\pm$ final state. The low photon energy is chosen to suppress $\pi^0\pi^0$-production mechanisms different to the $\gamma A \to \sigma A \to \pi^0\pi^0 A$ process

Using different targets one investigates the processes happening at different effective densities. The Carbon target has a much larger surface diameter to nuclear radius ratio than the Lead target, therefore the effective density in the Lead target is larger than in the Carbon target. The TAPS collaboration [M$^+$02] estimated their effective densities to be $0.35\rho_0$ for Carbon and $0.65\rho_0$ for Lead. They reported a shift of the invariant mass of the $\pi^0\pi^0$ final state in the medium and no shift in the $\pi^0\pi^\pm$ final state [M$^+$02].

Already in [MARBM04] we investigated $\gamma A \rightarrow A\pi\pi$. Hence we first want to compare the model presented in this thesis to the model described in the latter reference.

8.1 Comparison to [MARBM04]

Altough both models are based on BUU methods, the physical input differs. In contrast to the model described in [MARBM04] we use a different method to simulate the absorption of the pions in the final state, and we also use a different method to model the initial γ-absorption in the nucleus.

8.1.1 The treatment of the γ-absorption

In [MARBM04] a model based on effective field theory [NOVR01] [TO96] is exploited to describe the process

$$\gamma N \rightarrow \pi\pi\ N\ .$$

Our model uses elementary vacuum cross sections as input [Eff96]. In contrast to [MARBM04] we use just a phase-space distribution for the two correlated pions. We are aware of the fact that the model presented in [MARBM04] is superior in the distribution of the pions. Nevertheless we are using it to keep it simple.

8.1.2 The final state processes

The model presented in this thesis

The model presented in this thesis describes the final state interactions of the pions by a off-shell-resonance model. On top of the processes mediated by the resonances, we introduce background processes with cross sections deduced from elementary reactions. This model was described in chapter 5. We propagate explicitly the resonances and account for the medium by potentials for those resonances and we introduce modifications of their collisional width [Eff99].

The absorption of the pion is described by the explicit two-step process

$$\pi NN \rightarrow \Delta N \rightarrow NN$$

and the background process (see section 5.5.3)

$$\pi\ N\ N \rightarrow N\ N\ .$$

This process is isotropic in the simulation, which might be a problem one should eliminate in future calculations. For the scattering processes we introduced in our model besides the explicit two-step process

$$\pi N \rightarrow \Delta \rightarrow \pi N$$

a new background process

$$\pi N \rightarrow \pi N$$

such that we describe the experimental data for elementary collisions in vacuum (see section 5.5.1)

$$\sigma_{data} = \sigma_{\pi N \rightarrow \pi N} + \sigma_{\pi N \rightarrow N R \rightarrow \pi N}\ .$$

However, in the medium the

$$\pi N \rightarrow \Delta \rightarrow \pi N$$

scattering process is modified due to the in-medium modification of the resonance. We modify the dynamics by introducing a potential for the Δ (section 5.3.2) as well as the lifetime of the resonance by introducing an extra collisional width (Details in [Eff99] pages 248-249.).

The model presented in [MARBM04]

In [MARBM04] no resonances were included in the model, only pions and nucleons were propagated explictly. The absorption of the pion was described by an absorption rate Γ_{abs} exploiting optical potentials [NO93] [GRO$^+$91]. In appendix D.2 this is explained in the case of [NO93]. According to this rate, the pions were absorbed in each time step Δt with the probability

$$p_{abs} = 1 - \exp\left(\Gamma_{abs}\Delta t\right)\ .$$

The elastic scattering processes were simulated by the $\pi\ N \rightarrow \pi\ N$ process with cross sections deduced from experimental data on the elementary processes in vacuum. Here no in-medium modification of the cross section due to the modification of the resonances is implemented.

The potential for the nucleon is the same in both calculations. In [MARBM04] no potential for the pion was introduced.

8.2 Results

In figure 8.1 we show results for $\gamma A \to \pi\pi A$. The dotted curve is the result of [MARBM04]; the dashed curve represents the result of the model presented in this thesis without the real part of the hadronic potential and the solid curve shows the result with hadronic potential.

In the channel $\gamma A \to \pi^0\pi^0 A$ the result of [MARBM04] reproduces best the experimental results. Especially the first three points in the low-mass spectra of the Lead nucleus could not be reproduced with the model presented in this thesis. We observe in in this channels a downward shift of the invariant mass spectra going from Carbon to Lead. This downward shift is solely caused by final state effects and is the same with and without potential. For the model described in this thesis the shift is slightly larger than for [MARBM04]. This might be caused by the phase-space distribution of the initial $\pi^0\pi^0$ state, which is known to have shortcomings in this channel.

All results for the channel $\gamma A \to \pi^0\pi^\pm A$ disagree with the data. The absolute magnitude is roughly by a factor three too large. Also in this channel a downward shift of the invariant mass spectra going from Carbon to Lead can be observed for the theoretical models, but the experimental data do not show such a shift.

Let us compare the results obtained with the model of this thesis. The introduction of the hadronic potential leads to lower results, which means increased pion-absorption, in all channels while the peak position stays the same. The increase in the absorption can be understood by the short mean free path for the pions with $E_{kin} \leq 30\ MeV$ when including the hadronic potential (figure 6.7). For the more massive Lead nucleus the effect of the hadronic potential is more pronounced.

It is astonishing that both this model and the model described in [MARBM04] agree in a moderate manner with the data in the $\gamma A \to \pi^0\pi^0 A$ channel while they totally fail to reproduce the $\gamma A \to \pi^0\pi^\pm A$ channel. The two different models use very different physical input for the initial γ-absorption as well as for the final-state interactions of the pions. The big discrepancies in the comparison to the data sets is not understood.

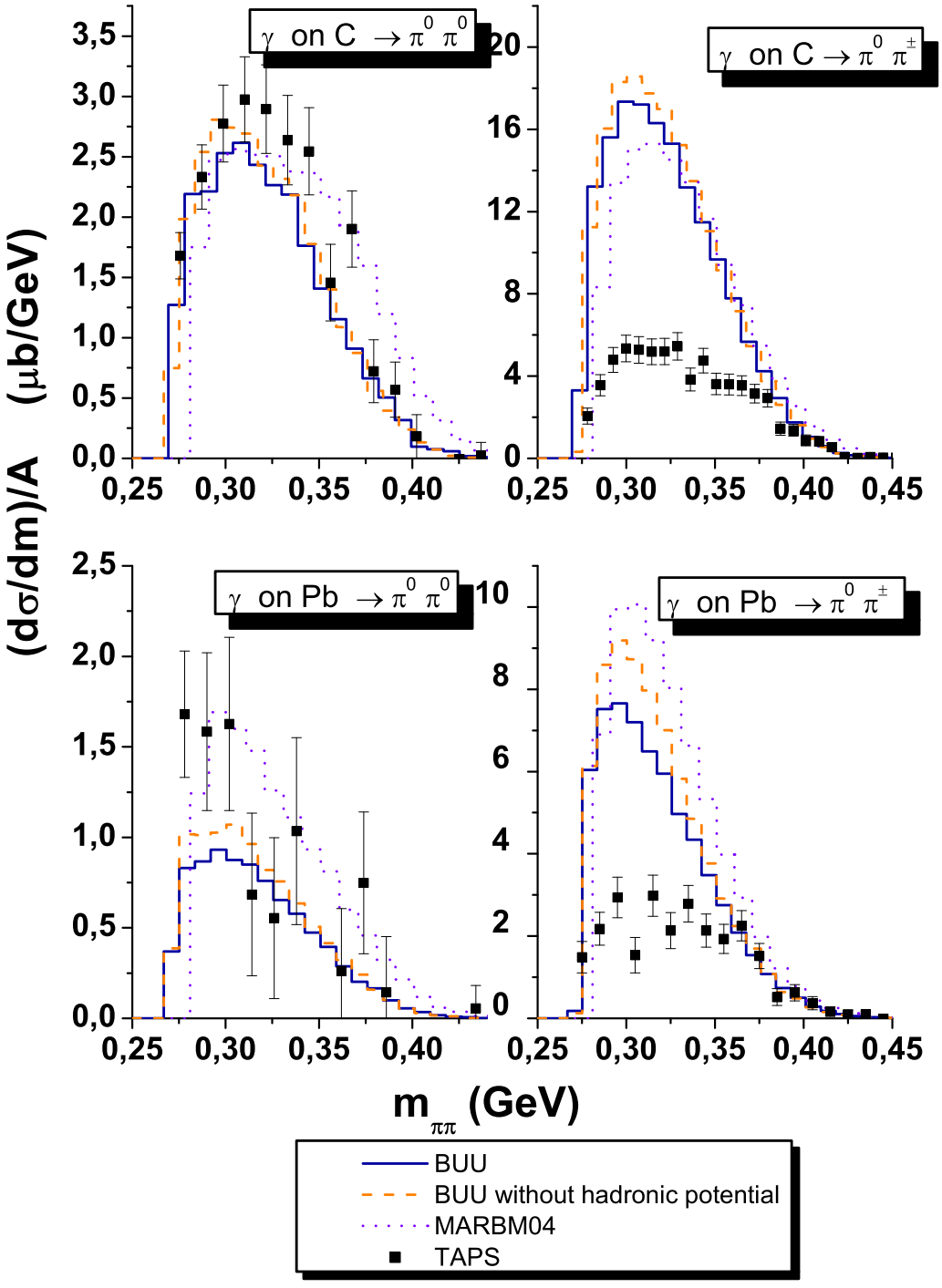

Figure 8.1: Results for $\gamma A \to \pi\pi A$. Data are taken out of [M+02].

Chapter 9

Summary and Outlook

Summary. In this thesis we investigated low energetic pions in the framework of a BUU transport model. We were able to show that also in a regime of large wave length the semi-classical BUU model still gives reasonable results.

Exploiting the Δ-hole model we derived a mean field potential for the pions. For low energies we utilized the model described in [NO93] and for higher energies a first order result was obtained.

We improved the final state cross sections for the pions and included the mean field derived by the Δ-hole model in the BUU simulation. Finally we investigated the influence of this mean field on parameters like the mean free path and the velocity of the pion inside the medium and observables like π- and γ-induced scattering events.

For the absorption cross sections we achieved very satisfactory agreement with the data sets [N^+80] [A^+81]. Here the inclusion of a hadronic potential for the pion lead to an increase in the cross sections due to the modifications of the dynamics of the pion. The agreement to data was very much improved by this mean field. In fully quantum mechanical calculations we were able to show that the real part of the pionic optical potential plays a crucial role in the analysis of reaction events. This could not be reproduced in the semi-classical BUU picture were the dependence on the real part was rather moderate for the reaction cross sections.

The results concerning the mean free path of the pion inside the nuclear medium were compared to fully quantum mechanical calculations [Hec81] [MRR84]. We observed that the classical picture overestimates the influence of the pionic hadronic potential on the mean free path of the pion below $E_{kin} = 30\ MeV$. This was also observed in the simulation of the π-induced experiments. We attribute this failure to the quantum mechanical tunneling mechanism which becomes im-

portant at very low energy and which can not be accounted for in a semi-classical model. Comparing to [MRR84] we found qualitative agreement while we were able to show that the vacuum approximation [EW88] is not appropriate at such low energies.

Finally we compared results of $\gamma A \to \pi\pi A$ to the experimental data by TAPS [M$^+$02]. Also with the model presented in this thesis we could not solve the problem in the $\gamma A \to \pi^0\pi^\pm A$ channel. Like in an earlier work [MARBM04] we overestimate the experimental data roughly by a factor of three. In the $\gamma A \to \pi^0\pi^0 A$ channel we observed moderate agreement with the data sets. Hence the channel $\gamma A \to \pi^0\pi^\pm A$ remains a puzzle.

Outlook. In this thesis we represented the pion by a classical quasi-particle with well defined mass. A next step of sophistication would be to include the spectral function of the pion in the simulation and to propagate the pion with a broad mass spectra. Therefore one needs to derive a consistent self energy which is fully relativistic to solve the problem of super-luminous pions which one is often confronted with in such an ansatz. At such low energies this fully relativistic self energy should include nucleon-hole-loop as well as Δ-hole-loop contributions. In [LM$^+$02] such an ansatz for the Δ resonance region was explored, but also here it was not possible to utilize the self energy in controlling the dynamics of the pions.

The nice results on absorption data are encouraging. The good results at such low energies have not been expected. Nevertheless one must be aware of the fact that such semi-classical models are rather designed for the simulation of high-energy events.

Part IV

Appendix

Appendix A

Units, Parameters, Abbreviations

Units

The work is presented in units where

$$\hbar = c = 1$$

Therefore one gets

$$[momentum] = [energy] = GeV = 1000 MeV$$

Parameters

$$\begin{aligned} f_\Delta &= 2.0 \\ g' &= \left(\frac{f_\Delta}{m_\pi}\right)^2 \hat{g} = 0.62 \\ \rho_0 &= 0.17\ fm^{-3} \end{aligned}$$

Abbreviations

$\wp$	Principal Value
$\Re$	Real part
$\Im$	Imaginary part
$h.c.$	hermitean conjugate

Appendix B

Useful tools

B.1 The formula $\frac{1}{x+i\eta} = \wp\frac{1}{x} - i\pi\delta(x)$

The symbolic formula $\frac{1}{x+i\eta} = \wp\frac{1}{x} - i\pi\delta(x)$ represents

$$\lim_{\eta\to 0}\int_a^b \frac{f(x)}{x+i\eta} = \wp\int_a^b \frac{dxf(x)}{x} - i\pi\int_a^b dxf(x)\delta(x) \tag{B.1}$$

B.2 Plot of vacuum dispersion relation

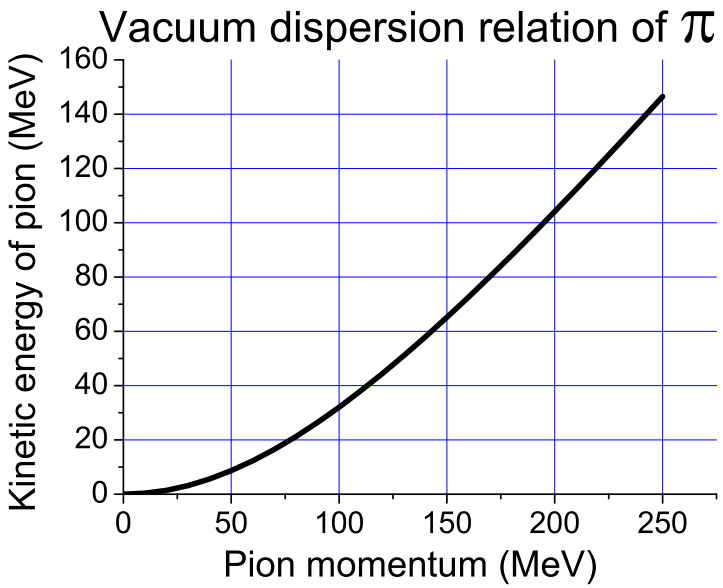

Appendix C

Details concerning the self energy of the π meson in the simple Δ-hole model

C.1 Feynman rules in the Δ-hole model

C.1.1 Vertices

The s_i indices stand for spin and i_i are isospin indices. The $S^\dagger, S$ and $T^\dagger, T$ operators of equation (2.2) translate into Clebsch-Gordan factors for each vertex. This can be seen directly in their definition in equation (2.3).

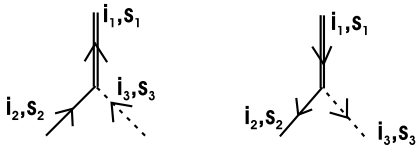

$$i\frac{f_\Delta}{m_\pi}\left(\tfrac{1}{2}, s_2; 1, s_3 | \tfrac{3}{2}, s_1\right)\left(\tfrac{1}{2}, i_2; 1, i_3 | \tfrac{3}{2}, i_1\right) \times \text{(momentum of pion)}$$

Table C.1: π-nucleon-Δ vertices

C.1.2 Propagators

Nucleon propagator:

$$G_N(E,p) = G_{particle}(E,p) + G_{hole}(E,p) = \frac{\theta(|p| - p_f)}{E - E_N(p) + i\eta} + \frac{\theta(p_f - |p|)}{E - E_N(p) - i\eta}$$

Δ-propagator without decay width of the Δ:

$$G_\Delta(E,p) = \frac{1}{E - E_\Delta(p) + i\eta}$$

C.2 Δ-hole loop

For the direct Δ-hole loop with pion charge q_π and nucleon charge q_N we get using the Feynman rules from above

$$i\Delta_N^{direct}(\omega,q) = (-1)\; i^2\widehat{F}\int \frac{dEd^3p}{(2\pi)^4} G_{hole}(E,p)G_\Delta(E+\omega,q+p).$$

We sum over the spin indices of the nucleon and the Δ. We average over the pion spin. The factor $\widehat{F}$ includes all isospin and spin factors. The expression is explicitly dependend on the charge of the nucleon N. In the end we are going to take care of the isospin sum in the loop. The vertices are actually treated as if they were $\pi-\Delta$-nucleon vertices. This is actually only true if the Δ-hole bubbles of figure (2.1) can be considered independent in spin and isospin, that means that the short range mediator carries well defined spin and isospin like the pion does.

$$\begin{aligned}\widehat{F} &= \underbrace{\frac{1}{3}\sum_{r,s,t}\left(\frac{1}{2},r;1,s|\frac{3}{2},t\right)^2}_{\text{spin sum and averaging}}\underbrace{\left(\frac{1}{2},q_N;1,q_\pi|\frac{3}{2},q_N+q_\pi\right)^2}_{\text{isospin factors}} \\ &= \frac{4}{3}\underbrace{\left(\frac{1}{2},q_N;1,q_\pi|\frac{3}{2},q_N+q_\pi\right)^2}_{\text{isospin factors}} \end{aligned} \tag{C.1}$$

First one solves the energy integration:

$$\begin{aligned}&\int \frac{dE}{2\pi} G_{hole}(E,p)G_\Delta(E+\omega,q+p) \\ =\;& \int_{-\infty}^{\infty}\frac{dE}{2\pi}\frac{\theta(p_f-|p|)}{(E-E_N(p)-i\eta)(E+\omega-E_\Delta(p+q)+i\eta)}).\end{aligned}$$

Now one can use complex calculus to close the integration contour in the upper complex halfplane C_u by Jordan's Lemma. The result is the residual at the $E=E_N(p)+i\eta$ pole.

$$\begin{aligned}&\int \frac{dE}{2\pi} G_{hole}(E,p)G_\Delta(E+\omega,q+p) \\ =\;& \theta(p_f-|p|)\frac{2\pi i}{2\pi}\left[\frac{1}{E+\omega-E_\Delta(p+q)+i\eta}\right]_{E=E_N(p)+i\eta} \\ =\;& \theta(p_f-|p|)\frac{i}{E_N(p)+i\eta+\omega-E_\Delta(p+q)+i\eta}\;.\end{aligned}$$

Therefore, in the limit $\eta\longrightarrow 0$,

$$i\Delta_N^{direct}(\omega,q) = \widehat{F}\int\frac{d^3p}{(2\pi)^3}\;\frac{i\theta(p_f-|p|)}{\omega+E_N(p)-E_\Delta(p+q)}\;.$$

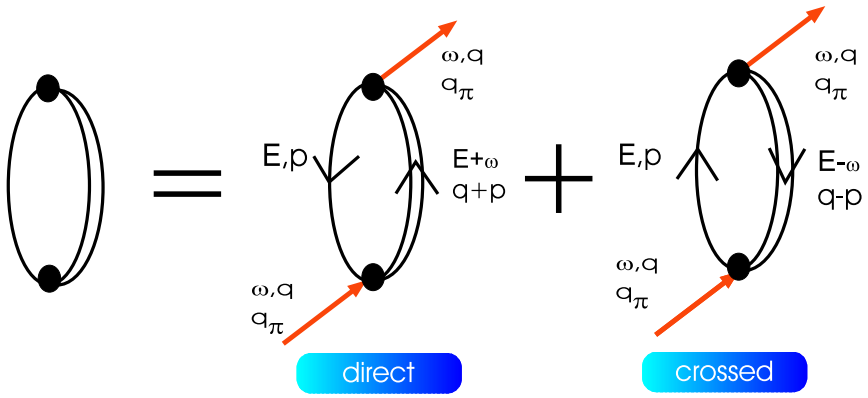

Figure C.1: The direct term and crossed term of the Δ-hole. The arrows are just meant to guide the eye and to make momentum,energy,spin and isospin flow clearly. In principle one is evaluating just the Δ-hole loop.

Now one introduces a non-relativistic approximation for the energies of the nucleon and Δ:

$$\begin{aligned} E_N(\vec{p}) &= \frac{\vec{p}^2}{2m_{Nuk}} + m_{Nuk} \\ E_\Delta(\vec{p}+\vec{q}) &= \frac{(\vec{p}+\vec{q})^2}{2m_\Delta} + m_\Delta \ . \end{aligned}$$

This leads to

$$\begin{aligned} i\Delta_N^{direct}(\omega,q) &= \widehat{F}\int \frac{d^3p}{(2\pi)^3}\ \frac{i\theta(p_f-|\vec{p}|)}{\omega + E_N(p) - E_\Delta(\vec{p}+\vec{q})} \\ &= \widehat{F}\int \frac{d^3p}{(2\pi)^3}\ \frac{i\theta(p_f-|\vec{p}|)}{\omega + m_{Nuk} - m_\Delta - \frac{\vec{q}^2}{2m_\Delta} - \frac{\vec{p}\vec{q}}{m_\Delta} + \vec{p}^2(\frac{1}{m_{Nuk}} - \frac{1}{m_\Delta})} \ . \end{aligned}$$

One now defines

$$\omega_\Delta = m_\Delta - m_{Nuk} + \frac{\vec{q}^2}{2m_\Delta} MeV.$$

Using

$$|\vec{p}| < p_f = (3\pi^2\rho_N)^{1/3} \cong 250\frac{MeV}{c}$$

one can neglect $\vec{p}^2(\frac{1}{m_{Nuk}} - \frac{1}{m_\Delta})$. Taking the low energy limit

$$\omega \to m_\pi \Rightarrow q \to 0$$

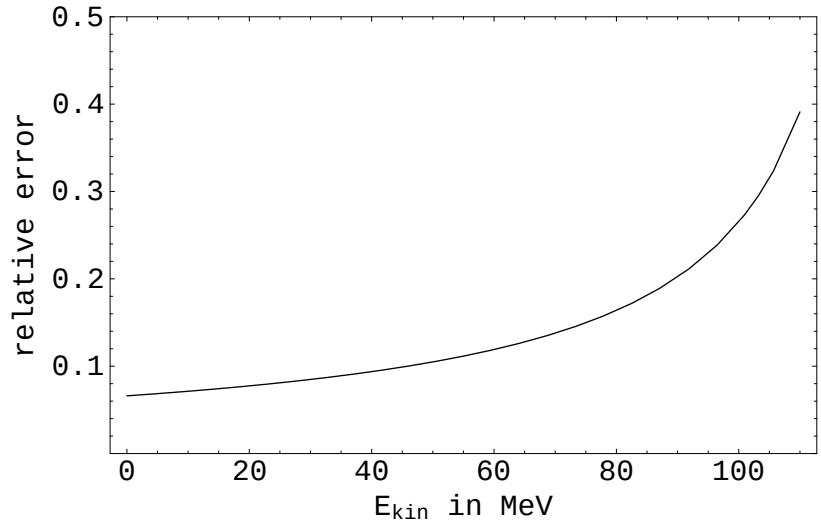

Figure C.2: Quality of the approximation of equation (C.2) in dependence of pionic kinetic energy.

one can neglect $\frac{\vec{p}\vec{q}}{m_\Delta}$ in comparison to $\omega_\Delta - \omega$. The density ρ_N is the density of the specific nucleon - either proton or neutron.

$$\begin{aligned} i\Delta_N^{direct}(\omega,q) &= \widehat{F}\int \frac{d^3p}{(2\pi)^3}\,\frac{i\theta(p_f-|\vec{p}|)}{\omega-\omega_\Delta-\frac{\vec{p}\vec{q}}{m_\Delta}+\vec{p}^2(\frac{1}{m_{Nuk}}-\frac{1}{m_\Delta})} \\ &= \widehat{F}4\pi\int_0^{p_f}\frac{dp}{(2\pi)^3}\,\frac{ip^2}{\omega-\omega_\Delta} \\ &= \widehat{F}4\pi\frac{1}{(2\pi)^3}\frac{1}{3}\frac{ip_f^3}{\omega-\omega_\Delta} \\ &= -i\widehat{F}\frac{1}{3\pi^2}\frac{p_f^3}{\omega_\Delta-\omega} \\ &= -i\widehat{F}\frac{1}{2}\rho_N\frac{1}{\omega_\Delta-\omega}\ . \end{aligned} \tag{C.2}$$

The quality of the approximation in equation (C.2) can be seen in figure C.2, where we have plotted

$$\begin{aligned} \text{relative error} &= \frac{f(E_{kin})-g(E_{kin})}{f(E_{kin})} \\ \text{with}\qquad f(E_{kin}) &= \int d^3p\frac{\theta(p_f-|\vec{p}|)}{\omega-\omega_\Delta-\frac{\vec{p}\vec{q}}{m_\Delta}+\vec{p}^2(\frac{1}{m_{Nuk}}-\frac{1}{m_\Delta})} \\ g(E_{kin}) &= \int d^3p\frac{\theta(p_f-|\vec{p}|)}{\omega-\omega_\Delta} = \frac{4\pi p_f}{3}\frac{1}{\omega-\omega_\Delta}\ . \end{aligned}$$

The error is small in a kinetic energy regime smaller 100 MeV. The crossed-term follows by $\omega \leftrightarrow -\omega$ and $q \leftrightarrow -q$ and $q_\Delta = q_\pi + q_N \Longrightarrow q_\Delta = -q_\pi + q_N$. Therefore

we get

$$i\Delta_N^{crossed}(\omega,q) = -i\frac{\widehat{G}}{2}\rho_N\frac{1}{\omega_\Delta+\omega}$$

with

$$\widehat{G} = \frac{4}{3}\underbrace{\left(\frac{1}{2},q_N;1,-q_\pi|\frac{3}{2},q_N-q_\pi\right)^2}_{\text{isospin factors}} . \tag{C.3}$$

Summing both parts up one finally gets:

$$\begin{aligned} i\Delta_N(\omega,q) &= i\Delta_N^{direct}(\omega,q)+i\Delta_N^{crossed}(\omega,q) \\ &= -i\,\frac{1}{2}\rho_N\left(\frac{\widehat{F}}{\omega_\Delta-\omega}+\frac{\widehat{G}}{\omega_\Delta+\omega}\right) . \end{aligned}$$

Now one has to take care of the nucleon-Δ isospin sum:

$$\begin{aligned} i\Delta(\omega,q) &= \sum_{N=proton,neutron} i\Delta_N(\omega,q) \\ &= -i\frac{2}{3}\left(A_{proton}+A_{neutron}\right) \end{aligned}$$

$$A_{proton} = \rho_{proton}\left(\frac{\left(\frac{1}{2},\frac{1}{2};1,q_\pi|\frac{3}{2},q_\pi+\frac{1}{2}\right)^2}{\omega_\Delta-\omega}+\frac{\left(\frac{1}{2},\frac{1}{2};1,-q_\pi|\frac{3}{2},-q_\pi+\frac{1}{2}\right)^2}{\omega_\Delta+\omega}\right)$$

$$A_{neutron} = \rho_{neutron}\left(\frac{\left(\frac{1}{2},-\frac{1}{2};1,q_\pi|\frac{3}{2},q_\pi-\frac{1}{2}\right)^2}{\omega_\Delta-\omega}+\frac{\left(\frac{1}{2},-\frac{1}{2};1,-q_\pi|\frac{3}{2},-q_\pi-\frac{1}{2}\right)^2}{\omega_\Delta+\omega}\right) .$$

Evaluating the Clebsch-Gordan elements one gets for π^- :

$$\begin{aligned} A_{Proton}+A_{Neutron} &= \rho_p\left(\frac{\frac{1}{3}}{\omega_\Delta-\omega}+\frac{1}{\omega_\Delta+\omega}\right)+\rho_n\left(\frac{1}{\omega_\Delta-\omega}+\frac{\frac{1}{3}}{\omega_\Delta+\omega}\right) \\ &= \frac{2}{3}\frac{1}{\omega_\Delta^2-\omega^2}\left(\rho_p(2\omega_\Delta-\omega)+\rho_n(2\omega_\Delta+\omega)\right) \\ &= \frac{4}{3}\frac{\omega_\Delta}{\omega_\Delta^2-\omega^2}\rho+\frac{2}{3}\frac{\omega}{\omega_\Delta^2-\omega^2}\left(\rho_n-\rho_p\right) , \end{aligned}$$

for π^0 :

$$\begin{aligned} A_{Proton}+A_{Neutron} &= \rho_p\left(\frac{\frac{2}{3}}{\omega_\Delta-\omega}+\frac{\frac{2}{3}}{\omega_\Delta+\omega}\right)+\rho_n\left(\frac{\frac{2}{3}}{\omega_\Delta-\omega}+\frac{\frac{2}{3}}{\omega_\Delta+\omega}\right) \\ &= \frac{4}{3}\frac{\omega_\Delta}{\omega_\Delta^2-\omega^2}\rho , \end{aligned}$$

for π^+ :

$$\begin{aligned} A_{Proton} + A_{Neutron} &= \rho_p \left(\frac{1}{\omega_\Delta - \omega} + \frac{\frac{1}{3}}{\omega_\Delta + \omega} \right) + \rho_n \left(\frac{\frac{1}{3}}{\omega_\Delta - \omega} + \frac{1}{\omega_\Delta + \omega} \right) \\ &= \frac{2}{3} \frac{1}{\omega_\Delta^2 - \omega^2} \left(\rho_p (2\omega_\Delta + \omega) + \rho_n (2\omega_\Delta - \omega) \right) \\ &= \frac{4}{3} \frac{\omega_\Delta}{\omega_\Delta^2 - \omega^2} \rho + \frac{2}{3} \frac{\omega}{\omega_\Delta^2 - \omega^2} \left(\rho_p - \rho_n \right) \ , \end{aligned} \tag{C.4}$$

with $\rho = \rho_p + \rho_n$. In the special case of isospin symmetric matter

$$\rho_{Neutron} = \rho_{Proton} = \frac{\rho}{2}$$

one can easily see that

$$i\Delta(\omega, q) = -i \frac{8}{9} \rho \frac{\omega_\Delta}{\omega_\Delta^2 - \omega^2} \tag{C.5}$$

becomes independent of the charge of the pion.

C.3 Dispersion relation

The dispersion relation which has to be solved is

$$\omega^2 - k^2 - m_\pi^2 - \Pi(\omega, k) = 0 \ . \tag{C.6}$$

C.3.1 Symmetric nuclear matter

For symmetric nuclear matter the dispersion relation can easily be solved [Hen94]. Using (C.5) one gets

$$\begin{aligned} \Pi &= k^2 \left(\frac{f_\Delta}{m_\pi} \right)^2 \frac{\Delta(\omega, k)}{1 - \hat{g} \Delta(\omega, k)} \\ &= k^2 \frac{C \omega_\Delta}{\omega^2 - \omega_\Delta^2 - g' C \omega_\Delta} \end{aligned}$$

with

$$\begin{aligned} f_\Delta &= 2.0 \\ g' &= \left(\frac{f_\Delta}{m_\pi} \right)^2 \hat{g} = 0.62 \\ C &= \frac{8}{9} \left(\frac{f_\Delta}{m_\pi} \right)^2 \rho. \end{aligned}$$

The dispersion relation therefore becomes

$$\begin{aligned} 0 &= \omega^2 - k^2 - m_\pi^2 - \Pi(\omega, k) \\ &= \omega^2 - k^2 - m_\pi^2 - k^2 \frac{C\omega_\Delta}{\omega^2 - \omega_\Delta^2 - g' C\omega_\Delta} \; . \end{aligned}$$

Which can be solved by

$$\omega_{1,2}^2(k) = \frac{1}{2}\left(\widehat{E}^2 + E_{free}^2 \pm \sqrt{\left(\widehat{E}^2 - E_{free}^2\right)^2 + 4k^2 C\omega_\Delta} \right)$$

with

$$\begin{aligned} \widehat{E} &= \sqrt{\omega_\Delta^2 + g' C\omega_\Delta} \\ E_{free} &= \sqrt{k^2 + m_\pi^2} \end{aligned}$$

Consequently the pion propagator can be split into two branches

$$G_\pi(\omega, k) = \frac{1}{\omega^2 - k^2 - m_\pi^2 - \Pi(\omega, k)} = \frac{Z_1}{\omega^2 - \omega_1^2 + i\eta} + \frac{Z_2}{\omega^2 - \omega_2^2 + i\eta}$$

with

$$\begin{aligned} Z_1 &= \frac{1}{2}\left(1 - \frac{\widehat{E}^2 - E_{free}^2}{\sqrt{\left(\widehat{E}^2 - E_{free}^2\right)^2 + 4k^2 C\omega_\Delta}} \right) \\ Z_2 &= \frac{1}{2}\left(1 + \frac{\widehat{E}^2 - E_{free}^2}{\sqrt{\left(\widehat{E}^2 - E_{free}^2\right)^2 + 4k^2 C\omega_\Delta}} \right) \; . \end{aligned}$$

C.3.2 Nonsymmetric nuclear matter

For asymmetric nuclear matter the situation is somewhat more difficult. Due to the factor

$$\frac{\omega}{\omega^2 - \omega_\Delta^2}$$

in $A_{proton} + A_{neutron}$ the polynomial in ω which stems from the dispersion relation (C.6) cannot be solved analytically. Therefore one solves the dispersion relation numerically. The example refers to a worst-case scenario of a lead nucleus, where the isospin asymmetry is very big. The absolute effect in the π^+- and π^--channel should be about the same size in both channels. In the π^0-channel there is no effect.

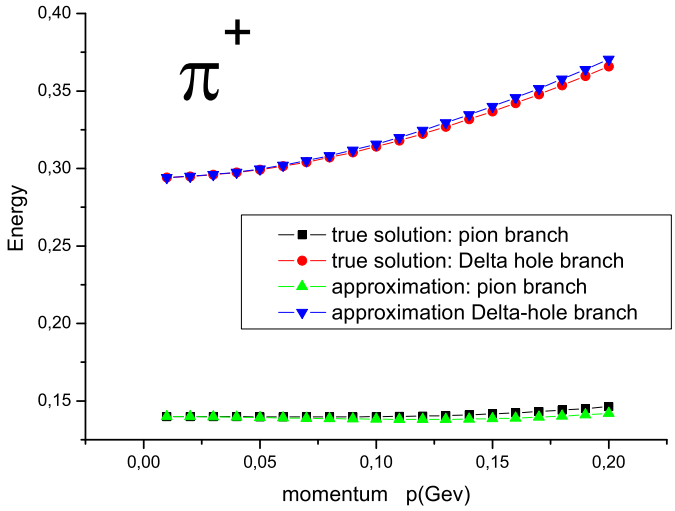

Figure C.3: Quality of the isospin approximation for a π^+ ($\rho = \rho_0$, Pb nucleus)

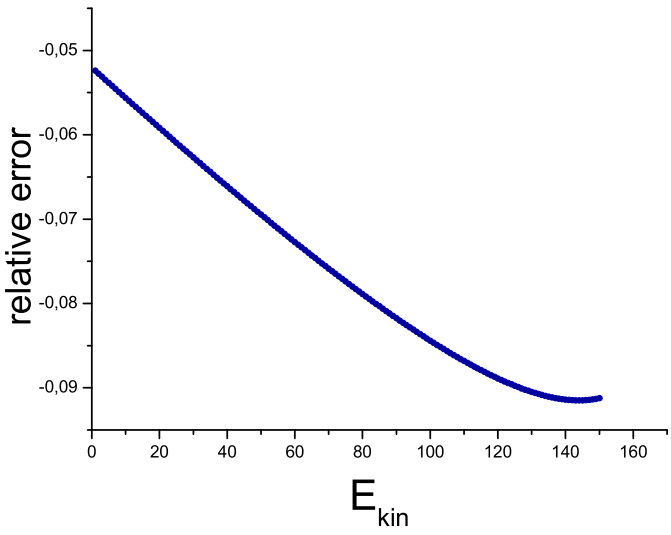

Figure C.4: Quality of the isospin approximation for a π^+ ($\rho = \rho_0$, Pb nucleus)

We compare the dispersion relation of a π^+ with and without the extra term proportional $\rho_{proton} - \rho_{neutron}$ of equation (C.4). The author concludes that this extra term is negligible. Therefore the extra term is set to zero and we use for all cores the results of the isospin symmetric case. The relative error of the selfenergy evaluated at the point

$$\left(p, E = \sqrt{p^2 + m_\pi^2}\right)$$

can be seen in figure C.4. The different dispersion relations are plotted in figure C.3.

Appendix D

Optical potential for pions with low energy

In [NO93] the authors presented a optical pionic potential for low energy pions. The results are based on the pion-nucleus optical potential derived in their work on pionic atoms [JNGR93]. There the pions were assumed to be at rest. Then the authors of [NO93] made some extrapolations to finite kinetic energies, such that their optical potential is assumed to be a good approximation for kinetic energies of the pions below 60 MeV.

The calculations are performed for a π^-. The result for a π^+ is obtained by isospin rotation. For π^0 we use the potential symmetrized in proton and neutron density which is also proposed in [EW88].

In the beginning of this section we will investigate the structure of this potential. It follows a description of the implementation of potential in the BUU simulations. The notation is chosen according to [NO93].

D.1 Structure of the optical potential

The optical potential has two distinct parts. The first part is due to s-wave scattering in the medium. It is derived from scattering data.

The second part is due to p-wave scattering in the medium, which is well described using the formalism of the Δ-hole model. The authors also included some small phenomenological term in their p-wave part to describe better the scattering data. This piece we are going to neglect because it is small and does not have a clear microscopical interpretation.

The full optical potential is the sum of both parts. Higher partial wave contributions can be neglected safely as experimental scattering phase shifts show.

$$V_{opt} = V_{opt}^{s-wave} + V_{opt}^{p-wave} \ .$$

D.1.1 The s-wave term

The s-wave term is given by

$$V_{opt}^{s-wave} = V_1^s + V_2^s \ .$$

The term V_1^s stems from the extrapolation of the theoretical potential used for the pionic atoms. It includes absorptive and quasielastic pieces. The term V_2^s includes only quasielastic contributions and is absent in the limit of $E_{kin} = 0$ of the pion.

D.1.2 The p-wave term

For the p-wave the authors get the following expression

$$2\omega V^{p-wave}(r) = 4\pi \frac{M_N^2}{s} \left[\bigtriangledown \frac{P(r)}{1 + 4\pi g' P(r)} \bigtriangledown - \frac{\epsilon}{2} \bigtriangledown^2 \left(\frac{P(r)}{1 + 4\pi g' P(r)} \right) \right] \ .$$

This expression implements the Lorentz-Lorentz correction, which has already been described in section 2.2.1. The structure of the gradients is a result of the so called angle transformation[1]. The susceptibility P(r) is given by

$$P(r) = P_1(r) + P_2(r) \ .$$

Like in the s-wave case P_1 stems from the pionic atoms potential and the P_2 piece incorporates only quasielastic contributions. The term P_1 has the following structure

$$P_1 = -\frac{1}{4\pi} \frac{2}{3} \left(\frac{f^*}{m_\pi} \right)^2 [\alpha_d + \alpha_c] + \alpha_n + \alpha_t \ .$$

The α_d comes from the direct Δ-hole excitations, α_c is the the crossed Δ-hole contribution. α_N is a result of crossed and direct nucleon-hole processes. The term α_t is a sum of various second order diagrams. Only the contributions α_d and α_t incorporate complex pieces, which lead to absorption. The nucleon-hole and crossed Δ-hole pieces are real and do not contribute to absorption.

D.2 Implementation in the BUU simulation

In the BUU simulation we are dealing with classical particles following classical trajectories with well defined momentum p and position r. Classical particles are described in quantum mechanics by packages of plane waves.

To use the p-wave part in our simulation we evaluate the optical potential matrix elements between plane waves $\langle x|p\rangle$. We assume a local density approximation (density is assumed constant) and approximate P(r)=const. Therefore the gradients get replaced by ip.

[1] derivation can be found in [EW88] pages 218-220

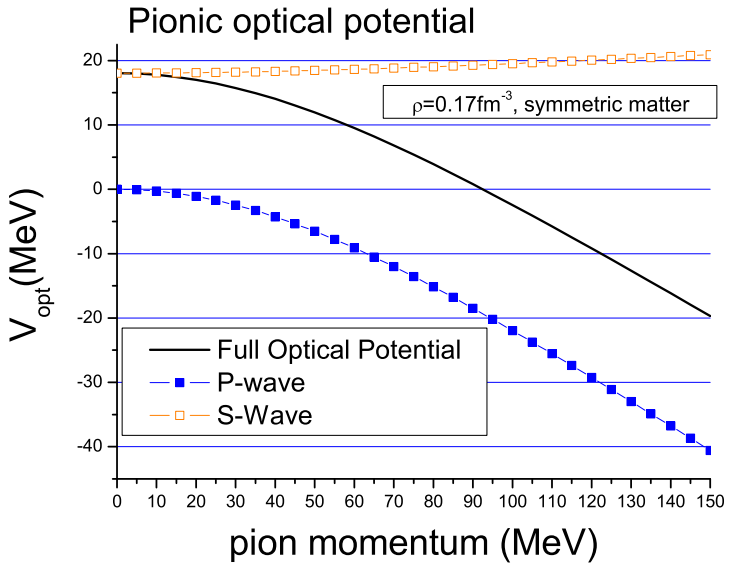

Figure D.1: The real part of the pionic optical potential.

$$
\begin{aligned}
V_{opt}^{p-wave}(x,p) &\equiv \frac{\langle x|V^{p-wave}|p\rangle}{\langle x|p\rangle} \\
&= -\frac{2\pi p^2}{\omega}\frac{M_N^2}{s}\left[1-\frac{\epsilon}{2}\right]\frac{P(\rho)}{1+4\pi g' P(\rho)} \; .
\end{aligned}
$$

In section 3.3.1 the connection between self energy and optical potential is discussed.

$$2E_{Free}V_{opt} = \Pi \; .$$

The real part of the self energy is therefore used as an input for the equations of motion in the BUU simulation. The imaginary parts of the self energy can be used to define a pion decay rate. In section 1.2.3 it was shown that

$$
\begin{aligned}
\Gamma_i\left(\omega_i,\vec{p}\right) &\simeq -\frac{\Im\left(\Pi\right)}{E_{Free}} && \text{(D.1)} \\
&= -\frac{\Im\left(2E_{Free}V_{opt}\right)}{E_{Free}} = -\Im\left(2V_{opt}\right) \; . && \text{(D.2)}
\end{aligned}
$$

Actually this decay rate expresses the loss of particles of a given momentum and energy. So it includes also the loss of a particles due to their scattering to some other momentum. Those processes are called quasielastic processes. The full decay constant can therefore be split into an absorptive part, where the particle

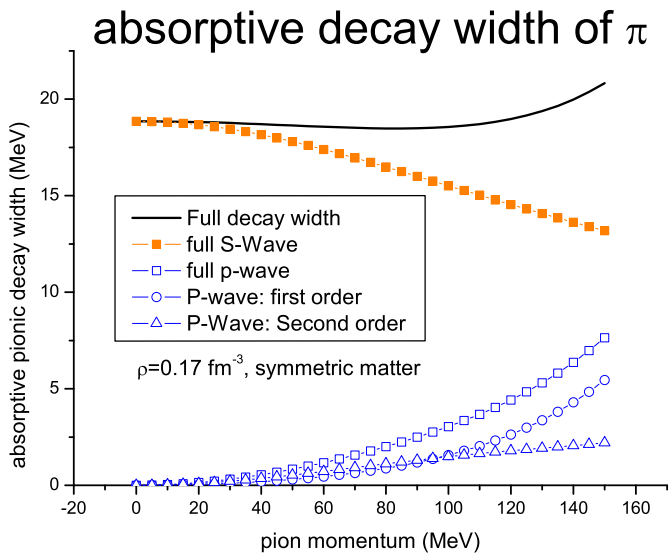

Figure D.2: The pionic decay width in the Valencia model

is annihilated, and a quasielastic part:

$$\Gamma = \Gamma_{abs} + \Gamma_{quasi} \ .$$

To define an absorption rate one now sums up all absorptive contributions of the s-wave and the p-wave terms. One defines

$$\Gamma_{abs} = \Gamma_{abs}^{s-wave} + \Gamma_{abs}^{p-wave}$$

with

$$\begin{aligned} \Gamma_{abs}^{s-wave} &= -\Im\left(2V_{opt}^{s-wave,absorptive}\right) \\ \Gamma_{abs}^{p-wave} &= -\Im\left(2V_{opt}^{p-wave,absorptive}\right) \ . \end{aligned}$$

D.2.1 S-wave absorption

The only s-wave contribution to Γ_{abs} is a piece of V_1:

$$\Gamma_{abs}^{s-wave} = -\frac{1}{E_{Free}}\left(-4\pi\right)\Im\left[B_0\right]\left(1+\frac{\epsilon}{2}\right)2\left(\rho_p^2+\rho_p\rho_n\right) \ .$$

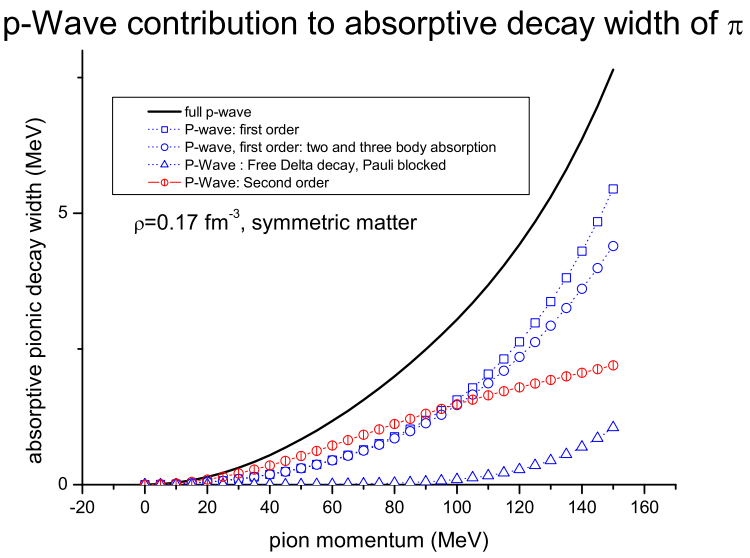

Figure D.3: The pionic decay width due to p-wave

D.2.2 P-wave absorption

Here the situation is a little more subtle due to the Lorentz-Lorenz correction. Let us study the term $\frac{P(r)}{1+4\pi g' P(r)}$ to examine the imaginary part of V_{opt}^{P-wave}:

$$\begin{aligned} \Im & \left[\frac{P(r)}{1+4\pi g' P(r)}\right] = \\ = & \frac{1}{2i}\left(\frac{P(r)-P^*(r)}{(1+4\pi g' P(r))\,(1+4\pi g' P^*(r))}\right) \\ = & \frac{\Im\left[P(r)\right]}{1+16\pi^2 g'^2 |P(r)|^2 + 8\pi g' \Re\left[P(r)\right]} \ . \end{aligned}$$

Now one has to extract the absorptive parts of

$$\Im\left[P(r)\right] = \Im\left[P_1 + P_2\right] \ .$$

The P_2 part is fully quasielastic. As a result one has to concentrate on P_1:

$$P_1 = -\frac{1}{4\pi}\frac{2}{3}\left(\frac{f^*}{m_\pi}\right)^2 \left[\alpha_d + \alpha_c\right] + \alpha_n + \alpha_t \ .$$

Now α_t and α_c are both real. The imaginary part of α_T can be accounted to the absorptive part. The term α_d is more complicated, because it contains the quasielastic width of the Δ_{1232}.

$$\alpha_d \ = \ \rho_n \frac{1}{A} + \frac{\rho_p}{3}\frac{1}{B}$$

with

$$\begin{aligned} A &= \sqrt{s} - M_\Delta - \Sigma_\Delta\left(\frac{2\rho_p}{\rho_0}\right) + i\left[\frac{\Gamma^\Delta}{2} - \Im\left[\Sigma_\Delta^{QA3}\left(\frac{\rho}{\rho_0}\right)\right]\right] \\ B &= \sqrt{s} - M_\Delta - \left[\frac{2}{3}\Sigma_\Delta\left(\frac{2\rho_p}{\rho_0}\right) + \frac{1}{3}\Sigma_\Delta\left(\frac{2\rho_n}{\rho_0}\right)\right] \\ &\quad + i\left[\frac{\Gamma^\Delta}{2} - \Im\left[\Sigma_\Delta^{QA3}\left(\frac{\rho}{\rho_0}\right)\right]\right] . \end{aligned}$$

Using the relation

$$\Im\left(\frac{1}{f}\right) = -\frac{\Im[f]}{|f|^2}$$

one gets the following result:

$$\begin{aligned} \Im[\alpha_d] &= \rho_n \frac{1}{|A|^2}\left[\Im\left(\Sigma_\Delta\left(\frac{2\rho_p}{\rho_0}\right)\right) - \frac{\Gamma^\Delta}{2} + \Im\left[\Sigma_\Delta^{QA3}\left(\frac{\rho}{\rho_0}\right)\right]\right] \\ &+ \frac{\rho_p}{3}\frac{1}{|B|^2}\left[\Im\left(\frac{2}{3}\Sigma_\Delta\left(\frac{2\rho_p}{\rho_0}\right) + \frac{1}{3}\Sigma_\Delta\left(\frac{2\rho_n}{\rho_0}\right)\right) - \frac{\Gamma^\Delta}{2}\right. \\ &\quad \left. + \Im\left[\Sigma_\Delta^{QA3}\left(\frac{\rho}{\rho_0}\right)\right]\right] . \end{aligned}$$

Σ_Δ^{QA3} is the width of the Δ due to three body processes. It incorporates both a quasielastic term and an absorptive term

$$\Im\left[\Sigma_\Delta^{QA3}\left(\frac{\rho}{\rho_0}\right)\right] = \underbrace{-C_q(T)\left(\frac{\rho}{\rho_0}\right)^{\alpha_q(T)}}_{\text{quasielastic}} \underbrace{-C_{A3}(T)\left(\frac{\rho}{\rho_0}\right)^{\alpha_{A3}(T)}}_{\text{absorptive}} .$$

For Γ_{abs} we are only interested in the last term, which stems out of three-body-absorption. Therefore

$$\Im[\alpha_d]_{absorptive} = \left(\rho_n\frac{1}{|A|^2} + \frac{\rho_p}{3}\frac{1}{|B|^2}\right)\left[-\frac{\Gamma^\Delta}{2} - C_{A3}(T)\left(\frac{\rho}{\rho_0}\right)^{\alpha_{A3}(T)}\right]$$

$$\begin{aligned} \Im[\alpha_d]_{absorptive} &= \rho_n\frac{1}{|A|^2}\left[\Im\left(\Sigma_\Delta\left(\frac{2\rho_p}{\rho_0}\right)\right) - \frac{\Gamma^\Delta}{2} - C_{A3}(T)\left(\frac{\rho}{\rho_0}\right)^{\alpha_{A3}(T)}\right] \\ &+ \frac{\rho_p}{3}\frac{1}{|B|^2}\left[\Im\left(\frac{2}{3}\Sigma_\Delta\left(\frac{2\rho_p}{\rho_0}\right) + \frac{1}{3}\Sigma_\Delta\left(\frac{2\rho_n}{\rho_0}\right)\right) - \frac{\Gamma^\Delta}{2}\right. \\ &\quad \left. - C_{A3}(T)\left(\frac{\rho}{\rho_0}\right)^{\alpha_{A3}(T)}\right] . \end{aligned}$$

The final result after the splitting is

$$\begin{aligned}\Gamma_{abs}^{p-wave} &= \Im\left[-2V_{opt}^{p-wave,absorptive}\right] \\ &= -\frac{2\pi p^2}{D_{Free}}\frac{M_N^2}{s}\left[1-\frac{\epsilon}{2}\right]\frac{\Im\left[P(r)\right]_{absorptive}}{1+16\pi^2 g'^2|P(r)|^2+8\pi g'\Re\left[P(r)\right]}(-2)\end{aligned}$$

with

$$\Im\left[P(r)\right]_{absorptive} = \Im\left[\alpha_t\right] - \frac{1}{4\pi}\frac{2}{3}\left(\frac{f^*}{m_\pi}\right)^2 \Im\left[\alpha_d\right]_{absorptive} \ .$$

Appendix E

Deutsche Zusammenfassung

> Wohlauf, laßt uns herniederfahren und da ihre Sprache verwirren,
> daß keiner des anderen Sprache verstehe.
> 1. Moses 10.11

Diese Diplomarbeit entstand im Rahmen der Forschung des "Instituts für theoretische Physik I" der JLU Giessen. Das Institut ist interessanterweise international besetzt und die damit verbundene babylonische Sprachvielfalt sorgt für eine englische Umgangssprache. Aus diesem Grund entstand auch diese Diplomarbeit in englischer Sprache.

Nach dem derzeitigen Wissen wird die Physik auf der subnuklearen Skala vollkommen von dem sogenannten Standardmodell beschrieben. Die elementaren Freiheitsgrade sind Leptonen, Quarks und Eichbosonen. Trotz aller Bemühungen war es bisher nicht möglich ein einzelnes freies Quark zu beobachten. Bisher konnten nur Vielteilchenzustände jener Quarks, die sogenannten Hadronen, im Experiment identifiziert werden. Die einfachsten Hadronen bestehen entweder aus drei Quarks (Baryonen) oder einem Quark und einem Antiquark (Mesonen). Bei niederen Energien bilden jene Vielteilchenzustände die relevanten Freiheitsgrade. Allerdings sind Vielteilchensysteme von Natur aus schwer zu beschreiben. Darum mag man den Sinn anzweifeln, nun jene komplizierten Zustände auch noch in einem nuklearen Medium betrachten zu wollen.

Trotz allem kann man viel über die elementaren Bausteine - also die Quarks - lernen, indem man diese hadronischen Quark-Vielteilchensysteme beobachtet. Besonders interessant sind die Abhängigkeiten der Eigenschaften der Hadronen vom umgebenden nuklearen Medium. Die "Quantumchromodynamik" (QCD) ist Teil des Standardmodells und beschreibt die Dynamik der Quarks und Gluonen. Jene QCD sagt voraus, dass bei hohen nuklearen Dichten die sogenannte "Chirale Symmetrie" wiederhergestellt wird [BW96], was dann auch nachhaltigen Einfluss auf die Eigenschaften der Hadronen haben sollte. Darum untersucht man Hadronen wie das π-, ω-, ϕ- oder ρ-Meson in nuklearer Materie und vergleicht

jene Beobachtungen mit den Eigenschaften der Hadronen im Vakuum. In dieser Arbeit besteht die betrachte Kernmaterie aus Kernen in derem Grundzustand. Komplementär dazu kann man auch Schwerionenkollisionen betrachten. In jenen Prozessen wird ein sogenannter Feuerball produziert, der aus angeregter und sehr dichter Kernmaterie besteht.

Intention der Arbeit In dieser Diplomarbeit wird der Einfluss der pionischen Selbstenergie auf Prozesse mit niederenergetische Pionen untersucht. Dabei stützen wir uns auf das sogenannte Boltzmann - Uehling - Uhlenbeck (BUU) Transportmodell, um niederenergetische Pion-Kern-Streuung und γ-Kern-Streuung zu simulieren. Ursprünglich wurden Transportmodelle wie das genannte BUU-Modell für die Simulation von Schwerionenkollisionen eingesetzt.

Unser Interesse an Niederenergie-Prozessen wurde durch ein Experiment der TAPS-Gruppe [M$^+$02] ausgelöst. Jenes Experiment untersucht die Produktion von Pionen durch Photonen, welche in einem komplexen Atomkern absorbiert werden. Mit der Einschussenergie von $400 - 460\ MeV$ können auch gleichzeitig zwei korrelierte Pionen in einem Absorptionsprozess produziert werden. Die kinetische Energie der korrelierten Pionen übersteigt dann selten $120\ MeV$. Die TAPS-Gruppe analysierte die invariante Masse dieses Zwei-Pionen-Endzustands außerhalb des nuklearen Mediums und berichtete, erste Hinweise auf die Wiederherstellung der Chiralen Symmetrie in Kernmaterie gefunden zu haben. Ein anderes Experiment, welches Pionen anstatt Photonen im Eingangskanal nutzt, wurde von der CHAOS-Gruppe betrieben. Sie betrachten Pionen im gleichen Energiefenster [B$^+$96][B$^+$00]. Auch hier wurden erste Anzeichen der Restauration der Chiralen Symmetrie gefunden.

In diesen Experimenten sind Endzustandswechselwirkungen extrem wichtig. Aus diesem Grund ist es entscheidend ein zuverlässiges Transportmodell zur Analyse jener Experimente heranzuziehen. Das BUU-Modell, welches über die letzten zwei Jahrzehnte in Giessen entwickelt wurde, ist ein solches Transportmodell. Es wurde sowohl in Schwerionenkollisionen [Ehe92] [Tei96] [LM$^+$02] als auch in γ-Kern Prozessen [Eff96] [Eff99] [Leh03] verwandt und hat eine lange Tradition in unserer Arbeitsgruppe.

Trotz seiner Meriten ist das Modell semiklassisch. Darum ist es wichtig zu überprüfen, ob das Modell auch dann noch sinnvolle Vorhersagen machen kann, wenn die Wellenlänge des Pions nahezu der Größe des Kerns entspricht.

Ergebnisse Mit Hilfe des Δ-Loch-Modells wurde ein mittleres Feld für das Pion abgeleitet. Dabei wurde für niedrige Energien $E_{kin} \leq 60\ MeV$ ein Modell von Nieves und Oset [NO93] verwandt, und bei höheren Energien wurde ein Resultat erster Ordnung Störungstheorie ausgenutzt.

Wir verbesserten die Wirkungsquerschnitte der Pionen in der BUU-Simulation und führten das mittlere Feld für die Pionen in die Simulation ein. Schließlich

untersuchten wir den Einfluß dieses mittleren Feldes auf Parameter wie die freie Weglänge und die Geschwindigkeit der Pionen im Atomkern und Observable wie π- und γ- induzierte Streuprozesse.

Im Bereich der π-induzierten Absorptionsprozesse erzielten wir sehr zufriedenstellende Übereinstimung mit dem Experiment [N$^+$80] [A$^+$81]. Die Hinzunahme des mittleren Feldes für das Pion führte zu einem Anstieg der Reaktionsquerschnitte durch die Modifikation der Pionen-Dynamik (siehe Graphen 5.6, 5.7 und 5.8). Durch dieses mittlere Feld war es möglich die Daten sehr gut zu beschreiben. In vollkommen quantenmechanischen Rechnungen konnten wir zeigen, dass der Realteil des optischen Potentials des Pions einen entscheidenden Einfluß auf Reaktionsquerschnitte besitzt (siehe Graph 7.2). Jener Realteil des optischen Potentials ist genau das oben diskutierte mittlere Feld. In den semiklassischen BUU-Rechnungen konnte dies im Falle der Reaktionsquerschnitte allerdings nicht bestätigt werden. In den BUU-Rechnungen hingen die Ergebnisse nur mäßig vom mittleren Feld ab (siehe Graph 7.3).

Wir verglichen die in BUU ermittelten freien Weglängen mit quantenmechanischen Rechnungen [Hec81] [MRR84]. Dabei beobachteten wir, dass die semiklassische BUU-Simulation den Einfluß des repulsiven pionischen mittleren Feldes bei Energien $E_{kin} \leq 30\ MeV$ überschätzt (Graphen 6.11 und 6.12). Hier sinkt die mittlere freie Weglänge zu rapide im Vergleich zu den quantenmechanischen Rechnungen. Diese Überschätzung konnte auch in π-induzierten Vorgängen bei sehr kleinen Energien beobachtet werden. Im Vergleich zu [MRR84] fanden wir eine gute qualitative Übereinstimmung. Wir zeigten weiterhin, dass die Vakuumnäherung [EW88] bei jenen kleinen Energien ungenügend ist (Graph 6.7).

Schließlich untersuchten wir $\gamma A \rightarrow \pi\pi A$ Produktionsprozesse und verglichen jene Resultate mit TAPS-Daten [M$^+$02]. Auch das Modell dieser Diplomarbeit konnte das Problem im $\gamma A \rightarrow \pi^0\pi^\pm A$ Kanal nicht lösen. Ähnlich einer früheren Arbeit [MARBM04] überschätzten wir die Daten in jenem Kanal ungefähr um einen Faktor drei. Im dazu komplementären $\gamma A \rightarrow \pi^0\pi^0 A$ Kanal erzielten wir eine moderate Übereinstimmung mit dem Experiment. Auch deshalb bleibt das Problem im $\gamma A \rightarrow \pi^0\pi^\pm A$ Kanal ein ungelöstes Rätsel.

Die guten Resultate bezüglich der Absorptionsquerschnitte sind sehr ermutigend. Man konnte diese Ergebnisse bei solch niedrigen Energien im Rahmen einer semiklassischen Theorie eigentlich kaum erwarten. Zukünftiges Ziel dürfte wohl die Implementierung der vollen Spektralfunktion der Pionen sein. Dabei wäre es notwendig eine relativistische Selbstenergie der Pionen abzuleiten, die sowohl Nukleon-Loch- als auch Δ-Loch Anregungen im nuklearen Medium berücksichtigen würde. In [LM$^+$02] wurde bereits das Pion mit seiner Spektralfunktion in eine BUU-Simulation implementiert, aber auch hier war es nicht möglich die abgeleitete Selbstenergie zur Bestimmung der Pionen-Dynamik zu implementieren.

Wir sahen, dass es durch Einführung des mittleren Feldes für die Pionen zu einer deutlichen Verbesserung in einigen Querschnitten kam. Darum sehen

wir das mittlere Feld als wichtigen Bestandteil einer Transportsimulation bei niedrigen Energien an. Allerdings sollte man immer im Hinterkopf behalten, dass die semiklassische Beschreibung im Rahmen des BUU-Modells bei niedrigen Energien auch an Grenzen stößt.

Bibliography

[A+81] D. Ashery et al. True absorption and scattering of pions on nuclei. *Physical Review*, C23(5):2173–2185, 1981.

[A+88] Andreev et al. Measurement of the cross section of the reaction $pp \rightarrow pp\pi^0$ in the region of dibaryon resonance. *Zeitschrift für Physik*, A329:371–373, 1988.

[AR02] L. J. Abu-Raddad. Pion-nucleus optical potential up to the delta-resonance region. *arXiv:nucl-th*, (0211028 v1), November 2002.

[B+95] Bondar et al. The $pp \rightarrow pp\pi^0$ reaction near the kinematical treshold. *Physics Letters*, B356:8–12, 1995.

[B+96] F. Bonutti et al. A Dependence of the $(\pi^{\pm}, \pi^+\pi^{\pm})$ Reaction near the $2m_\pi$ Threshold. *Physics Review Letters*, 77:603, 1996.

[B+00] F. Bonutti et al. The $\pi\pi$ interaction in nuclear matter from a study of the $\pi^+ A \rightarrow \pi^+\pi^{\pm}A'$ reactions. *Nuclear Physics*, A677:213, 2000.

[BG88] G. F. Bertsch and S. Das Gupta. A guide to microscopic models for intermediate energy heavy ion collisions. *Physics Reports*, 160(4):189–233, 1988.

[BK84] G. F. Bertsch and H. Kruse. Boltzmann equation for heavy ion collisions. *Physical Review*, C29(2):673–675, 1984.

[BKL+52] H. Byfield, J. Kessler, L. M. Lederman, et al. Scattering and absorption of π-mesons in carbon. *Physicsal Review*, 86(1):17–21, April 1952.

[BW75] G. E. Brown and W. Weise. *Physics Reports*, 22:279, 1975.

[BW96] R. Brockmann and W. Weise. The chiral condensate in nuclear matter. *Physics Letters*, B367:40–44, 1996.

[CMMN90] W. Cassing, V. Metag, U. Mosel, and K. Niita. Production of energetic particles in heavy-ion collisions. *Physics Reports*, 188(6), 1990.

[CR79] J. Chai and D. O. Riska. *Nuclear Physics*, A329:429, 1979.

[CWB+71] A. A. Carter, J. R. Williams, D. V. Bugg, P. J. Bussey, D. R. Dance, et al. The total cross section for pion-proton scattering between 70 MeV and 290 MeV. *Nuclear Physics*, B26:445–460, 1971.

[D+01] M. Daum et al. The reaction $np \to np\pi^0$ from treshold up to 570 MeV. *arXiv:nucl-ex*, (0108008v1), August 2001.

[Eff96] Martin Effenberger. Gammaabsorption an Kernen, 1996. Diploma thesis, JLU Giessen, Institut für theoretisches Physik I.

[Eff99] Martin Effenberger. *Eigenschaften von Hadronen in einem vereinheitlichten Transportmodell*. PhD thesis, JLU Giessen, Institut für theoretisches Physik I, 1999.

[Ehe92] Wolfgang Ehehalt. Effekte hadronischer Selbstenergien in der Kern-Kern-Dynamik, 1992. Diploma thesis, JLU Giessen, Institut für theoretische Physik I.

[EW88] Torleif Ericson and Wolfram Weise. *Pions and nuclei*. Clarendon Press,Oxford, 1988.

[F+91] E. Friedmann et al. Total reaction cross sections for 20-30 MeV pions and the anomaly of pionic atoms. *Physics Letters*, B257(1-2):17–20, March 1991.

[Fli99] Thorsten Fliessbach. *Statistische Physik*. Spektrum, Heidelberg Berlin, 1999.

[FW71] Alexander L. Fetter and John Dirk Walecka. *Quantum theory of many-particle systems*. McGraw-Hill Book Company, 1971.

[G+02] Geissel et al. Deeply Bound 1s and 2p Pionic States in ^{205}Pb and Determination of the s-Wave Part of the Pion-Nucleus Interaction. *Physics Review Letters*, 88(12), 2002.

[GRO+91] C. Gracia-Recio, E. Oset, et al. *Nuclear Physics*, A526:685, 1991.

[H+95] J. G Hardie et al. Kinematically complete measurement of $pp \to pn\pi^+$ near treshold. *Physics Review*, C56(56), 1995.

[H+02a] K. Hagiwara et al. Review of particle physics. Technical report, Particle Data Group, 2002. http://pdg.lbl.gov.

[H+02b] K. Hagiwara et al. Review of Particle Physics. *Physical Review D*, 66:010001+, 2002.

[Hec81] Patrick Hecking. Pion mean free path in nuclear matter. *Physics Letters*, B103(6):401–404, 1981.

[Hen94] P. A. Henning. Thermo field dynamics for quantum fields with continous mass spectra. Technical Report ISSN 0171-4546, GSI, April 1994.

[JNGR93] E. Oset J. Nieves and C. Garcia-Recio. A theoretical approach to pionic atoms and the problem of anomalies. *Nuclear Physics*, A554:509–553, 1993.

[Joa75] Charles J. Joachain. *Quantum Collision Theory*. North Holland Publishing Company Amsterdam and Oxford, 1975.

[K+01] M. Kohl et al. Self energies of the pion and the Δ isobar from the $^3He(e,e'\pi^+)^3H$ reaction. *arXiv:nucl-ex*, 0104004, April 2001.

[Kod84] T. Kodama. Causality and relativistic effects in intranuclear cascade calculations. *Physical Review*, C29(2146), 1984.

[LB88] Landoldt and Boernstein, editors. *New Series*, volume 12. Springer Verlag, Berlin, 1988.

[Leh03] Jürgen Lehr. *In-Medium-Eigenschaften von Nukleonen und Nukleonresonanzen in einem semiklassischen Transportmodell*. PhD thesis, JLU Giessen, Institut für theoretisches Physik I, 2003.

[LM+02] A. B. Larionov, U. Mosel, et al. Off-shell pions in Boltzmann-Uehling-Uhlenbeck transport theory. *Physical Review*, C66, 2002.

[LP03] L. B. Leinson and A. Pérez. Relativistic short-range correlation effects on the pion dynamics in nuclear matter. *arXiv:nucl-th*, (0307025 v1), July 2003.

[M+92] H. O. Meyer et al. Total cross section for $pp \to pp\pi^0$ close to treshold. *Nuclear Physics*, A539:633–661, 1992.

[M+02] J. G. Messchendorp et al. In-medium modification of the $\pi\pi$ interaction in photon-induced reactions. *Physics Review Letters*, 89(222302), 2002. arXiv:nucl-ex/0205009v2.

[MARBM04] P. Mühlich, L. Alvarez-Ruso, O. Buß, and U. Mosel. Low-energy $\pi\pi$ photoproduction of nuclei. arXiv:nucl-th/0401042v1, January 2004.

[Mes76] Albert Messiah. *Quantenmechanik Band I*. Walter de Gruyter, 1976.

[Mos] Ulrich Mosel. Quantentheorie 2. Lecture notes.

[Mos99] Ulrich Mosel. *Fields,Symmetries and Quarks*. Springer Verlag Berlin Heidelberg, 1999.

[MRR84] R. A. Mehrem, H. M. A. Radi, and J. O. Rasmussen. Behavior of pions incident on a slab of uniform complex nuclear material. *Physical Review*, C30(1):301–304, 1984.

[MS+92] D. M. Manley, E. M. Saleski, et al. Multichannel parametrization of πN scattering amplitudes. *Physical Review*, D45(4002), 1992.

[N+80] K. Nakai et al. Measurements of cross sections for pion absorption by nuclei. *Physical review letters*, 44(22):1446–1449, 1980.

[NO93] J. Nieves and E. Oset. Many-body approach to low energy pion-nucleus scattering. *Nuclear Physics*, A554:554–579, 1993.

[Nol97] Wolfgang Nolting. *Grundkurs theoretische Physik 5: Quantenmechanik*. Friedrich Vieweg & Sohn Verlagsgesellschaft mbH, Braunschweig/Wiesbaden, fourth edition, 1997.

[NOVR01] J. C. Nacher, E. Oset, M. J. Vicente, and L. Roca. *Nuclear Physics*, A695:295, 2001.

[OS87] E. Oset and L. L. Salcedo. Delta self energy in nuclear matter. *Nuclear Physics*, A468:631, 1987.

[Pet98] Wolfram Peters. *Die kohärente Photoproduktion von Pionen und Eta-Mesonen an sphährischen Kernen in einem relativistischen,nicht-lokalen Modell*. PhD thesis, JLU Giessen, Institut für theoretische Physik I, 1998.

[PS95] Michael E. Peskin and Daniel V. Schroeder. *Quantum Field Theory*. Perseus Books Publishing,Reading (Massachusetts), 1995.

[S+82] Shimizu et al. Measurement of the pp cross sections in the momentum range 0.9-2 GeV/c. *Nuclear Physics*, A386:571–588, 1982.

[Shy] Radhey Shyam. private communications.

[SMC79] K. Stricker, H. McManus, and J. A. Carr. Nuclear scattering of low energy pions. *Physical review*, C19(3):929–947, March 1979.

[T+88] T. Tsuboyama et al. Study of the $np \to pp\pi^-$ in the incident neutron momentum range 1-1.9 GEV/c. *Nuclear Physics*, A486(669), 1988.

[Tei96] Stefan Teis. *Transporttheoretische Beschreibung von relativistischen Schwerionenkollisionen bei SIS-Energien.* PhD thesis, JLU Giessen, Institut für theoretisches Physik I, 1996.

[Tho03] Markus Thoma. Einführung in die Transporttheorie. Lecture notes, 2003.

[TO96] J. A. Gomez Tejedor and E. Oset. *Nuclear Physics*, A600:413, 1996.

[WPK+88] G. M. Welke, M. Prakash, T. T. S. Kuo, S. Das Gupta, and C. Gale. Azimuthal distribution in heavy ion collisions and the nuclear equation of state. *Physical Review*, C38(2101), 1988.

Acknowledgments

In the first place I wish to thank Prof. Ulrich Mosel, both for giving me the opportunity to join his institute, and for the helpful and stimulating criticism and guidance.

I would also like to acknowledge the help of Prof. Radhey Shyam of the Saha Institute of Nuclear Physics. He helped me calculating the quantum mechanical reaction cross sections with his code to solve the Klein-Gordon equation.

Special thanks go also to Dr. Luis Alvarez-Ruso and Dr. Jürgen Lehr who have been open-minded and patient enought to introduce me to the BUU transport code and pion physics at low energy. They also made valuable comments concerning this diploma thesis and helped to reduce typos. Also frequent discussion with Dr. Markus Post have been very stimulating. I also wish to thank Dr. Alexej Larionov, Thomas Falter and Pascal Mühlich for valuable discussions on the BUU code.

I wish to thank my room mate Markus Wagner for the really good atmosphere in our office and for discussions on physics and non-physics. Having attended already the same school and the same lectures both in the JLU Giessen and in our time at the UW Seattle, we have shared a lot of good time.

In addition, I want to thank the computer crew who have been doing a really great job. And I also want to thank all the rest of the institute for the nice atmosphere and the sunny BBQ's.

Special thanks go also to Elke Jung for the immense help with the bureaucracy.

Schließlich danke ich meinen Eltern für die mentale und großzügige finanzielle Unterstützung während meiner Studienzeit in Giessen und Seattle. Vielen Dank für die Freiheiten, welche Ihr mir ermöglicht habt!